



Simulation and Economic Analysis of 5-Hydroxymethylfurfural Conversion to 2,5-Furandicarboxylic Acid

Diploma Thesis

to obtain the academic degree of 'Diplom-Ingenieur'
at Leoben University of Mining

presented by Christoph Triebel, B.Sc.

Graz, August 2012

First advisor: Univ.-Prof. Dipl.-Ing. Dr. techn. Harald Raupenstrauch
Chair of Thermal Processing Technology
Leoben University of Mining

Second advisor: Prof. Marianthi G. Ierapetritou
Department of Chemical and Biochemical Engineering
Rutgers - The State University of New Jersey

To my Grandmother Aloisia

Eidesstattliche Erklärung

Ich erkläre an Eides statt, dass ich diese Arbeit selbstständig verfasst, andere als die angegebenen Quellen und Hilfsmittel nicht benutzt und mich auch sonst keiner unerlaubten Hilfsmittel bedient habe.

Affidavit

I declare in lieu of oath, that I wrote this thesis and performed the associated research myself, using only literature cited in this volume.

Seiersberg, 08/20/2012

Christoph Triebel

Acknowledgements

I gratefully acknowledge the Marshall Plan Scholarship for the financial support of my research at Rutgers, the State University of New Jersey in the USA.

I would like to thank Prof. Harald Raupenstrauch for attending my work and enabling research abroad. He was a great help through my whole master program and had always time for my questions and concerns.

I am thankful to Prof. Thomas Farris for permitting my research at the School of Engineering at Rutgers University.

I owe my gratitude to Prof. Marianthi Ierapetritou for the supervision of my work. She gave me good advices and was always willing to listen to my problems.

I would like to thank Vladimiros Nikolakis for helpful discussions. Zhaojia Lin is acknowledged for supporting me in process simulations and economy analysis during my research.

I am deeply grateful to my parents and my whole family, who have always been there for me and helped me in all regards.

Last but not least I would like to thank my girlfriend Christina for all her love and support.

Zusammenfassung

Aufgrund des ansteigenden Ölpreises und umwelttechnischer Aspekte gewinnt in den letzten Jahren die Entwicklung von Alternativen zu erdölbasierten Chemikalien und Treibstoffen immer mehr an Bedeutung. Biomasse ist ein mögliches erneuerbares Ausgangsmaterial für die Herstellung von Chemikalien und Treibstoffen. Um die gleichen Produkte wie durch erdölbasierte Prozesse zu erzeugen, sind unterschiedliche Katalysatoren und Reaktionsmechanismen notwendig.

Ein viel versprechender Rohstoff für Chemikalien, die auf Biomasse basieren, ist 5-Hydroxymethylfurfural (HMF), das aus Monosacchariden, wie zum Beispiel Glukose und Fruktose, erzeugt wird. Ein mögliches Produkt aus HMF ist 2,5-Furandicarboxylische Säure (FDCA), die aus der katalytischen Oxidation von HMF hergestellt wird. Laut einem Bericht des Departments für Energie von den Vereinigten Staaten von Amerika im Jahre 2004 gehören HMF und FDCA zu den 12 biobasierten Bausteinen für Chemikalien der Zukunft.

Im Rahmen der vorliegenden Arbeit wurden Prozesssimulationen zur Herstellung von gereinigtem FDCA aus HMF durchgeführt. Hierfür wurde ein Rohrreaktor simuliert, um FDCA aus HMF in einer wässrigen Lösung zu erzeugen, wobei Luft als Oxidationsmittel benutzt wurde. Des Weiteren wurden zwei unterschiedliche FDCA-Reinigungsverfahren untersucht.

Im ersten Prozess erstarrt FDCA in einem Kristallisator und wird in einem Hydrozyklon oder einem Filter abgeschieden, wobei die Reinheit im Produktstrom in den beiden Verfahren bei 3 Gew% beziehungsweise 98 Gew% FDCA liegt.

In einem weiteren Prozess wird flüssiges FDCA mit einer Reinheit von 97 Gew% hergestellt. Aufgrund des hohen Siedepunktes von FDCA ist eine Trennung von der wässrigen Essigsäurelösung nicht möglich. Hierfür wird FDCA vom Lösungsmittel Trioctylamin aus der wässrigen Lösung extrahiert und in einer Destillationskolonne gereinigt. Die Essigsäure und Trioctylamin werden in einer zweiten Destillationskolonne getrennt, wobei das Destillat nicht verflüssigt wird, um die Kühlkosten gering zu halten.

Es wurden bei allen Prozessen Wirtschaftlichkeitsberechnungen durchgeführt, um den geringstmöglichen Verkaufspreis von FDCA zu ermitteln. In den Prozessen mit dem Hydrozyklon und dem Filter wurde der Preis für FDCA auf

4435 \$/t beziehungsweise 3157 \$/t errechnet. Der niedrigste Verkaufspreis von FDCA im Prozess mit den Destillationskolonnen wurde mit 3885 \$/t ermittelt.

Die durchgeführten Empfindlichkeitsstudien zeigen, dass die Selektivität von FDCA und die Umwandlung von HMF und den Zwischenprodukten einen geringen Einfluss auf den errechneten kleinsten Preis für FDCA haben, wobei die Anlagenkapazität und die Kosten für den Katalysator und HMF sich stark auf den geringsten Verkaufspreis von FDCA auswirken.

Abstract

Due to rising oil price and environmental aspects, research on alternatives for petroleum based chemicals and fuels is growing in recent years. Biomass is one potential raw material for producing non-petroleum derived chemicals and fuels. Different catalysts and reaction steps are required to generate the same products in comparison with the petroleum based processes.

One possible starting material for biobased chemicals is 5-hydroxymethylfurfural (HMF), which is derived from monosaccharides, such as glucose and fructose. HMF could be converted into different chemicals and fuels, such as 2,5-furandicarboxylic acid (FDCA), which is generated by catalytic oxidation of HMF. According to a report of the Department of Energy (DOE) in 2004, HMF and FDCA are one of the 12 biobased building blocks of the future.

Simulations on the processes for producing and purifying FDCA from HMF were performed. A tubular reactor was used to generate FDCA from HMF in aqueous solvent using air as oxidant. For purification, two different processes were designed.

In the first process, FDCA is solidified at a crystallizer and fed to a filter or a hydrocyclone. The purity of FDCA in the product stream in the processes using the hydrocyclone and the filter are 3 wt% and 98 wt%, respectively.

The second process produces liquid FDCA at a purity of 97 wt%. Due to the high boiling point of FDCA, separation from the aqueous acetic acid solvent is impossible. For this purpose FDCA is extracted by the solvent trioctylamine and removed using distillation. Acetic acid and trioctylamine are separated in a second distillation column, at which a partial condenser is used to minimize cooling cost.

At all processes, economy analysis was carried out to estimate minimum sale price of FDCA. In the processes with the hydrocyclone and the filter, FDCA price is estimated to be 4435 \$/t and 3157 \$/t, respectively. Estimated minimum sale price of FDCA in the process with the distillation columns is 3885 \$/t.

Sensitivity analysis shows that selectivity of FDCA and conversion of HMF have small impact on FDCA price due to recycling of HMF and the intermediates, whereas plant capacity, catalyst cost and HMF cost have more profound effect on the price of FDCA.

Table of Contents

1	Motivation.....	1
2	Literature on Biomass Conversion.....	3
2.1	Alternative paths to petroleum based products.....	3
2.2	Biomass conversion	4
2.3	Biobased chemicals	5
2.3.1	HMF	8
2.3.2	FDCA	9
2.3.3	PEF	11
2.3.4	Others	12
2.4	Petroleum based chemicals	12
2.4.1	Terephthalic acid.....	12
2.4.2	PET.....	13
2.5	FDCA production from HMF	15
3	Process Simulation	22
3.1	Solvent, catalyst and oxidant.....	22
3.2	First estimations	23
3.3	Flowsheet design	25
3.3.1	Process using crystallization	27
3.3.2	Process using distillation	38
4	Economic Analysis	43
4.1	Capital costs	43
4.2	Operating costs	43
4.3	Economic assumptions	44
5	Results.....	45
5.1	Process simulation using crystallization	45
5.1.1	Process simulation using centrifugation	45
5.1.2	Process simulation using filtration	50
5.2	Process simulation using distillation	55
5.3	Process optimization	65
5.3.1	Process simulation using crystallization and filtration	65
5.3.2	Process simulation using distillation	72
5.4	Economic analysis of the process using crystallization.....	85
5.4.1	Process using centrifugation	85
5.4.2	Process using filtration	87

5.5	Economic analysis of the process using distillation	90
5.5.1	Decreased trioctylamine flow rate	92
5.6	Sensitivity analysis.....	94
6	Summary and Outlook	99
7	Bibliography	103
8	Appendix: Theory of Simulated Unit Operations.....	106
8.1	Distillation	106
8.2	Liquid-liquid extraction	111
8.3	Crystallization	112
8.3.1	Classical Nucleation Model	112
8.3.2	Continuous Crystallization.....	113
8.3.3	Nucleation.....	113
8.3.4	Crystal Growth Rate.....	114
8.3.5	Population Balance	116
8.3.6	Magma Density.....	118
8.4	Thermodynamics	119
8.4.1	Equation-of-state models	119
8.4.2	NRTL	120

Table of Figures

Figure 1: Biomass conversion processes. a thermodynamical route, b biological route, c hybrid biological and thermodynamical route [12].....	4
Figure 2: Sugars that can be used as starting materials for the building blocks HMF, FDCA, DFF, BHF and DMF [6].....	5
Figure 3: Molecular structure of HMF	8
Figure 4: Molecular structure of FDCA	9
Figure 5: Possible products from FDCA [15].....	10
Figure 6: Polyesterification of diester diol over high vacuum and Sb_2O_3 catalyst [11]	11
Figure 7: Molecular structure of terephthalic acid	12
Figure 8: Reaction steps of HMF oxidation according to Partenheimer et al. [23].....	15
Figure 9: HMF conversion to solute FDCA according to Gorbanev et al. [24].....	16
Figure 10: Yields of HMFCA (●) and FDCA (□) according to Gorbanev et al. in aqueous solution using 1 wt% Au/TiO ₂ at 20 bar and 30°C. [24].....	16
Figure 11: Reaction steps of HMF oxidation according to Casanova et al. [19]	17
Figure 12: Membrane reactor for converting HMF to FDCA developed by Kröger et al. [25].....	18
Figure 13: Batch reactor using silicone beads for HMF conversion to FDCA developed by Kröger et al. [25].....	18
Figure 14: Reaction steps of HMF conversion to FDCA according to Lilga et al. [17]	19
Figure 15: Conversion of HMF and selectivity to FDCA, FFCA, DFF and other byproducts in a tubular reactor over 5 % Pt/ZrO ₂ catalyst at 10 bar and 100°C with varying liquid hourly space velocity (LHSV) according to Lilga et al. [17]	20
Figure 16: Molecular structure of FDCA (R = H), FDCA monomethylester (R = Me) and FDCA monoethylester (R = Et).....	20
Figure 17: Flowsheet of HMF conversion to FDCA using a distillation column for FDCA separation from the solvent	23
Figure 18: Temperature and liquid mass fraction profiles of the distillation column for removing FDCA.....	24
Figure 19: Flowsheet of HMF conversion to FDCA with air and fractional solvent recycle flows.....	26
Figure 20: Flowsheet of HMF conversion to FDCA using a crystallizer for obtaining solid FDCA	27
Figure 21: Molecular structure of the FDCA ion, $FDCA^{2-}$	28
Figure 22: Specified components for simulations using a crystallizer	28
Figure 23: Operating conditions and saturation calculation method for simulated MSMR crystallizer	29
Figure 24: Stoichiometric reaction for simulated MSMR crystallizer	29
Figure 25: Solubility specifications for simulated MSMR crystallizer.....	30
Figure 26: Input box for ideal gas heat capacity data of $FDCA^{2-}$	30
Figure 27: Estimated physical properties of $FDCA^{2-}$	31
Figure 28: Estimated parameters for unknown components.....	32
Figure 29: Estimated Wagner parameters of defined molecules.....	33
Figure 30: Estimation options for missing parameters	33
Figure 31: Structure sheet of $FDCA^{2-}$	34

Figure 32: Flowsheet of HMF conversion to FDCA using a crystallizer and a hydrocyclone for separating solid FDCA from aqueous solvent.....	35
Figure 33: Specifications at hydrocyclone for separating FDCA from solvent.....	36
Figure 34: Flowsheet of HMF conversion to FDCA using a crystallizer and a filter for removing solid FDCA	37
Figure 35: Specifications at filter for separating FDCA from solvent.....	38
Figure 36: Settings of the filter cake for separating FDCA from solvent.....	38
Figure 37: Flowsheet of HMF conversion to FDCA introducing high boiling point solvent trioctylamine and using a column for separating FDCA from trioctylamine	39
Figure 38: Molecular structure of trioctylamine	39
Figure 39: Settings at first column for separating FDCA from solvent.....	41
Figure 40: Settings at second column for separating acetic acid and water from trioctylamine.....	42
Figure 41: Mass fractions of liquid phase and temperature profile of distillation column B8	61
Figure 42: Mass fractions of liquid phase and temperature profile of distillation column B18	63
Figure 43: Flowsheet of HMF conversion to FDCA using a crystallizer and a filter for removing solid FDCA with a splitter for discharging solvent at a fraction	65
Figure 44: Flowsheet of HMF conversion to FDCA using a crystallizer and a filter for removing solid FDCA with a splitter for discharging solvent at a fraction and pure O ₂ as oxidant	68
Figure 45: Flowsheet of HMF conversion to FDCA introducing high boiling point solvent trioctylamine and using a column for separating FDCA from trioctylamine with gaseous distillate at second column	72
Figure 46: Mass fractions of vapor phase and temperature profile of column B18 with gaseous distillate	75
Figure 47: Mass fractions of liquid phase and temperature profile of column B8 at the process with reduced trioctylamine flow rate	79
Figure 48: Mass fractions of vapor phase and temperature profile of column B18 with gaseous distillate	81
Figure 49: Flowsheet of HMF conversion to FDCA introducing high boiling point solvent trioctylamine and using a column for separating FDCA from trioctylamine with gaseous distillate at both columns and no flash downstream the extractor	82
Figure 50: Mass fractions of liquid phase and temperature profile of column B8 at the process with reduced trioctylamine flow rate and no flash separator	85
Figure 51: Minimum sale price of FDCA as a function of the plant capacity	96
Figure 52: Annual costs of the process with the crystallizer and the filter using pure oxygen as oxidant	97
Figure 53: Minimum sale price of FDCA as a function of raw material market prices	98
Figure 54: Schematic illustration of a distillation column with reboiler and total condenser [44].....	107
Figure 55: Mass flows and fractions of the rectifying section for component balance [44]	107
Figure 56: Mass flows and fractions of the stripping section for component balance [44]	108
Figure 57: SOL, ROL and q-line in the McCabe-Thiele diagram [44].....	109

Figure 58: Graphical evaluation of the number of stages in McCabe-Thiele diagram using SOL and ROL [28].....	110
Figure 59: Minimum number of stages at a distillation column with total reflux (distillate is zero) [28].....	110
Figure 60: Infinite number of stages at a distillation column with no reflux [28].....	111
Figure 61: Schematic illustration of crosscurrent and countercurrent liquid-liquid extraction [28].....	112
Figure 62: Population density (n): Number of particles in a specific size range (ΔN_i) divided by this size range (ΔL_i) [28].....	117

List of Tables

Table 1: Criteria used by Bozell in evaluating products from biobased technologies [14]	7
Table 2: Solubility of FDCA in water/acetic acid mixtures [17]	22
Table 3: Particle size distribution at crystallizer	32
Table 4: Flow rate and mass fractions of feed stream of the process with the hydrocyclone	45
Table 5: Fractions and flow rates of reactor inputs at the process with the hydrocyclone	46
Table 6: Mass fractions and flow rate of crystallizer input at the process with the hydrocyclone	46
Table 7: Mass fractions and flow rate of crystallizer output at the process with the hydrocyclone	47
Table 8: Overflow and underflow of the hydrocyclone	47
Table 9: Dimensions of the hydrocyclones	48
Table 10: Mass fractions and flow rate of vapor phase of flash separator B4 at the process with the hydrocyclone	49
Table 11: Mass fraction of liquid phase and mole fraction of vapor phase of flash separator B10 at the process with the hydrocyclone	49
Table 12: Flow rate and mass fractions of feed stream of the process with the filter	50
Table 13: Fractions and flow rates of reactor inputs at the process with the filter	50
Table 14: Mass fractions and flow rate of crystallizer input at the process with the filter	51
Table 15: Mass fractions and flow rate of crystallizer output at the process with the filter	52
Table 16: Average mass flow and fractions of the filter cake	52
Table 17: Mass fraction of liquid phase and mole fraction of vapor phase of flash separator B8	53
Table 18: Flow rate and mole fractions of vapor phase of flash separator B4 at the process with the filter	54
Table 19: Mass fraction of liquid phase and mole fraction of vapor phase of flash separator B10 at the process with the filter	54
Table 20: Flow rate and mass fractions of feed stream of the process with the distillation column	55
Table 21: Fractions and flow rates of reactor inputs at the process with the distillation column	56
Table 22: Flow rate and mole fractions of vapor phase of flash separator B4 at the process with the distillation column	56
Table 23: Mass fraction of liquid phase and mole fraction of vapor phase of flash separator B9 at the process with the distillation column	57
Table 24: Mass fractions and flow rate of aqueous extractor input	58
Table 25: K-values of the components in the 4 stages of the extractor	58
Table 26: Mass fractions and flow rates of the aqueous and organic outlet streams of the extractor	59
Table 27: Mass fractions and flow rates of liquid and vapor phase of flash separator B7 at the process with the distillation column	59
Table 28: Mass fraction and flow rate of distillate and bottoms of distillation column B8	60
Table 29: Mass fraction and flow rate of the input of distillation column B18	61

Table 30: Split fraction in the distillate and bottoms of distillation column B18	62
Table 31: Mass fraction and flow rate of distillate and bottoms of distillation column B18	63
Table 32: Mass fraction and flow rate of the organic input of the extractor	64
Table 33: Flow rate and mass fractions of feed stream of the process with the filter and splitter	66
Table 34: Fractions and flow rates of the reactor inputs at the process with the filter and splitter	66
Table 35: Mass fractions and flow rate of the crystallizer input at the process with the filter and splitter	67
Table 36: Average mass flow and fractions of the filter cake at the process with the filter and splitter	67
Table 37: Mass flows of outlet streams 11 of both processes using a filter	68
Table 38: Flow rate and mass fractions of feed stream of the process with filter, splitter and pure O ₂ as oxidant.....	69
Table 39: Fractions and flow rates of the reactor inputs at the process with filter, splitter and pure O ₂ as oxidant.....	69
Table 40: Flow rate and mole fractions of vapor phase of flash separator B4 at the process with the filter, splitter and pure O ₂ as oxidant	70
Table 41: Mass fraction of liquid phase and mole fraction of vapor phase of flash separator B10 at the process with the filter, splitter and pure O ₂ as oxidant	71
Table 42: Mass fractions and flow rate of crystallizer input at the process with filter, splitter and pure O ₂ as oxidant	71
Table 43: Average mass flow and fractions of the filter cake at the process with filter, splitter and pure O ₂ as oxidant	72
Table 44: Mass fractions and flow rate of the input of distillation column B18 with gaseous distillate.....	73
Table 45: Mass fractions and flow rate of distillate and bottoms of column B18 with gaseous distillate.....	74
Table 46: Mass fractions and flow rate of the aqueous extractor input at the process with reduced trioctylamine flow rate	76
Table 47: K-values of the components in the 4 stages of the extractor at the process with reduced trioctylamine flow rate.....	76
Table 48: Mass fractions and flow rates of the aqueous and organic outlet streams of the extractor at the process with reduced trioctylamine flow rate.....	77
Table 49: Mass fractions and flow rates of liquid and vapor phase of flash separator B7 at the process with reduced trioctylamine flow rate.....	78
Table 50: Mass fractions and flow rates of distillate and bottoms of column B8 at the process with reduced trioctylamine flow rate	79
Table 51: Mass fractions and flow rate of the input of column B18 with gaseous distillate	80
Table 52: Mass fractions and flow rates of distillate and bottoms of column B18 at the process with reduced trioctylamine flow rate	81
Table 53: Mass fractions and flow rate of distillation column B8 input at the process with reduced trioctylamine flow rate and no flash separator.....	83
Table 54: Mass fractions and flow rates of distillate and bottoms of column B8 at the process with reduced trioctylamine flow rate and no flash separator	84
Table 55: Capital costs of the process with the hydrocyclone	86

Table 56: Operating costs of the process with the hydrocyclone	87
Table 57: Capital costs of the processes with the filter	87
Table 58: Operating costs of the processes with the filter	88
Table 59: Capital costs of the process with the filter and pure O ₂	89
Table 60: Operating costs of the process with the filter and pure O ₂	90
Table 61: Capital costs of the processes with distillation columns	91
Table 62: Operating costs of the processes with distillation columns	92
Table 63: Capital costs of the processes with distillation columns and reduced trioctylamine flow rate	93
Table 64: Operating costs of the processes with distillation columns and reduced trioctylamine flow rate	94
Table 65: Influence of temperature and pressure at the crystallizer, and conversion and selectivity at the reactor at the process with the filter and pure oxygen as oxidant	95

Table of Symbols

Latin characters

a	constant	[-]
AcOH	acetic acid	
AMF	5-acetoxymethylfurfural	
b	constant	[-]
B	number of formed crystals, birth density function	[-], [$\text{m}^{-1}\text{s}^{-1}$]
BHF	2,5-bis(hydroxymethyl)-furan	
C	concentration	
Cat.	catalyst	
CIPSD	conventional solid substreams with particle size distribution	
Conv.	conversion	[-]
c_p	specific heat capacity	[$\text{J kg}^{-1} \text{K}^{-1}$]
CSTR	continuous stirred tank reactor	
D	distillate flow rate, death density function	[kg/s], [$\text{m}^{-1}\text{s}^{-1}$]
DHAFQM	aqueous heat of formation at infinite dilution	[W]
DFF	diformylfuran	
DMF	2,5-dimethylfuran	
DOE	Department of Energy	
E	extract	[kg/s]
ELECNRTL	Electrolyte non-random two-liquid model	
EMF	5-ethoxymethylfurfural	
F	feed	[kg/s]
FDCA	2,5-furandicarboxylic acid	
FFCA	5-formyl-2-furancarboxylic acid	
FFA	5-formyl-2-furancarboxylic acid (in Figure 9)	
g	interaction energies of molecular pairs	[J]
G	crystal growth rate	[m/s]
G and A	General and Administrative	
h	specific enthalpy	[J/kg]
H	enthalpy	[J]
HMF	5-hydroxymethylfurfural	
HMFA	5-hydroxymethyl-2-furancarboxylic acid	

i	constant	[-]
J	molecular flux	[n/s]
k	constant	[-]
L	liquid flow rate, length	[kg/s], [m]
LHSV	liquid hourly space velocity	[h ⁻¹]
M	molar mass	[g/mol]
m	constant	[-]
MIBK	methyl isobutyl ketone	
MIXCIPSD	mixed conventional solid substreams with particle size distribution	
MMF	5-methoxymethylfurfural	
m%	mole percent	[-]
MSMPR	mixed-suspension, mixed-product-removal	
M _T	density of crystal slurry	[kg/m ³]
n	constant, population density	[-], [m ⁻¹]
N	number of moles	[-]
NRTL	non-random two-liquid model	
NRTL-RK	non-random two-liquid Redlich Kwong model	
p	constant	[-]
P	pressure	[N/m ²]
PEF	poly(ethylene 2,5-furandicarboxylate)	
PET	polyethylene terephthalate	
Pres.	pressure	[bar]
PTA	purified terephthalic acid	
PTFE	polytetrafluoroethylene	
q	constant	[-]
Q	flow rate	[kg/s]
R	raffinate, rotation rate, gas constant	[kg/s], [rpm], [J mol ⁻¹ K ⁻¹]
ROL	rectifying operation line	
s	specific entropy	[J kg ⁻¹ K ⁻¹]
S	solvent, supersaturation	[kg/s], [g/l]
Sel.	selectivity	[-]
SOL	stripping operation line	
SRK	Soave-Redlich-Kwong	
t	time	[s]

Temp.	temperature	[°C]
TOA	trioctylamine	
v	specific volume	[m ³ /kg]
V	vapor flow rate, volume	[kg/s], [m ³]
vol%	volume percent	[-]
wt%	weight percent	[-]
x	mass or mole fraction in the liquid phase	[-]
y	mass fraction in the vapor phase	[-]

Greek characters

α	parameter	[-]
γ	activity coefficient	[-]
ρ	density	[kg/m ³]
τ	crystal residence time	[s]
ω	acentric factor	[-]

Indices

aqu	aqueous
c	surface of the crystal, critical
D	distillate
e	crystal impeller contact
f	formation
gas	gaseous
i	component
j	component
n	stage number, crystallization step
r	reduced
R	rectifying section
s	solute saturation
S	stripping section
ss	driving force of supersaturation
V	vapor
0	start condition, reference condition
1-7	indices of constants

1 Motivation

A large number of chemicals produced today are based on petroleum. Therefore, this market is heavily depended on the oil market. Due to limited resources, economic and environmental reasons, biomass is considered as an alternative raw material for the production of many organic chemicals. Hence the logistic infrastructure of existing products can be utilized, which diminishes the investment costs and enables the change from petroleum to biomass-based processes.

Due to higher oxygen content of biomass compared to petroleum, different reaction steps are performed, such as dehydration, decarbonylation and hydrodeoxygenation. The catalysts used for producing biobased chemicals are similar to those used in petroleum based processes, such as mineral acid, organic acid, solid acid and heterogeneous metal catalysts. For production of chemicals derived from biomass those are competitive to petroleum based chemicals, economic and recycling aspects should not be disregarded.

At present time, manufacturing of chemicals using biomass as starting material is limited to laboratory scale. An important point is the simulation of the upscaling, including optimization of conversion and selectivity and economic analysis of the processes. Main part for estimating weighting of different costs is sensitivity analysis.

A possible feedstock for organic chemicals or fuels is 5-hydroxymethylfurfural (HMF), which is derived from hexose sugars and could be converted into several molecules through condensation, hydrolysis, hydrogenation, oxidation and hydrogenolysis. One of these molecules is 2,5-furandicarboxylic acid (FDCA), generated by catalytic oxidation of HMF.

According to the U.S. Department of Energy (DOE), FDCA is one of the twelve building blocks of the future and could be used as starting material for biobased fuels, plastics and chemicals. A promising application of FDCA is the substitution of terephthalic acid in the manufacturing of polyethylene terephthalate (PET), which is used for bottles, cans, foils, fibers, and is part of food, cosmetics, detergents and pharmaceuticals. Another field of application of FDCA is the production of poly(ethylene 2,5-furandicarboxylate) (PEF), a polymer similar to

PET. PEF is synthesized in a similar way as PET, using FDCA for transesterification instead of terephthalic acid as starting material.

No large-scale plants exist for continuous production of FDCA using HMF as starting material. Biomass based processes using HMF and FDCA may be promising alternatives to petroleum based refinery.

The present work describes the process of HMF conversion to FDCA, based on published literature. For simulation and economic analysis, Aspen Plus and Aspen Process Economy Analyzer were used [1, 2]. The main reaction step in all different paths is a catalytic oxidation that uses aqueous acetic acid as solvent, Pt/ZrO₂ as catalyst, and air as oxidant.

The first process investigated involves a mixed-suspension, mixed-product-removal (MSMPR) crystallizer for solidifying FDCA at ambient temperature, and a filter or a hydrocyclone for separating the purified solid FDCA from aqueous acetic acid solvent.

The second alternative considered includes the production of purified liquid FDCA. Due to the high melting point of FDCA, trioctylamine is introduced as solvent to facilitate separation of liquid FDCA from the solvent using a distillation column.

Process optimization and economic analysis were performed to estimate the minimum sale price of FDCA. Sensitivity analysis was carried out to investigate the impact of selectivity of FDCA and conversion of HMF on FDCA price. The effects of plant capacity and HMF cost on the minimum sale price of FDCA are also discussed.

2 Literature on Biomass Conversion

2.1 Alternative paths to petroleum based products

In the production of fuels and chemicals, petroleum is the most common raw material. Due to increasing cost, diminishing supply and environmental impact of petroleum, the generation of renewable biobased raw materials and alternative energy is rising. Focus on wind, solar and geothermal energy production cannot solve the challenge to find alternative starting materials for fabricating organic chemicals. [3-5]

In recent years, research on developing sustainable technologies and renewable raw materials increases. Processes have to be developed to convert renewable starting materials, such as carbohydrates and oils generated from plants. Chemicals based on renewable biomass push technologies for nonfood transformation of carbohydrates, the largest source of renewable substances on earth, into industrial chemicals. [6-9]

Annually, 200 billion tons of biomass are produced, thereof 95 % are carbohydrates. For food and other aims 3 to 4 % of the carbohydrates are used. Hence plenty of biomass can be used for producing chemicals from renewable sources. [10]

Molecules containing furan heterocycles are alternative feedstocks for synthesizing polymers. These molecules, which have similar properties to the building blocks in the chemical industry, are produced among others from furfural or 5-hydroxymethylfurfural (HMF) those are generated from saccharide sources. In recent years, focus on the furan ring is also directed due to its main part in the Diels-Alder reaction to synthesize new functional materials. [11]

2.2 Biomass conversion

Biomass conversion is accomplished by thermochemical processes using heat and metal catalysts or biological processes using enzymes and microorganisms (Figure 1). Both systems can be combined in a catalytic technique to yield furans from fructose or glucose, which are monosaccharides found in many plants. These furans can be used for generation of building blocks for industrial chemistry. [12]

In the thermochemical process carbohydrates from plants, whose have large polymer chains, have to be converted in several steps to generate building blocks for chemicals or have to be split and deoxidized in order to produce fuels for engines. Synthetic gas is refined for producing synthetic diesel, but at this process half of the origin carbohydrate's energy is lost. [12]

The biological process uses enzymes to crack large polymer chains of the carbohydrates to produce glucose. Microorganisms generate biobased building blocks or bioethanol out of the produced glucose. Currently the yeast *Saccharomyces cerevisiae* is used to ferment glucose into two equivalents of ethanol. One advantage of biological processes is that tailored molecules can be generated, but compared to chemical processes, the capacity is low. [12]

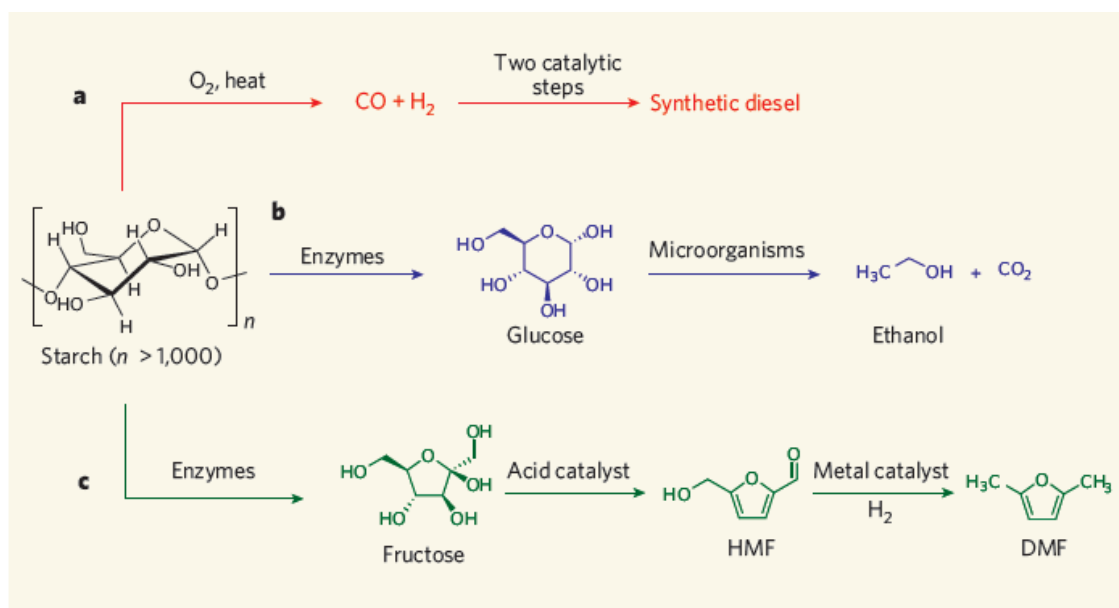


Figure 1: Biomass conversion processes. a thermodynamical route, b biological route, c hybrid biological and thermodynamical route [12]

One of the most important processes is the conversion of sugars to building block chemicals. Especially the hexoses D-fructose and glucose are used as starting materials. Biomass has to be pretreated to produce cellulosic components, whose are dehydrated to generate sugars. In the next step the sugars are converted via fermentation or chemical reaction, such as dehydration, rehydration, hydrogenation, condensation and oxidation, to yield fuels. Particular attention shall be paid to the furans 5-hydroxymethylfurfural (HMF), 2,5-diformylfuran (DFF), 2,5-furandicarboxylic acid (FDCA), 2,5-bis(hydroxymethyl)-furan (BHF) and 2,5-dimethylfuran (DMF) (Figure 2), because they can be used as building blocks for new chemicals as well as substitution for common petroleum-based chemicals. [6, 13]

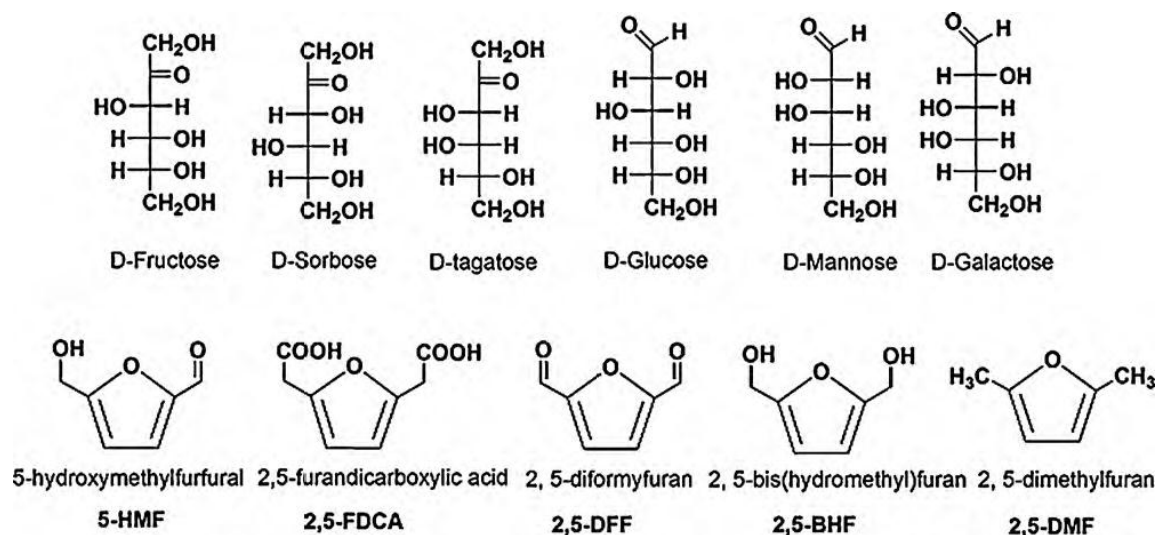


Figure 2: Sugars that can be used as starting materials for the building blocks HMF, FDCA, DFF, BHF and DMF [6]

2.3 Biobased chemicals

Biorefinery has two important goals to achieve: the substitution of renewable raw material for petroleum and the development of a bio-based industry. It is difficult to build up an economic industry for producing biofuels, because fuel is a very low value product. A better economic goal would be to combine production of low value biofuels and high value chemicals made out of renewable sources. [14]

To raise profitability, optimization of the process steps to produce a more competitive product by using renewable raw materials is required. Enhanced use

of basic materials, recycling waste streams, minimizing energy consumption and using economy of scale are further points to optimize industrial production. [15]

In 2004, the US Department of Energy (DOE) reported a list of important chemicals generated by biorefinery carbohydrates and the processes and technology for producing these compounds. These chemicals were selected due to known processes, economics, industrial viability, size of markets, and the feasibility of the compounds for generating derivatives. Chemicals of the DOE report are [15]:

- 1,4-succinic, fumaric and malic acids
- 2,5-furandicarboxylic acid
- 3-hydroxypropionic acid
- aspartic acid
- glucaric acid
- glutamic acid
- itaconic acid
- levulinic acid
- 3-hydroxybutyrolactone
- glycerol
- sorbitol
- xylitol/arabinitol

Conversion of these building blocks contains synthesis of sugars into the building blocks and transforming them to useful chemicals. [15]

Based on the report of the DOE, Bozell developed a list of criteria to evaluate products from biobased technologies, which is shown in Table 1. [14]

Table 1: Criteria used by Bozell in evaluating products from biobased technologies [14]

<i>The compound or technology has received significant attention in the literature.</i>	A high level of reported research identifies both broad technology areas and structures of importance to the biorefinery.
<i>The compound illustrates a broad technology applicable to multiple products.</i>	As in the petrochemical industry, the most valuable technologies are those that can be adapted to the production of several different structures.
<i>The technology provides direct substitutes for existing petrochemicals.</i>	Products recognized by the chemical industry provide a valuable interface with existing infrastructure and utility.
<i>The technology is applicable to high volume products.</i>	Conversion processes leading to high volume functional equivalents or utility within key industrial segments will have particular impact.
<i>A compound exhibits strong potential as a platform.</i>	Compounds that serve as starting materials for the production of derivatives offer important flexibility and breadth to the biorefinery.
<i>Scale up of the product or a technology to pilot, demo, or full scale is underway.</i>	The impact of a biobased product and the technology for its production is greatly enhanced upon scale up.
<i>The biobased compound is an existing commercial product, prepared at intermediate or commodity levels.</i>	Research leading to production improvements or new uses for existing biobased chemicals improves their utility.
<i>The compound may serve as a primary building block of the biorefinery.</i>	The petrochemical refinery is built on a small number of initial building blocks: olefins, BTX, methane, CO. Those compounds that are able to serve an analogous role in the biorefinery will be of high importance.
<i>Commercial production of the compound from renewable carbon is well established.</i>	The potential utility of a given compound is improved if its manufacturing process is already recognized within the industry.

The list of important chemicals made out of renewable raw materials in the DOE report is updated in 2010 by Bozell, including following substances [14]:

- Ethanol
- Furans (HMF, FDCA)
- Glycerol and derivatives
- Biohydrocarbons
- Lactic acid
- Succinic
- Hydroxypropionic acid
- Levulinic acid
- Sorbitol
- Xylitol

The following sections describe possible alternatives for petroleum based chemicals derived from biomass.

2.3.1 HMF

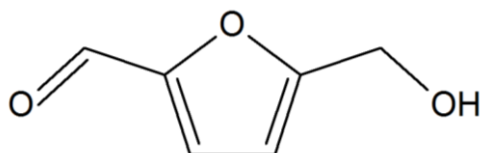


Figure 3: Molecular structure of HMF

CAS Registry Number: 67-47-0

Molecular Formula: C₆H₆O₃

Molecular Weight: 126.11

Density: 1.29 g/cm³

Boiling Point: 291°C (at 760 torr)

Melting Point: 30 - 34°C

Risk Codes: 36/37/38-52/53

Safety Statements: S24/S25

Hazard Symbols: Xi: Irritant, Hazard Class: 3 [16]

5-hydroxymethylfurfural (HMF) is derived from C₆ sugars and is convertible to levulinic acid and formic acid. Starting materials for this process are fructose, mono-, di-, and polysaccharides, such as glucose, sucrose, and starch. HMF is derived from the conversion of fructose via acid-catalyzed dehydration, using solid acids to prevent disposal behavior. Biphasic method of fructose transformation to produce HMF has a selectivity of HMF of up to 80 % at 90 % fructose conversion. Due to cross-polymerization, the yield of HMF with water as solvent is low. [5, 9, 14]

The yield of HMF increases in ionic liquid media, for example dehydration of fructose in methyl imadizolium chloride achieves a yield of HMF of 92 %. Another research shows that the yield of HMF with glucose as starting material in 1-ethyl-3-methylimidazolium chloride using a CrCl₂ catalyst is up to 70 %. Due to the difficult separation of HMF from the ionic liquid, an alternative dehydration

process using choline chloride/citric acid with a HMF yield of 90 % has been invented. [14]

HMF was first separated in the last decade of the 19th century with a yield of 20 % from a mixture of fructose and sucrose with oxalic acid as catalyst. The structure of HMF was found in 1909. Reichstein and Zschokke, and Haworth and Jones developed a synthesis method for generating HMF that is still today in use. In 1980s, van Dam et al. and Cottier et al. demonstrated that an aqueous and a non-aqueous process lead to a yield of HMF of 37 %. [6]

Due to its keto and hydroxyl functionalities, HMF can be converted into valuable chemicals through condensation, hydrolysis, hydrogenation, oxidation and hydrogenolysis. Through oxidation of HMF 2,5-diformylfuran (DFF), 5-hydroxymethyl-2-furancarboxylic acid (HMFCFA), 5-formyl-2-furancarboxylic acid (FFCA), and 2,5-furandicarboxylic acid (FDCA) can be generated, whose are used for adhesives, sealants, composites, coatings, binders, foams, curatives, monomers and resins. [7, 17]

HMF can be used as starting material for producing antifungal compounds, thermo resistant polymers and macrocyclic compounds, especially for the synthesis of dialdehydes, ethers, amino alcohols and other organic intermediates. HMF can also be used for producing disubstituted furan derivatives, a major component of pharmacologically active compounds. Due to economic aspects, furanic intermediates are still derived from petroleum, instead from HMF. [6]

For the production of HMF, economic processes have to be developed and the storage of this unstable substance has to be solved.

2.3.2 FDCA

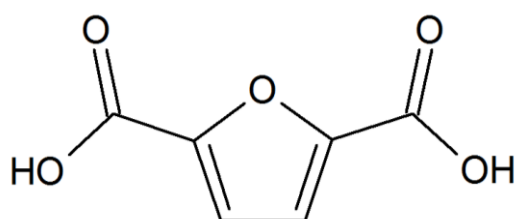


Figure 4: Molecular structure of FDCA

CAS Registry Number: 3238-40-2

Molecular Formula: $C_6H_4O_5$

Molecular Weight: 156.09

Boiling Point: 419.2°C (at 760 torr)

Density: 1.604 g/cm³

Risk Codes: 36/37/38

Safety Statements: S26S36/S37/S39 [18]

2,5-furandicarboxylic acid (FDCA) is produced by oxidizing HMF with different catalysts in two steps: alcohol oxidation to aldehyde and aldehyde oxidation to carboxylic acid. Challenges of transforming sugars to FDCA are developing selective dehydrations without side reactions, finding solid acid catalysts instead of liquid catalysts, developing dehydration steps to anhydrides and lactones, oxidizing aldehydes to alcohols and alcohols to acids, using air as oxidant, allowing inhibitory substances in process flows due to biomass sources, and avoiding producing hydrogen peroxide. Challenges in transforming FDCA to polymers are controlling esterification and avoiding side reactions. [15, 19]

FDCA can be converted to succinic acid, 2,5-bis(aminomethyl)-tetrahydrofuran, 2,5-dihydroxymethyl-tetrahydrofuran, 2,5-dihydroxymethyl-furan and 2,5-furandicarbaldehyde (Figure 5). [15]

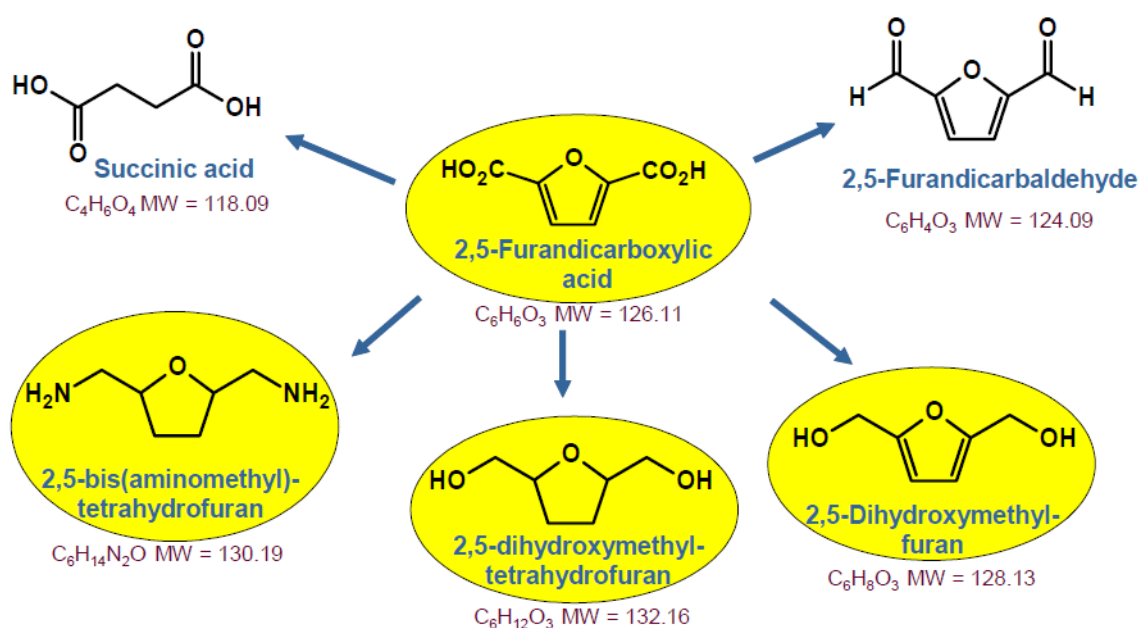


Figure 5: Possible products from FDCA [15]

FDCA can be used as fungicide, corrosion inhibitor and melting agent for foundry sands or as an intermediate in pharmaceutical and photography fields. FDCA is also used for amine-based curatives for polyureas, hybrid epoxy- and urea-urethanes, and polyester polyols, which are used in the production of corrosion- and flame-resistance coatings. [6, 19]

In the production of polyethylene terephthalate (PET), terephthalic acid can be substituted for FDCA. Due to its similarity to terephthalic acid that has a market value of 0.80 \$/kg, FDCA can be used as a building block for producing poly(ethylene 2,5-furandicarboxylate) (PEF), a polymer similar to PET. FDCA is also capable of preparing Schiff bases and as a starting material for polybutylene terephthalate. [5, 9, 14, 19]

Market sizes for polyethylene terephthalate and polybutylene terephthalate are 1.8 million t/a and 450.000 t/a, respectively. Prices of PET products range from 0.45 \$/kg to 1.40 \$/kg. Manufacturing new nylons from FDCA could attain a market size of about 4 million t/a, with values of 0.40 \$/kg to 1.00 \$/kg. [15, 20]

2.3.3 PEF

Poly(ethylene 2,5-furandicarboxylate) (PEF) can be synthesized from FDCA and ethylene glycol, whose are converted at 75°C for 6 h over vacuum and small amounts of aqueous hydrochloric acid to diester diol with a yield of 98 %. PEF is produced by polytransesterification of diester diol over high vacuum and a Sb_2O_3 catalyst at increasing temperature from 70°C to 220°C (Figure 6). Ethylene glycol has to be trapped continuously at liquid nitrogen temperature. [11]

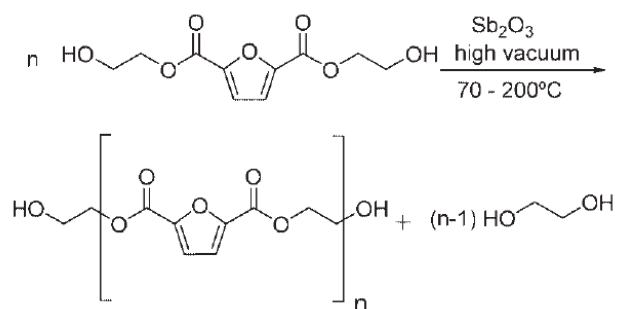


Figure 6: Polyesterification of diester diol over high vacuum and Sb_2O_3 catalyst [11]

2.3.4 Others

2,5-furfuryldiamine, 2,5-furfuryldiisocyanate and 5-hydroxymethyl furfurylidene ester, those are derivatives of HMF, can be used for producing polymers, such as polyesters, polyamides and polyurethane. [6]

2,5-diformylfuran (DFF) is used for producing polymers, pharmaceuticals, antifungal agents, macrocyclic ligands or in the production of poly(vinyl alcohol) as a cross-linking agent. [6]

2,5-bis(hydroxymethyl)-furan (BHF) and 2,5-dimethylfuran (DMF) are produced by the hydrogenation of HMF and can be produced in the one-pot dehydration and hydrogenation processes of hexoses. Due to its high energy density of 31.5 MJ/L, which is similar to that of gasoline (35 MJ/L) and 40 % higher than that of ethanol, DMF has good requirements for being used as a fuel in the future. Furthermore, it is immiscible with water and has a higher boiling point (92 - 94°C) than ethanol. [6]

2.4 Petroleum based chemicals

2.4.1 Terephthalic acid

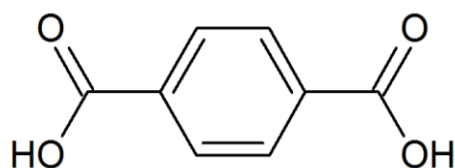


Figure 7: Molecular structure of terephthalic acid

Terephthalic acid is used for producing polyesters, generally by reaction with ethylene glycol or higher alkylene glycols. Polyesters are used for manufacturing fibers, films, containers, bottles and other packing materials, and molded articles. [10]

Aromatic carboxylic acids are produced in an aqueous acid solvent of methyl-substituted benzene and naphthalene as raw materials by exothermic liquid-phase oxidation with an oxygen source and a bromine-promoted catalyst. The positions of the methyl substitute comply with the positions of carboxyl groups in the product. Byproducts of this reaction are water, oxidation products of the aromatic source, and acetic acid degradation products, for instance methanol, methyl acetate, and methyl bromide. A vessel is used for producing aromatic carboxylic acids at elevated temperature and pressure. In the vessel, a liquid-phase mixture is retained and a vapor-phase, containing water vapor, acetic acid and small amounts of byproducts, is distilled from the vessel to control temperature. Due to the high temperature, high pressure and corrosive behavior of the vapor-phase stream, separating or recovering substances features technically and economically challenges. [10]

For production of polyesters for important employment, such as fibers and bottles, purified aromatic carboxylic acids, such as purified terephthalic acid (PTA), are used, because impurities may correlate with color formation in polyesters. Catalytically hydrogenations with noble metal catalysts are used for purifying aromatic carboxylic acids, minimizing impurities and reducing the level of color bodies, amount of metals, acetic acids and bromine compounds. One approach for purification may be developing new processes using alternative raw materials. [10]

2.4.2 PET

Polyethylene terephthalate (PET) is a thermoplastic polyester used for bottles, cans, foils, fibers, and is part of food, cosmetics, detergents and pharmaceuticals. PET is a hard, stiff, strong and dimensionally stable resin. It is highly transparent, colorless and absorbs very little water. It has good chemical resistance to mineral oils, solvents and acids, but not to bases. Various synthetic processes lead to amorphous or fairly high crystalline characteristics. In contrast to semi-crystalline PET, amorphous PET is more ductile, but less stiff and hard. [21]

Starting materials for manufacturing thermoplastic polymers are dicarboxylic acids and dihydric alcohols, at which terephthalic acid is the most important one.

High purification of the raw material is necessary, because impurities may lead to chain termination, branching, second reactions or discoloration. [22]

Thermoplastic polyesters are produced in two steps. First step is transesterification of dicarboxylic diesters or esterification of dicarboxylic acid in presence of dihydric alcohol to produce a precondensate. In the second step the high molecular mass polyester is generated by elimination of dihydric alcohol. Both steps are catalytic reactions producing water as byproduct. [22]

Using terephthalic acid and ethylene glycol as raw materials, PET is produced by direct esterification under pressure and temperatures of 220 – 260°C. Water, which is the byproduct of the esterification, is removed continuously by distillation. Catalysts are not necessary, but can be used, such as amines or Sb_2O_3 . After esterification, pressure is decreased and the temperature enhanced to distillate ethylene glycol. The next step is polycondensation, where the temperature is increased to up to 280°C at a pressure of < 1 mbar. In the polycondensation, the same catalysts can be used as in the esterification. Other catalysts for the polycondensation are antimony, germanium, titanium, or lead compounds. When a defined melt density is reached, the process stops and vacuum is removed in the vessel with nitrogen. The product is quenched with water and for avoiding oxidation crushed into pellets or chips. In the next step, the product is dried to reduce water. [22]

PET is a starting material for producing synthetic fibers such as polyester, dacron, and terylene. Due to its good gas barrier properties against carbon dioxide and oxygen, PET is used for manufacturing bottles. Another range of uses are food trays for oven use, roasting bags, audio or video tapes, mechanical components and containers for different usages. PET films are used for packaging and in electrical applications, such as dielectric metal foil capacitors. 60 % of the world's PET production is used for producing synthetic fibers, at which 30 % of the global bottle manufacturing is covered. Textile synthesizing makes up 18 % of the world's polymer production. Polyester is the most common synthetic fiber, implying polyester filament and polyester staple, used for manufacturing clothing and furnishing. [21]

2.5 FDCA production from HMF

Partenheimer et al. describe the oxidation of HMF at 70 bar with air in aqueous acetic acid solution over a homogenous metal/bromide catalyst using a Co/Mn/Br composition. Products and route of the autoxidation are shown in Figure 8. FDCA is derived from HMF via oxidation producing the intermediates 2,5-diformylfuran and 2-carboxy-5-(formyl)furan. [23]

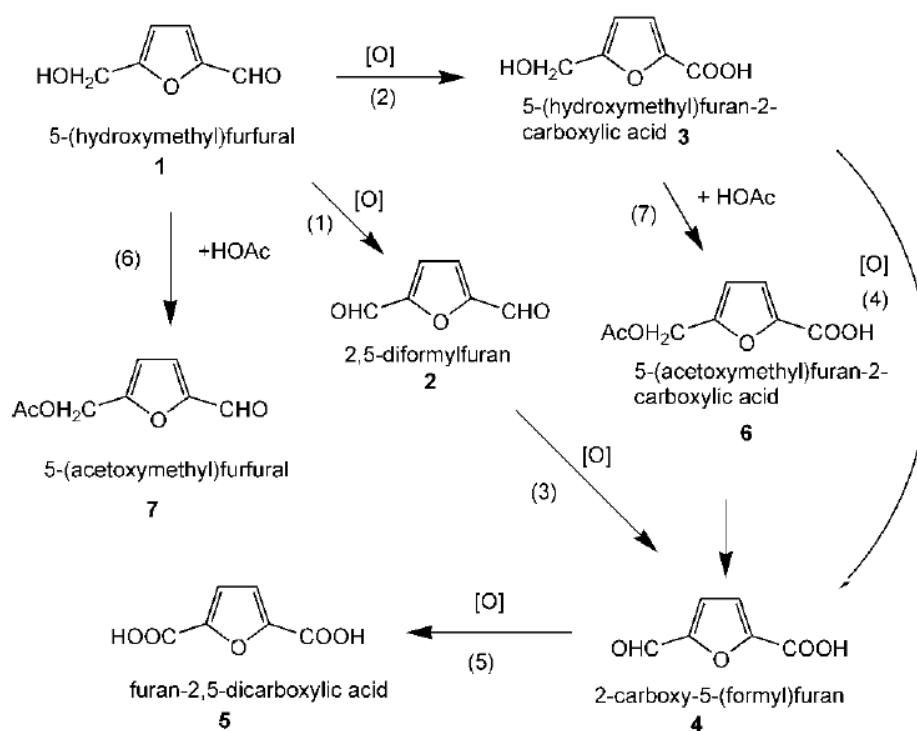


Figure 8: Reaction steps of HMF oxidation according to Partenheimer et al. [23]

The yield is directly proportional to the concentration of the catalyst and the temperature, but is limited to about 60 %. [23]

In addition, Gorbanev et al. reported the aerobic oxidation of HMF using Au/TiO₂ catalysts in aqueous sodium hydroxide solution at 20 bar oxygen pressure. Reaction steps of HMF conversion to FDCA are shown in Figure 9. First HMF is oxidized in a fast reaction to 5-hydroxymethyl-2-furancarboxylic acid (HMFCa). The limiting reaction step is the oxidation of HMFCa to 5-formyl-2-furancarboxylic acid (FFA) that is converted finally to FDCA. [24]

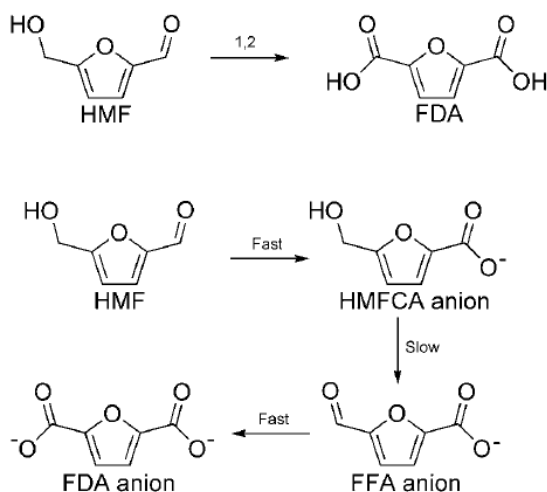


Figure 9: HMF conversion to solute FDCA according to Gorbanev et al. [24]

The yield characteristics of FDCA and HMFCa are shown in Figure 10. The maximum achieved yield of FDCA is 71 % at 30°C. [24]

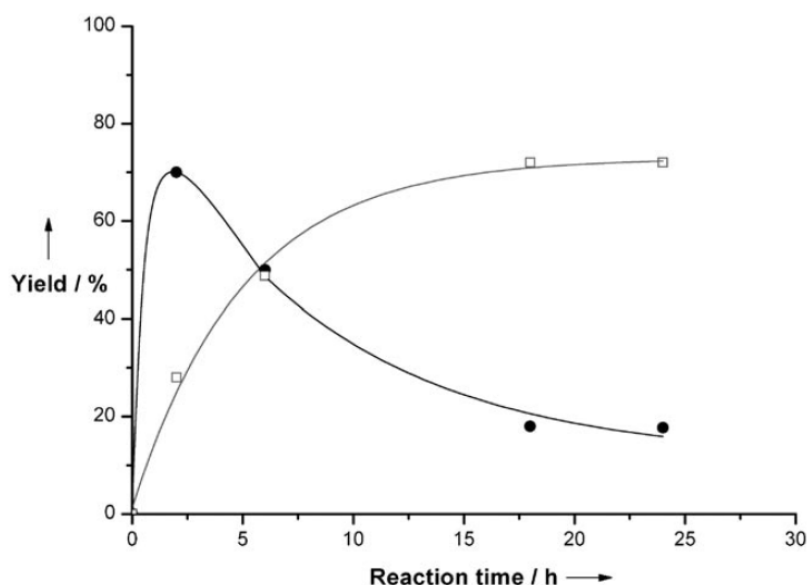


Figure 10: Yields of HMFCa (●) and FDCA (□) according to Gorbanev et al. in aqueous solution using 1 wt% Au/TiO₂ at 20 bar and 30°C. [24]

Casanova et al. reported that using Au/CeO₂ or Au/TiO₂ catalysts leads to a yield of FDCA of over 99 %. Reaction conditions are 65°C and 65 bar in aqueous sodium hydroxide solution. HMF is converted to HMFCa, which is transformed into 5-formyl-2-furandicarboxylic acid (FFCA), before FDCA is generated (Figure 11). The limiting reaction step of this process is the conversion of HMFCa to FFCA. [19]

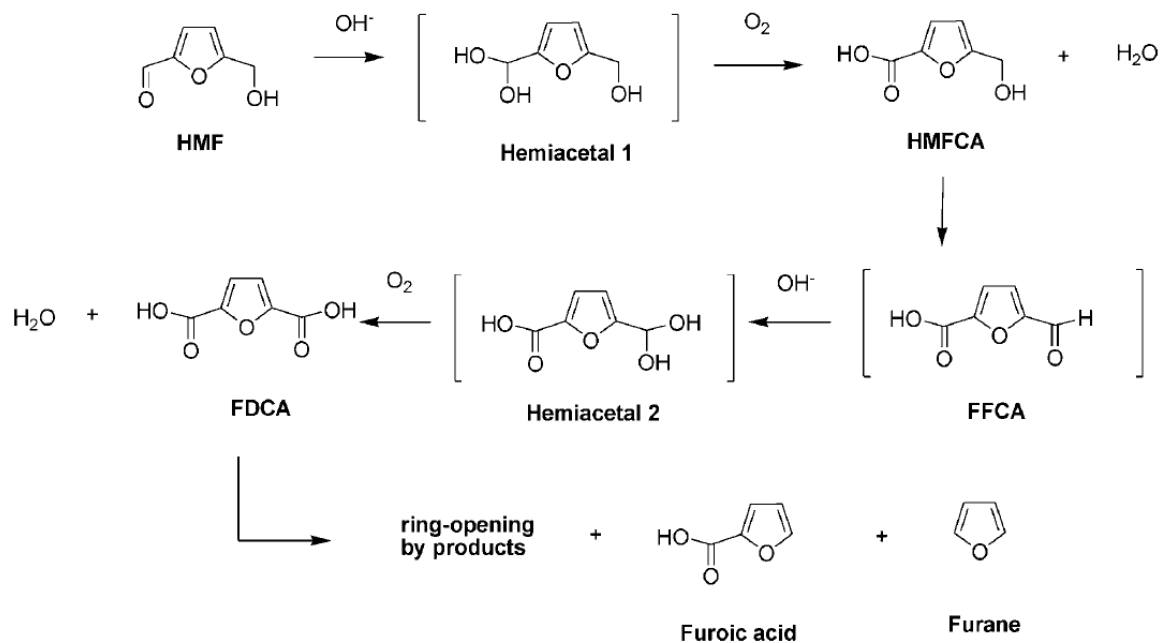


Figure 11: Reaction steps of HMF oxidation according to Casanova et al. [19]

Keeping the temperature constant at 130°C , best results were achieved, but at this temperature recycling of the catalyst is impossible. However, increasing the temperature from 25°C to 130°C after HMF conversion to HMFCA allows a recycle of the catalysts with a FDCA selectivity of 93% in the third cycle. [19]

Conversion methods using Pt/C, Pd/C, Au/C and Au/TiO₂ catalysts were compared in literature under same conditions. Using Au as catalyst, a fast conversion of HMF to HMFCA can be achieved, due to the oxidation of the aldehyde side chain of HMF. HMFCA is oxidized to FDCA using Pt or Pd as catalyst, revealing that these catalysts contrary to Au activate the side chain of HMFCA. The conversion of HMFCA to FDCA over gold catalysts requires high concentrations of the used base and high oxygen pressure. [5]

Ribeiro et al. describe the one pot conversion from fructose to FDCA, which requires a special catalyst with acid characteristics for producing HMF from fructose and metallic characteristics for obtaining FDCA. Co(acac)₃ catalyst in SiO₂-gel was fabricated to accomplish an one-pot conversion, but results show that the selectivity of HMF is low. [8]

A challenge in the in-situ conversion from fructose to FDCA is that fructose is also oxidized, which would decrease the yield of HMF. Therefore two models of

the two-phase system water/methyl isobutyl ketone (MIBK) were developed by Kröger et al. with a maximum yield of FDCA of approximately 25 %. [25]

In the first model the separation of the two phases is realized with a PTFE-membrane. In aqueous solution fructose is converted to HMF, and in the MIBK solution FDCA is produced from HMF. As shown in Figure 12, fructose is not able to pass through the membrane. [25]

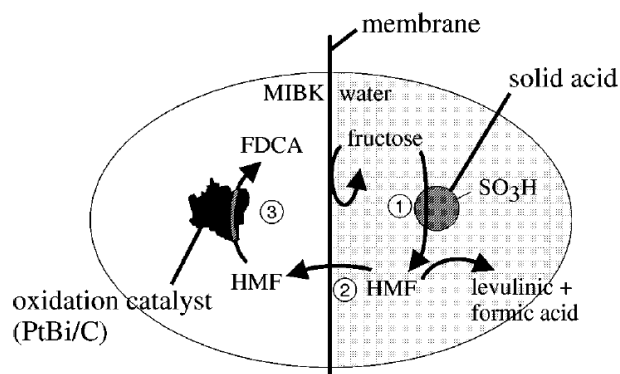


Figure 12: Membrane reactor for converting HMF to FDCA developed by Kröger et al. [25]

The second model involves a batch reactor with aqueous solid acid solvent using a PtBi/C catalyst enclosed in MIBK-swollen silicone. HMF is produced in aqueous solution from fructose, which cannot go through the encapsulated catalyst. FDCA is derived from HMF that passes the PtBi/C catalyst enclosed in silicone beads (Figure 13). [25]

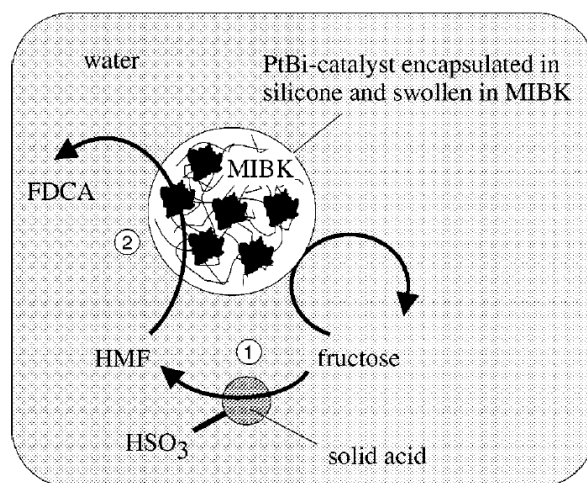


Figure 13: Batch reactor using silicone beads for HMF conversion to FDCA developed by Kröger et al. [25]

Lilga et al. describe in an US patent HMF conversion by the intermediates DFF, HMFCFA and FFCA (Figure 14). [17]

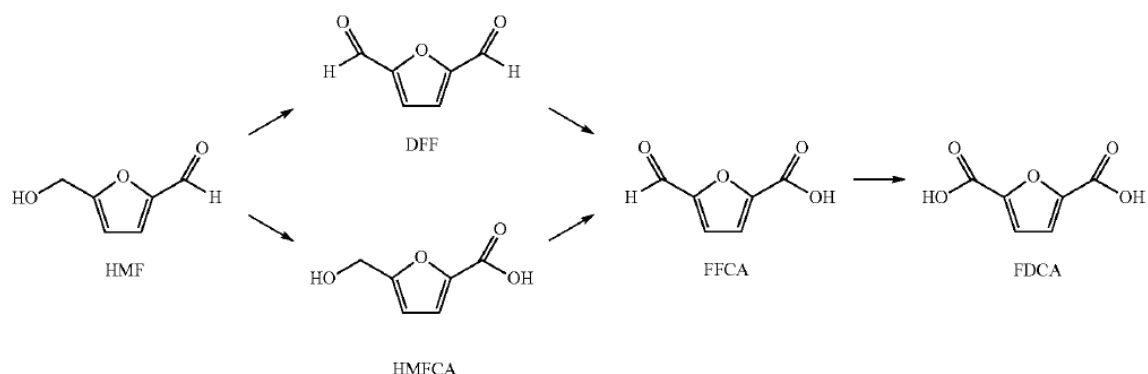


Figure 14: Reaction steps of HMF conversion to FDCA according to Lilga et al. [17]

The operating conditions are 10 bar and 100°C over different catalysts, namely Pt/C, Pt/ZrO₂, Pt/Al₂O₃, Pt/SiO₂ and Pt/TiO₂. Aqueous acetic acid solvent is used in a ratio of 40/60 of acetic acid/water to enhance the solubility of FDCA. Feed for the batch processes is 1 to 3 wt% HMF in aqueous acetic acid solution and 0.5 wt% HMF in the same solvent for steady state operation. [17]

The US patent describes several experiments carried out in a tubular reactor. Figure 15 shows the selectivity of FDCA, FFCA and DFF, and the HMF conversion in a tubular reactor over Pt/ZrO₂ catalyst at 10 bar and 100°C. Liquid hourly space velocity, which is the ratio of the hourly volume of feed to the volume of the catalyst, is varied from 7.5 h⁻¹ to 3 h⁻¹. Selectivity of FDCA and FFCA are approximately 98 wt% and 2 wt%, respectively. [17]

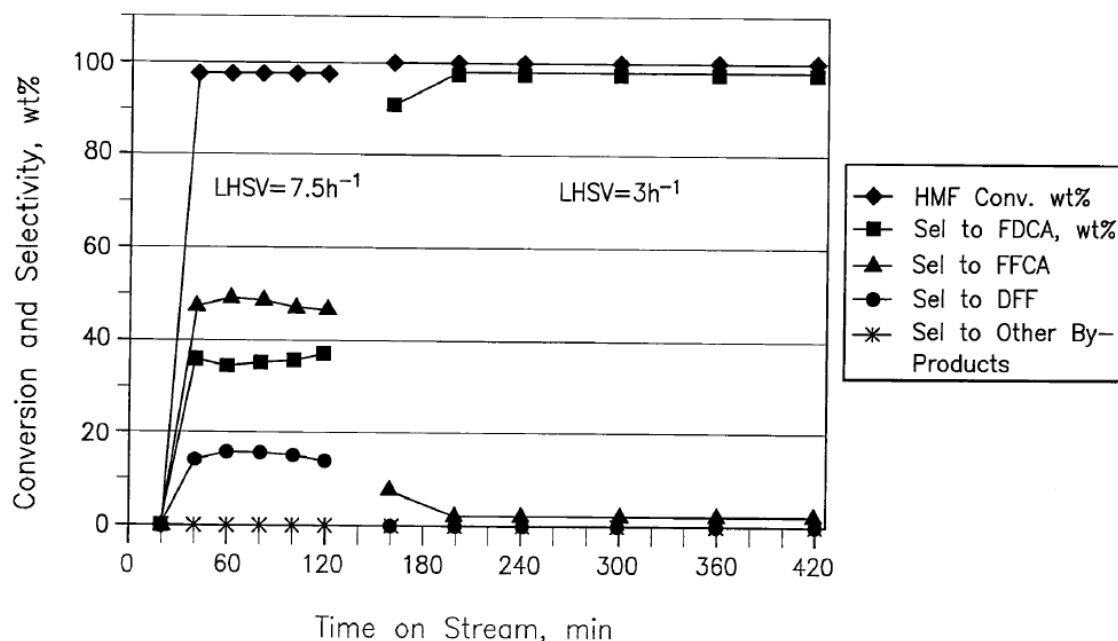


Figure 15: Conversion of HMF and selectivity to FDCA, FFCA, DFF and other byproducts in a tubular reactor over 5 % Pt/ZrO₂ catalyst at 10 bar and 100°C with varying liquid hourly space velocity (LHSV) according to Lilga et al. [17]

The Dutch company Avantium patented a process for producing FDCA from alkyl ethers of HMF, such as 5-methoxymethylfurfural (MMF) and 5-ethoxymethylfurfural (EMF) or 2,5-bis(alkoxymethyl)furan. Using these substances as starting materials avoids problems caused by the instability of HMF. Products of the oxidation are FDCA and FDCA esters, such as monomethylester and monoethylester of FDCA (Figure 16), at a yield of 70 to 85 %, which can be used for manufacturing polyesters via transesterification using diol. Feed material for the catalytic reaction using Co/Mn/Br catalysts is an aqueous acetic acid solution containing MMF, EMF and HMF. Preferred temperature ranges from 160 to 190°C at a pressure of 20 to 60 bar. [26]

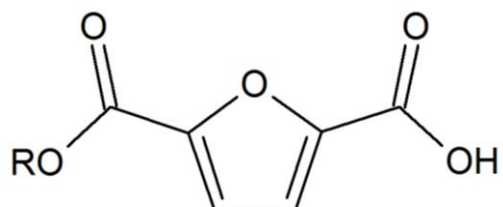


Figure 16: Molecular structure of FDCA (R = H), FDCA monomethylester (R = Me) and FDCA monoethylester (R = Et)

Another patent of Avantium describes the production of FDCA at a yield of up to 78 %. Starting materials are HMF, 5-acetoxymethylfurfural (AMF), which is an ester of HMF, 5-methylfurfural, 5-(chloromethyl)furfural, 5-methylfuroic acid, 5-(chloromethyl)furoic acid, 2,5-dimethylfuran and mixtures thereof. AMF is the preferred feed substance, because it is more stable than HMF. FDCA and FDCA esters can be used as basic materials for producing polymers by transesterification using a diol. Temperature of the oxidation for generating FDCA, using air as oxidant, is between 160 and 190°C at a pressure of 20 to 60 bar. The solvent is an aqueous acetic acid solution, using Co/Mn/Br catalysts. [27]

3 Process Simulation

3.1 Solvent, catalyst and oxidant

Deriving FDCA from HMF requires an oxidation step, which is performed in an aqueous solution to disperse FDCA in water for steady state operation. Air is used as oxidant due to economic and environmental reasons.

Adding acetic acid or a weak base to the aqueous solution enhances solubility of FDCA. Introducing acetic acid in the solution leads to a lower selectivity of FDCA, with a yield loss up to 8 wt% [23]. Table 2 shows solubility of FDCA in solutions with different water/acetic acid ratios. In a water/acetic acid mixture with a ratio of 60/40, the solubility of FDCA is at 70°C more than twice as high as in pure water. Enhancing the acetic acid fraction leads to decreasing miscibility of the solvent and FDCA at 70°C. At 25°C, maximum solubility of FDCA is between a water/acetic acid ratio of 50/50 to 60/40. Higher acetic acid concentrations lead also to decreasing miscibility. [17]

Table 2: Solubility of FDCA in water/acetic acid mixtures [17]

vol% H ₂ O	vol% AcOH	wt% 70°C	wt% 25°C
100	0	0.327	0.086
60	40	0.779	0.153
50	50	0.746	0.173
40	60	0.596	0.171
30	70	0.592	0.143
10	90	0.458	0.138
0	100	0.193	0.080

A catalyst, which consists of a metal on a support material, is embedded in the tubular reactor for faster reaction and increasing yield of FDCA. According to the patent, metal of the catalyst is preferably Pt and support material contains C, ZrO₂, Al₂O₃, SiO₂, or TiO₂. [17]

3.2 First estimations

For simulation of HMF conversion to FDCA, Aspen Plus User Interface V7.3 [1] was used. Based on the US patent of Lilga et al., a reactor was designed to convert HMF to FDCA [17]. One opportunity to produce purified FDCA is to use distillation, which requires high temperatures. Heating up flow streams imply high energy input and subsequently high degradation of energy.

The flowsheet that is designed for first estimations is shown in Figure 17. According to the patent of Lilga et al., feed stream F containing 0.5 wt% HMF in water/acetic acid solution and air stream 9 are fed at a volume ratio of 1/100 into reactor B1 at 10 bar [17]. The RYield-reactor in Aspen was chosen for first estimations to accomplish the process. Input data of the RYield reactor are composition and amount of the feed flow, yields, and operating temperature and pressure in the reactor. The yields of the HMF conversion in the reactor are according to Lilga et al. 90 wt% FDCA, 2 wt% FFCA, and 0.05 wt% DFF [17]. Water, acetic acid and, due to its low conversion rate, air were specified as inert substances.

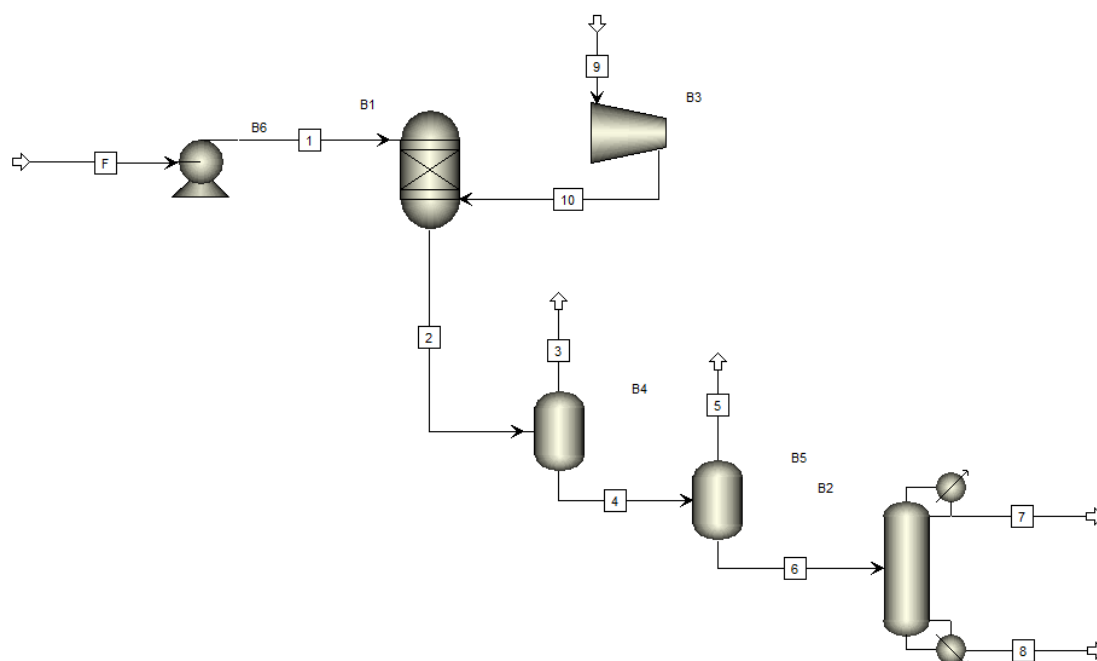


Figure 17: Flowsheet of HMF conversion to FDCA using a distillation column for FDCA separation from the solvent

In accordance with the patent, the solubility of FDCA in an acetic acid/water mixture at the ratio of 40/60 is 0.779 wt% at 70°C, increasing at higher temperatures [17]. Due to a HMF concentration of 0.5 wt% in the feed stream and a yield of FDCA of 90 wt%, FDCA fraction in the product stream is about 0.45 wt%. Hence, FDCA is completely soluble in the product stream due to its low concentration.

Two flash drums are installed downstream the reactor to recycle air and part of the solvent to obtain a minimum distillation column input. Operation conditions of the flash separators are 70°C and 3 bar, and 131°C and 2.5 bar, respectively.

12 stages were estimated for the separation at the distillation column. Due to the low fraction of heavy components in the feed stream of the column, the top tray was chosen as feed stage. The pressure was determined at 2 bar, reflux ratio was set to 1.1 and the distillate rate was varied to obtain a mole purity of 0.01 m% in bottoms.

Figure 18 shows temperature profile and mass fractions of each stage. The stage above the bottom stage contains 21 wt% FDCA in the liquid phase at a temperature of 219°C. As a result, FDCA would crystallize in that stage.

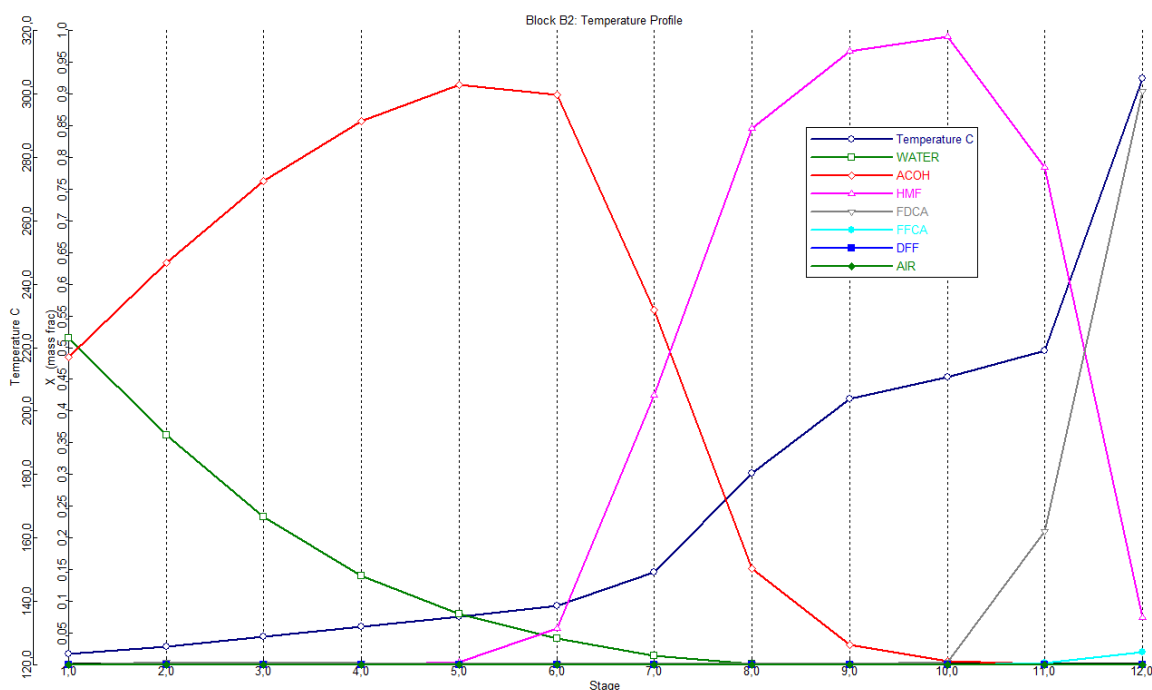


Figure 18: Temperature and liquid mass fraction profiles of the distillation column for removing FDCA

Adding heat streams and varying operating conditions (changing number of stages, reflux ratio, pressure, input concentrations etc.) have not improved results. At the bottom stage the reboiler is vaporizing flow stream and the equilibrium leads to a temperature of 219°C in the 11th stage. The concentration of FDCA is high in the stage above the reboiler, because it is condensing in that tray due to its high boiling point.

Due to the low boiling points of water and acetic acid in comparison to the melting point of FDCA, a distillation column could not be used for separating FDCA from the water/acetic acid solvent, because temperatures in the trays are too low, which leads to crystallization of FDCA in the distillation column.

First estimations show that separation of FDCA from water and acetic acid could not be obtained in a distillation column due to low temperature profile in the trays. Crystallization or the introduction of a new solvent with a high boiling point could lead to desired results. Therefore, processes were designed using crystallization or distillation for removing FDCA, where at latter an extractor is used for introducing a new solvent.

3.3 Flowsheet design

HMF, FDCA, FFCA and DFF are not included in Aspen database. Therefore, physical properties have to be estimated based on given boiling points, molecular weights and molecular structures of these substances. Also the melting points are specified to calculate crystallization.

The RStoic-reactor in Aspen Plus was chosen to model the processes. Input data for the RStoic reactor are stoichiometric reactions, operating temperature and pressure in the reactor and fractional conversions. According to the patent of Lilga et al., air and a feed solution with 0.5 wt% of HMF are streaming through a tubular reactor with an embedded 5 wt% Pt/ZrO₂ catalyst [17].

Operating conditions in the reactor are according to the US patent 100°C and 10 bar. The feed solution of the reactor in Aspen Plus simulation has a ratio of water/acetic acid of 60/40. The weight concentrations of the feed stream are 0.5 wt% HMF, 59.7 wt% water and 39.8 wt% acetic acid. Air is selected as

oxidant with a flow rate calculated based on the patent, which declines a volume ratio of air to feed flow in the reactor of 100/1 [17].

Figure 19 shows the process flow sheet of the reactor with two flash separators for recycling air and part of the solvent. Operating conditions of feed stream F and air flow A1 are ambient conditions, 25°C and 1 atm. The pressure of feed stream F is increased by a pump to 10 bar, which matches reactor conditions. A compressor is installed upstream the reactor to accomplish air pressure of 10 bar.

Downstream the reactor a flash drum is installed for separating gaseous from liquid phase. The gaseous phase contains water, acetic acid and air. To separate latter from rest, another flash separator is installed. Due to lower oxygen concentration compared to ambient air, a part of the recycled air is emitted (stream 7) and fresh air is sucked into the compressor (stream A1). The liquid phase of the second flash separator (stream 6) containing water and acetic acid is mixed with the feed stream and led into the pump. Pressures in the flash separators are 9.5 bar and 9 bar, respectively, to minimize pressure losses in the recycling stream.

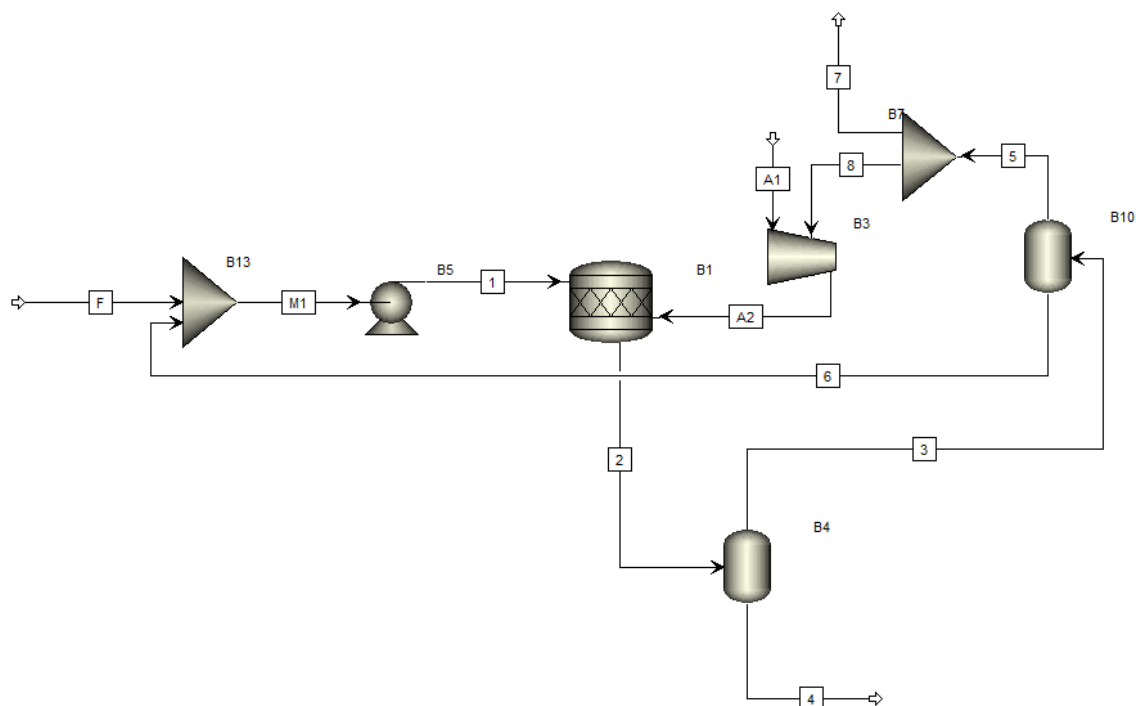


Figure 19: Flowsheet of HMF conversion to FDCA with air and fractional solvent recycle flows

The yields of the HMF conversion in the tubular reactor are in compliance with Lilga et al. 90 wt% FDCA, 2 wt% FFCA, and 0.05 wt% DFF. According to the patent the yield of FDCA is about 98 wt%, but using aqueous acetic acid as solvent decreases the selectivity [17]. Due to the huge ratio of air to HMF, air is reacting at a part with HMF. As mentioned above, FDCA is fully soluble in the solvent.

3.3.1 Process using crystallization

For removing FDCA, a crystallizer is installed downstream the flash drum B4 to obtain solid FDCA, which could be separated from the solvent by solid-liquid separation (Figure 20).

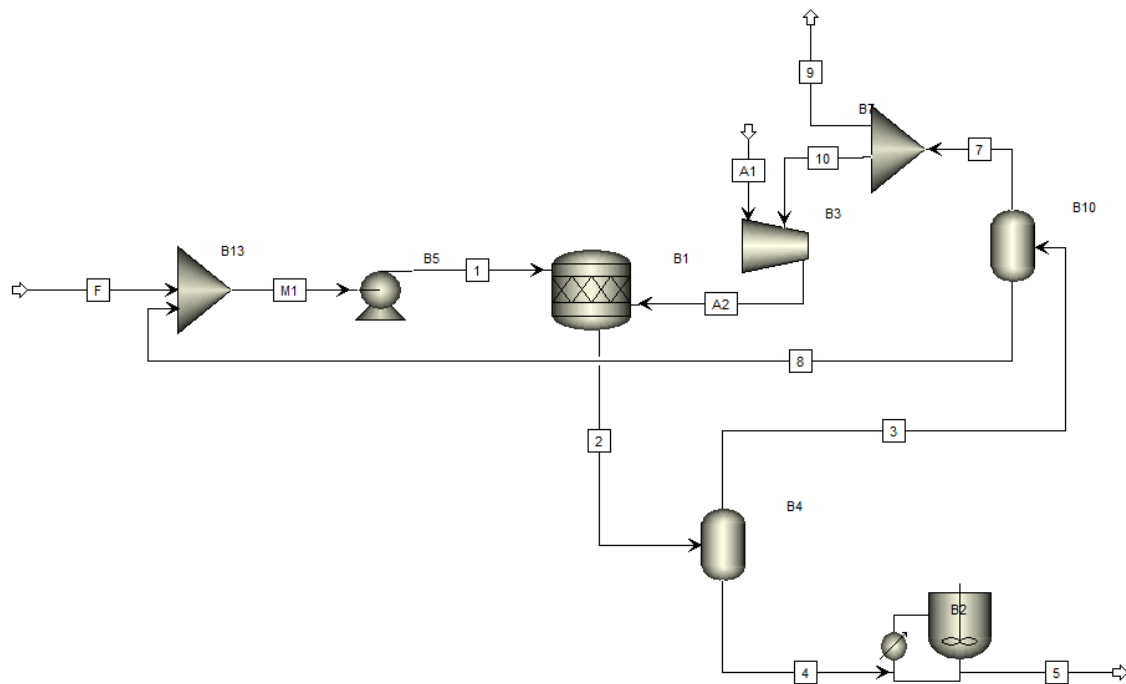


Figure 20: Flowsheet of HMF conversion to FDCA using a crystallizer for obtaining solid FDCA

Therefore, FDCA has to be specified as a solid component and the solute form of FDCA, FDCA^{2-} , has to be given in the simulation (Figure 21).

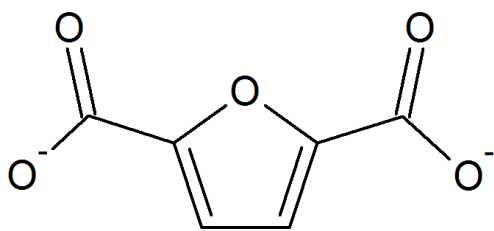


Figure 21: Molecular structure of the FDCA ion, FDCA^{2-}

Components set for the simulations using crystallization are shown in Figure 22.

Component ID	Type	Component name	Alias
▶ WATER	Conventional	WATER	H2O
ACOH	Conventional	ACETIC-ACID	C2H4O2-1
HMF	Conventional		
FDCA	Solid		
FFCA	Conventional		
DFF	Conventional		
FDCA2-	Conventional		
H+	Conventional	H+	H+
OH-	Conventional	OH-	OH-
N2	Conventional	NITROGEN	N2
O2	Conventional	OXYGEN	O2
*			

Figure 22: Specified components for simulations using a crystallizer

H^+ and OH^- have to be specified for crystallization of FDCA in an aqueous solution.

The component “Crystallizer” at Aspen Plus is simulating a mixed-suspension, mixed-product-removal (MSMPR) crystallizer, at which the mother liquor in the product stream is saturated. Feed of the crystallizer is mixed with the recycled flow of the crystallizer, streams a heat exchanger for manipulating temperature and is fed into the crystallizer. The specified component is crystallizing according to the defined saturation calculation method. For this purpose the solubility or the chemical reactions of the component has to be specified (Figure 23). Operating conditions are 25°C and 2.5 bar for economic reasons. Size of the crystallizer is determined at 10 m^3 .

Figure 23: Operating conditions and saturation calculation method for simulated MSMPR crystallizer

Choosing the saturation calculation method “solubility”, the stoichiometry of the reactants and the crystal product have to be specified. Latter has to have the form CIPSD (conventional solid substream with particle size distribution), which means that the particle size distribution is given or calculated to simulate solid-liquid separation (Figure 24). Accordingly the stream class MIXCIPSD is chosen, which requires solid particles with given particle size distribution.

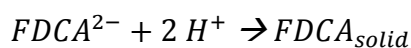
Component	Coefficient
FDCA2-	-1
H+	-2
*	

Crystal product: FDCA (CIPSD)
Coefficient: 1

Stoichiometry:
FDCA2- + 2 H+ -> FDCA(Cipsd)

Figure 24: Stoichiometric reaction for simulated MSMPR crystallizer

The stoichiometry of the crystallization of FDCA is as follows:



For estimating solubility, data of the US patent of Lilga et al. is used [17]. As shown in Figure 25, the solubility of FDCA in a 60/40 water/acetic acid solution at 25°C and 70°C are entered and water is specified as solvent.

Screenshot of the Solubility specifications dialog box. The 'Solubility basis' section has 'Solvent' selected with 'WATER' in the dropdown. The 'Solubility data' section has 'Concentration' selected for the data type. A table shows data for temperatures 70 and 25, with concentrations 7.79 and 1.53 kg/cum respectively.

Solubility data type:	Temperature	Concentration
Concentration	C	kg/cum
	70	7.79
	25	1.53
	*	

Figure 25: Solubility specifications for simulated MSMR crystallizer

For calculating crystallization, solid heat capacity of FDCA has to be estimated. For this purpose the atomic element contribution method of Hurst and Harrison is used (Figure 26) [28].

Screenshot of the 'Conventional Component Additional Data' dialog box. The dialog is open over a 'Define components' table. The table lists components like WATER, ACOH, HMF, FDCA, FFFCA, DFF, FDCA2-, H+, OH-, N2, O2, and an asterisk. The dialog box has five numbered buttons: 1. Liquid volume, 2. Vapor pressure data, 3. Extended Antoine vapor pressure coefficients, 4. Ideal gas heat capacity data (selected), and 5. Ideal gas heat capacity polynomial coefficients. There are also radio buttons for 'Evaluate using TDE' and 'Estimate using Aspen Plus property estimate system'.

Component ID	Type	Component name	Alias
WATER	Conventional	WATER	H2O
ACOH	Conventional	ACETIC-ACID	C2H
HMF	Conventional		
FDCA	Solid		
FFCA	Conventional		
DFF	Conventional		
FDCA2-	Conventional		
H+	Conventional	H+	H+
OH-	Conventional	OH-	OH-
N2	Conventional	NITROGEN	N2
O2	Conventional	OXYGEN	O2
*			

Figure 26: Input box for ideal gas heat capacity data of FDCA²⁻

For calculating charge balance, standard heat of formation for gas phase (Figure 27) and aqueous heat of formation at infinite dilution of FDCA^{2-} (DHAFQM in Figure 28) have to be specified. Former is given in the NIST database and set at user defined components specifications [29]. Latter is entered at the path “Properties – Parameters – Pure Component – USRDEF” and is calculated using following estimated equation:

$$\Delta H_{\text{aqu}}^{\infty} = f \Delta H_{\text{gas}}^0 \cdot 1.2 \quad 3-1$$

where H_{aqu}^{∞} is the aqueous heat of formation at infinite dilution and $f \Delta H_{\text{gas}}^0$ is the standard heat of formation for gas phase.

This equation is developed by calculating the ratio of the aqueous heat of formation at infinite dilution and the standard heat of formation for gas phase of OH^- , terephthalic acid and acetic acid. All of them have a similar ratio of approximately 1.2.

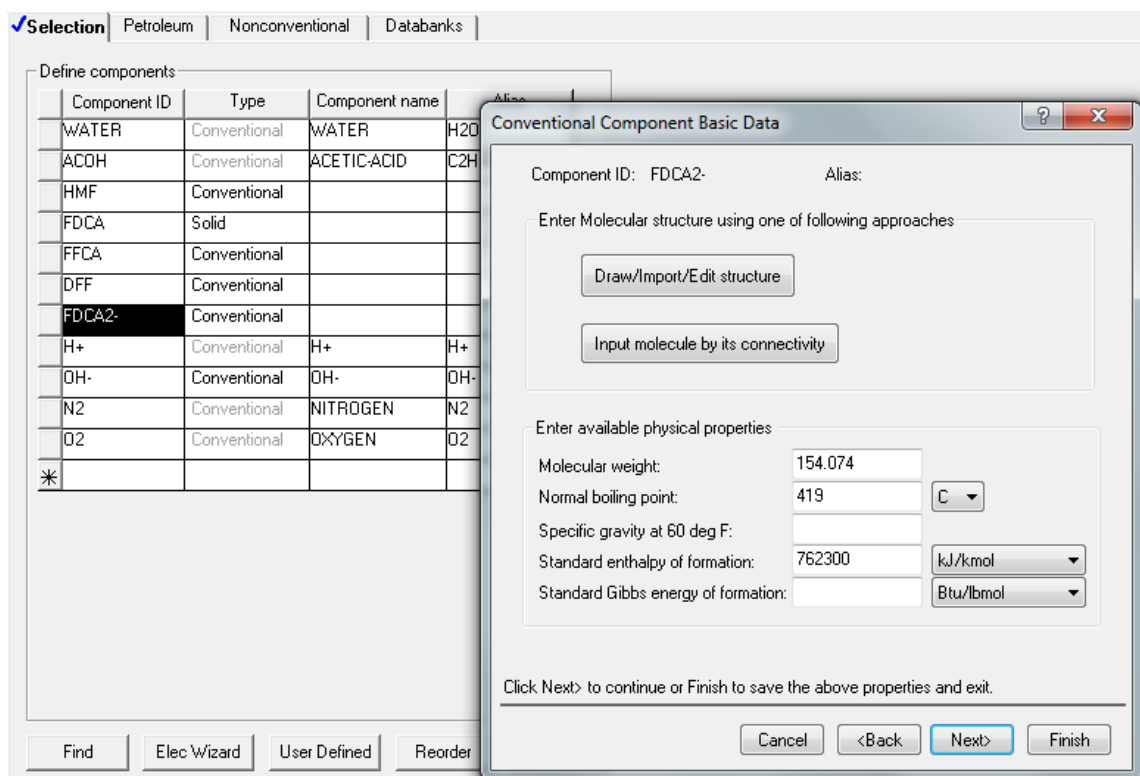


Figure 27: Estimated physical properties of FDCA^{2-}

Input									
Pure component scalar parameters									
Parameters	Units	Data set	Component	Component	Component	Component	Component	Component	Component
			HMF	FDCA	FFCA	DFF	FDCA2-		
TB	C	1	291	419,2	356,9	276,8	419		
MW		1	126,11	156,09	140,09	124,09	154,074		
TFP	C	1	32	342	209	110	342		
CHARGE		1					-2		
DHFORM	kJ/kmol	1					762300		
DHAQFM	kJ/kmol	1					900000		
*									

Figure 28: Estimated parameters for unknown components

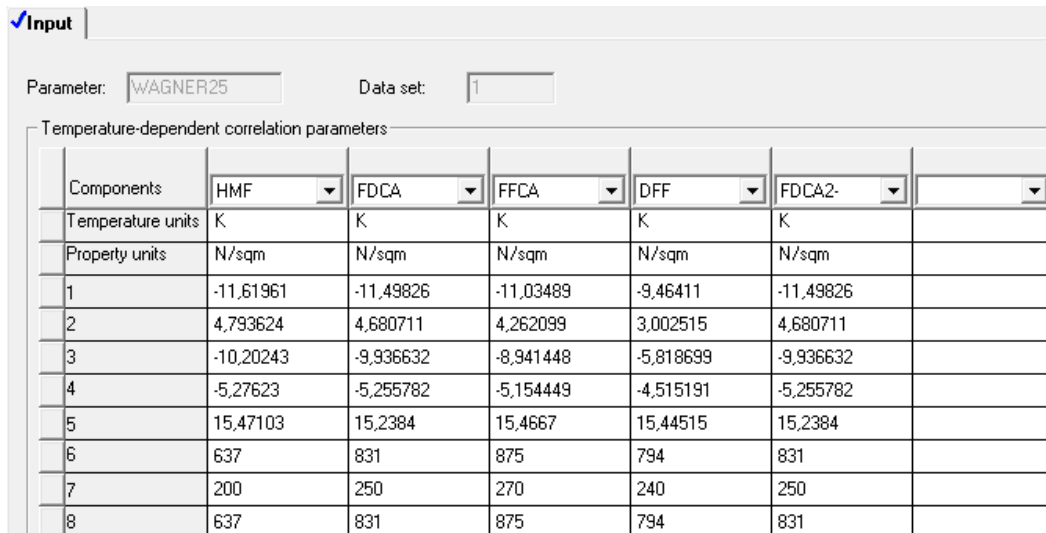
Particle size distribution at the crystallizer is estimated in accordance with the standardized normal distribution as follows:

Table 3: Particle size distribution at crystallizer

Particle size [μm]	Distribution [%]
0 – 20	2
20 – 40	4
40 – 60	9
60 – 80	15
80 – 100	20
100 – 120	20
120 – 140	15
140 – 160	9
160 – 180	4
180 – 200	2

For simulating the processes using crystallization, the property method ELECNRTL (Electrolyte-NRTL) was chosen, because it is the most versatile property method for electrolyte systems, used for aqueous and mixed solvent systems. ELECNRTL is based on NRTL-RK, modeling molecular interactions identically. NRTL-RK models liquid phase using NRTL property method and estimates liquid molar volume by using Rackett model. The solubility of supercritical gases is calculated by Henry's Law. For modeling vapor phase properties, Redlich-Kwong equation of state is used. Required parameters are provided by Aspen database, at which missing parameters are estimated or entered at the path "Properties – Advanced – Tabpoly". The only parameter that has to be specified at the crystallization processes is the solid volume of FDCA.

Due to a wrong calculated vapor pressure of FDCA using WAGN25 parameters, these values have to be deleted for FDCA²⁻ at the path “Properties – Parameters – Pure Component – WAGN25-1” (Figure 29).




Parameter: Data set:

Temperature-dependent correlation parameters

Components	HMF	FDCA	FFCA	DFF	FDCA2-	
Temperature units	K	K	K	K	K	
Property units	N/sqm	N/sqm	N/sqm	N/sqm	N/sqm	
1	-11,61961	-11,49826	-11,03489	-9,46411	-11,49826	
2	4,793624	4,680711	4,262099	3,002515	4,680711	
3	-10,20243	-9,936632	-8,941448	-5,818699	-9,936632	
4	-5,27623	-5,255782	-5,154449	-4,515191	-5,255782	
5	15,47103	15,2384	15,4667	15,44515	15,2384	
6	637	831	875	794	831	
7	200	250	270	240	250	
8	637	831	875	794	831	

Figure 29: Estimated Wagner parameters of defined molecules

For estimating all missing parameter, “Estimate all missing parameters” at the path “Properties – Estimation – Input” has to be selected.



Setup | Pure Component | T-Dependent | Binary | UNIFAC Group

Estimation options

Do not estimate any parameters

Estimate all missing parameters

Estimate only the selected parameters

Parameter types

Pure component scalar parameters

Pure component temperature-dependent property correlation parameters

Binary interaction parameters

UNIFAC group parameters

Figure 30: Estimation options for missing parameters

The bonds of FDCA²⁻ have to be calculated at the path “Properties – Molecular Structure – FDCA2- – Structure” (Figure 31).

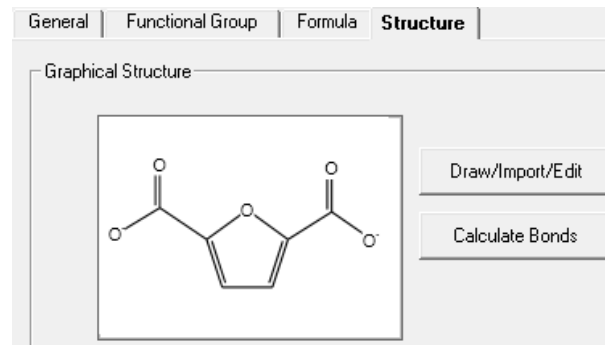


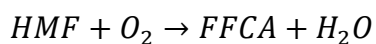
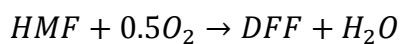
Figure 31: Structure sheet of FDCA²⁻

For separating solid FDCA from the solvent, a hydrocyclone or a filter is installed, depending on the requirement of the product stream.

3.3.1.1 Centrifugation

One opportunity for separating solid FDCA from the aqueous solvent is to install a hydrocyclone downstream the crystallizer. For simulation the component “HyCyc” at Aspen Plus is used to obtain the solid enriched product stream P. The overflow of the hydrocyclone is recycled and mixed with the feed stream F and the liquid recycling stream 8 of the flash separator B10 (Figure 32).

At the reactor, following stoichiometric reactions are given:



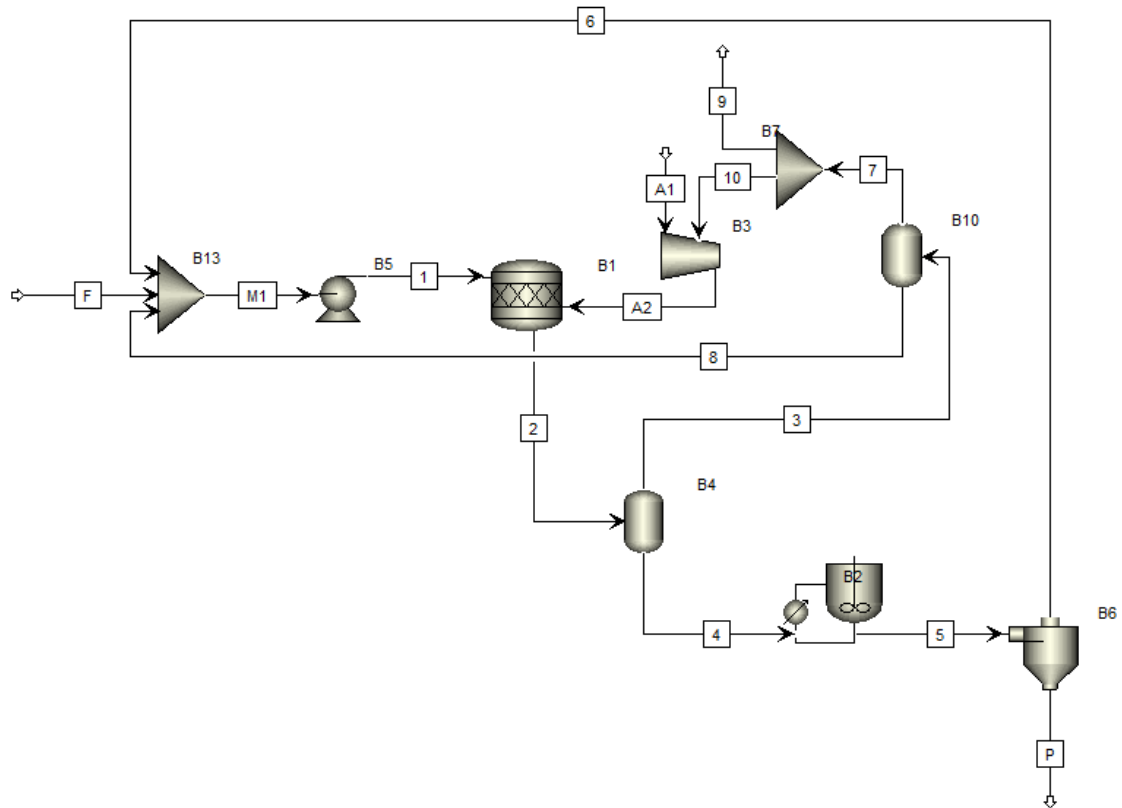


Figure 32: Flowsheet of HMF conversion to FDCA using a crystallizer and a hydrocyclone for separating solid FDCA from aqueous solvent

The hydrocyclone is separating solids from liquids due to centrifugal force of the liquid vortex. There are two different options at Aspen Plus to simulate the hydrocyclone, namely simulation mode and design mode. The hydrocyclone models in simulation mode the particle size that is separated at an efficiency of 50 % at a given diameter of the hydrocyclone. In design mode, dimensions of the hydrocyclone are calculated according to specified diameter of the particles, separation efficiency, maximum diameter, maximum pressure drop and density of the solid particles. [30]

For the process producing solid FDCA, the hydrocyclone is modeled in the design mode, at which the estimated diameter of the particles is 100 μm , the separation efficiency is set to 95 % and the density of the solid particles is given according to literature at 1.604 g/cm^3 [31]. Maximum diameter and pressure drop are determined at 4 m and 0.2 bar, respectively.

The image shows a software interface with four tabs: 'Specifications' (selected), 'Dimensions', 'Velocity Correlation', and 'Efficiency'. The 'Specifications' tab contains the following settings:

- Calculation mode:** Mode is set to 'Design' and Efficiency correlation is set to 'Built-in'.
- Design parameters:**
 - Diameter of solid particles: 100 (unit: mu)
 - Separation efficiency: 0,9
 - Maximum diameter: 4 (unit: meter)
 - Maximum pressure drop: 0,2 (unit: bar)
- Optional:** Density of solid particles: 1,604 (unit: gm/cc)

Figure 33: Specifications at hydrocyclone for separating FDCA from solvent

3.3.1.2 Filtration

Another possibility for separating FDCA from liquid is to install a filter. The component “Filter” at Aspen Plus is simulating rotary vacuum filters, whose can be modeled in a similar way as the hydrocyclone in simulation mode or design mode. The product streams of the filter are a solid filter cake, which is defined in the simulation as product stream P, and the filtrate 6, which is recycled to the reactor (Figure 34). Since water is formed at the reactor, a flash separator has to be installed downstream the filter to vaporize water and other volatile components.

Specifications		Filter Cake
Calculation options		
Mode:	Design	
Design parameters		
Maximum pressure drop:	0,5	bar
Width to diameter ratio:	2	
Operating conditions and parameters		
Rate of revolution:	60	Hz
Angle of filtration:	2,0945	rad
Filter medium resistance:		1/meter

Figure 35: Specifications at filter for separating FDCA from solvent

The mass fraction of solid FDCA in the filter cake is specified at 98 wt% to yield almost pure FDCA.

Specifications		Filter Cake
Filter cake specifications		
Filtration resistance:		meter/kg
Specific cake resistance:	2000000	meter/kg
Compressibility:	0	
Porosity:	0,45	
Solid particles in filter cake		
Mass fraction:	0,98	
Average sphericity:	0,75	
Average diameter:		meter

Figure 36: Settings of the filter cake for separating FDCA from solvent

3.3.2 Process using distillation

As shown in chapter 3.2, a distillation column can not separate FDCA from water and acetic acid due to comparatively low boiling points of the latter. For this reason trioctylamine is introduced as a new solvent downstream the flash separator B4 in the 4 stages liquid-liquid extractor B6 at 4 bar (Figure 37). Trioctylamine and water are specified as key components at the adiabatic extractor. The mole ratio of trioctylamine to water plus acetic acid is approximately 1/1. Literature affirm high solubility of organic acids in trioctylamine [32-36].

Density: 0.805 - 0.815 g/cm³

Solubility in water: insoluble [37]

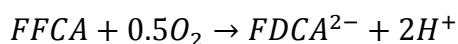
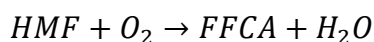
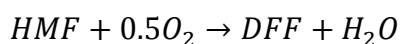
Price: 4800 - 5000 \$/t [38]

Triethylamine is used as a solvent and an intermediate in the manufacture of pharmaceuticals, quaternary ammonium compounds, agrochemicals, surfactants, lubricant additives, corrosion inhibitors, vulcanization accelerators and dyes.

3.3.2.2 Process specifications

For simulating liquid-liquid extraction, Soave-Redlich-Kwong (SRK) property method was chosen, because it is used for estimating water-hydrocarbon immiscibilities, using Kabadi-Danner mixing rules. Residual process is modeled by NRTL property method, which can be used for both, ideal and non-ideal chemical systems. NRTL property method models liquid phase by using NRTL activity coefficient and vapor phase by using ideal gas equation of state. Liquid molar volume is calculated by Rackett model. [30]

The water and acetic acid rich liquid phase is mixed with the feed stream F and recycled to the reactor (streams 16, 18 and 19). A part of the recycling stream has to be removed using a splitter (stream 17) to comply with mass balance, because water is formed in the reactor. In a similar way as in the process using crystallization and filtration, FFCA and DFF are recycled in large part and have to be fractional converted in the reactor to FDCA. In this scenario, conversion of FFCA and DFF to FDCA is also set to 10 %, respectively. Hence, following stoichiometric reactions are estimated at the reactor:



To minimize input of the first distillation column, the trioctylamine and FDCA-rich liquid phase (stream 5) is fed to a flash separator to evaporize water and acetic acid at 300°C and 3.5 bar.

The first distillation column separates FDCA from trioctylamine to produce FDCA at a purity of 97 wt% (product stream P). Due to high trioctylamine to FDCA ratio, the bottom stream is small relating to the feed stream of the distillation column. Therefore the feed stage is set to the top tray. Due to economic reasons, reflux ratio is estimated to be 0.1 and the number of stages is set to 17 at a pressure of 3 bar (Figure 39). Distillate to feed ratio is varied using a design specification to get a FDCA concentration of 97 wt% in bottoms. A total condenser is estimated and both distillate and bottoms phases are defined as liquid streams.

Configuration | Streams | Pressure | Condenser | Thermosiphon Co

Setup options

Calculation type: Equilibrium

Number of stages: 14 Stage wizard

Condenser: Total

Reboiler: Kettle

Valid phases: Vapor-Liquid

Convergence: Standard

Operating specifications

Reflux ratio: Mole 0,2

Distillate to feed ratio: Mole 0,9

Free water reflux ratio: Feed basis

Figure 39: Settings at first column for separating FDCA from solvent

The distillate of the first column is mixed with the liquid phase of the flash separator B7 and fed to the second distillation column, where trioctylamine is separated from water and acetic acid. The number of stages is set to 9 at a reflux ratio of 0.6, at which the 7th stage is specified as the feed stage (Figure 40). Distillate to feed ratio is varied using a design specification to get a mass flow of trioctylamine of 0.001 kg/s in the distillate. A total condenser is used at this distillation column and liquid distillate and bottoms are specified. The pressure of the second distillation column is estimated to be 2.5 bar.

Configuration | Streams | Pressure | Condenser | Thermosiphon Co

Setup options:

Calculation type: Equilibrium

Number of stages: 12 Stage wizard

Condenser: Total

Reboiler: Kettle

Valid phases: Vapor-Liquid

Convergence: Standard

Operating specifications:

Reflux ratio: Mole 0,8

Distillate to feed ratio: Mole 0,2055

Free water reflux ratio: Feed basis

Figure 40: Settings at second column for separating acetic acid and water from trioctylamine

The distillate containing water and acetic acid is recycled and mixed with the recycle stream of flash separator B9 and the water-rich phase of the liquid-liquid extractor to minimize feed stream of the reactor. The bottoms consisting of trioctylamine and FDCA is cooled down in a heat exchanger at 2.5 bar to 50°C and mixed with the pure trioctylamine inlet stream 12 to compensate the loss of the solvent due to its fraction in the bottoms of the first distillation column. The pressure of the trioctylamine recycling stream 14 is increased to 4 bar, which is fed into the liquid-liquid extractor.

4 Economic Analysis

Economic analysis of the process flowsheets is performed using Aspen Process Economic Analyzer [2]. This program calculates the total costs of the simulated plant over a specified period, consisting of capital costs and operating costs. Based on the results, the minimum sale price of the produced FDCA is estimated.

4.1 Capital costs

Capital costs imply all non-variable costs expended before startup and are split into direct costs and indirect costs. Former include all expenses to construct facility, such as costs for equipment, equipment installation, instrumentation and control, piping, electrical equipment and materials, process and auxiliary buildings, maintenance shops, building services, utilities, facilities, non-process equipment, and distribution and packaging. Indirect costs imply engineering and supervision expenses, construction costs, contractor's fees, and contingency. [39]

4.2 Operating costs

Operating costs include all fees for failure-free running processes, split into manufacturing costs and general expenses. Manufacturing costs imply expenses for raw materials, utilities, maintenance and repairs, operating supplies, operating labor, direct supervision and clerical labor, laboratory charges, patents and royalties, depreciation, local taxes, insurance, rent interest, and plant upkeep and overhead. General expenses consist of administrative costs, distribution and selling expenses, and research and development costs. [39]

4.3 Economic assumptions

To estimate the minimum sale price of FDCA, assumptions for the costs have to be made. The plants are assumed to operate in a continuous steady state mode for 8000 hours per year. The assessed payback time and lifetime of the plants are 20 years. The tax rate is set to 30 % and the assumed salvage value is 10 % of the initial capital cost. For depreciation method, straight line model is chosen. The assessed annual escalation is 3.5 % and the desired rate of return is set to 15 % per year.

For estimating the minimum sale price of FDCA, no profit is assumed. Since no byproducts are produced in the processes, the sale price of FDCA has to cover all costs, including total capital expenses and total operating costs.

In accordance with economic analysis of Kazi et al. [4], price of HMF is assumed at 1070 \$/t. Market price of trioctylamine and acetic acid are listed at 5000 \$/t [38] and 550 \$/t [40], respectively. Price of water as solvent and oxygen as oxidant are assumed at 0.1 \$/t and 250 \$/t, respectively.

For Pt/ZrO₂ catalyst, acquisition price of \$35 million is estimated based on the patent of Lilga et al. [17] and the market price of Pt/Al₂O₃ [41], assuming that Pt/Zr₂O₃ has a similar price compared to Pt/Al₂O₃ due to the high cost of Pt compared to the cost of the support material. Additional annual cost of \$100 T for recycling the catalyst is added [4]. Sensitivity analysis shows the impact of the catalyst cost on the minimum sale price of FDCA.

5 Results

5.1 Process simulation using crystallization

5.1.1 Process simulation using centrifugation

Figure 32 shows the process using crystallization for producing solid FDCA and downstream separation of solid particles from the solvent by a hydrocyclone. Feed stream of the process is estimated to gain input concentrations of the reactor according to the US patent of Lilga et al. (Table 4) [17]. Due to the low FDCA fraction in the product stream of approximately 3 wt%, high solvent input in comparison to the HMF feed is required for the process.

Table 4: Flow rate and mass fractions of feed stream of the process with the hydrocyclone

Component	Mass fraction Feed Stream F [wt%]
Water	53.6
Acetic acid	42.5
HMF	2.9
Total [t/d]	374

200.3 t/d water, 162.6 t/d acetic acid, 10.72 t/d HMF and 4313 m³/h air are required for the simulated process. In accordance with Lilga et al., the inputs of the reactor are shown in Table 5, in which, due to the low concentration, FDCA should be solute in a real process [17]. Calculated heat duty of the reactor is 4.28 MW and outlet vapor fraction is 35.88 %.

Table 5: Fractions and flow rates of reactor inputs at the process with the hydrocyclone

Component Liquid phase	Mass fraction	Mole fraction
	Feed Stream 1 [wt%]	Air Stream A2 [m%]
Water	59.19	0.228
Acetic acid	38.81	0.022
HMF	0.525	2.0e-9
FFCA	0.030	0
DFF	6.7e-4	0
FDCA ²⁻	0.036	0
H ⁺	4.7e-4	0
N ₂	0.841	81.02
O ₂	0.567	18.73
Solid FDCA	2.31 t/d	0 t/d
Total	2169 t/d	222944 m³/d

After removing air and part of the solvent by a flash separator, product stream 4 of the reactor is fed to the crystallizer at 150°C and 9.5 bar containing 54.58 wt% water, 44.02 wt% acetic acid and 1.01 wt% solute FDCA (Table 6).

Table 6: Mass fractions and flow rate of crystallizer input at the process with the hydrocyclone

Component Liquid phase	Mass fraction Stream 4 [wt%]
Water	54.58
Acetic acid	44.02
HMF	0.066
FFCA	0.068
DFF	1.5e-3
FDCA ²⁻	1.010
H ⁺	0.013
N ₂	0.149
O ₂	0.084
Solid FDCA [t/d]	2.31
Total [t/d]	1320

Linear extrapolation of Table 2 leads to a solubility of FDCA of 1.9 wt% at 150°C and 1 atm. Due to the low pressure dependence of the solubility of solids, FDCA should be completely soluble in the feed stream of the crystallizer in a real process, despite the high pressure of 9.5 bar [28].

In the next step, FDCA is crystallized at 25°C and 2.5 bar, obtaining a solid fraction in the product stream of the crystallizer of 1.11 wt%. The mass fraction of the liquid phase and the yield of solid FDCA are shown in Table 7, in which, due to crystallized FDCA, slight changes of the mass fractions in the liquid phase occur compared to the input of the crystallizer.

At a determined volume of the crystallizer of 10 m³, a residence time of 11 min is calculated, obtaining 14.7 t/d crystallized FDCA (Table 7). The estimated cooling duty of the crystallizer is 6.64 MW at a temperature of 25°C.

Table 7: Mass fractions and flow rate of crystallizer output at the process with the hydrocyclone

Component	Mass fraction
Liquid phase	Stream 5 [wt%]
Water	55.10
Acetic acid	44.44
HMF	0.066
FFCA	0.069
DFF	1.5e-3
FDCA ²⁻	0.084
H ⁺	1.1e-3
N ₂	0.151
O ₂	0.084
Solid FDCA [t/d]	14.69
Total [t/d]	1320

The product stream of the crystallizer is fed into the hydrocyclone to get a product stream containing 3.27 wt% solid FDCA at 14.3°C and 2.32 bar (Table 8).

Table 8: Overflow and underflow of the hydrocyclone

Hydrocyclone	Overflow	Underflow
Solid FDCA [t/d]	2.31	12.37
Total [t/d]	942	378
Solid fraction [wt%]	0.25	3.27

For the defined separation efficiency of 95 %, 8 hydrocyclones are estimated with a liquid volumetric flow rate of 6.72 m³/h per cyclone and a pressure drop of 0.178 bar. Dimensions of the hydrocyclones are as follow:

Table 9: Dimensions of the hydrocyclones

Dimension	[m]
Length of cylinder	1.077
Diameter of cylinder	0.215
Diameter of inlet	0.031
Diameter of overflow	0.043
Diameter of underflow	0.032

The overflow of the hydrocyclone is recycled, mixed with the feed stream F and the recycling stream 8 and led to pump B5. The input of the pump contains 0.143 wt% FDCA, which should be solute in large part at the estimated temperature of 19°C. Attention at pump design should be paid on the vapor fraction of the pump input, which is 0.86 %. Calculated required net work of the pump is 244.16 kW at a pump efficiency of 84.69 %. Estimated volumetric flow rate of the pump is 828.3 m³/h.

The underflow of the hydrocyclone comprises 53.30 wt% water, 42.99 wt% acetic acid and 3.27 wt% solid FDCA at a mass flow of solid FDCA of 12.37 t/d and could be used for downstream processes those require water and acetic acid for FDCA conversion. For economic reasons, acetic acid should be recycled and mixed with the feed stream of the reactor. The overall yield of FDCA in reference to the HMF conversion is 93.21 %.

As shown in Table 10, the vapor phase of the first flash separator B4 comprises 53.85 m% air, 40.54 m% water and 5.613 m% acetic acid. Estimated heat duty of the flash separator is 17.66 MW.

Table 10: Mass fractions and flow rate of vapor phase of flash separator B4 at the process with the hydrocyclone

Component	Mole fraction Stream 3 [m%]
Water	40.54
Acetic acid	5.613
HMF	3.6e-4
FFCA	3.5e-7
DFF	5.3e-7
FDCA ²⁻	0
H ⁺	0
N ₂	43.64
O ₂	10.21
Total [m³/d]	282161

Air is separated from water and acetic acid in the flash separator B10 at a cooling duty of 20.95 MW and recycled at 9 bar to the compressor, at which 10 % of the flow stream have to be removed due to the lower oxygen concentration of 18.47 m% in the recycled airstream compared to ambient air. Mass fraction of the liquid phase and molar fraction of the vapor phase of flash separator B10 are shown in Table 11. Mass fraction of water in stream 8 is higher than in feed stream F due to the higher volatility of water in comparison to acetic acid.

Table 11: Mass fraction of liquid phase and mole fraction of vapor phase of flash separator B10 at the process with the hydrocyclone

Component	Mole fraction Stream 7 [m%]	Mass fraction Stream 8 [wt%]
Water	0.254	66.13
Acetic acid	0.025	30.55
HMF	2.3e-9	4.2e-3
FFCA	0	4.5e-6
DFF	0	5.9e-6
FDCA ²⁻	0	0
H ⁺	0	0
N ₂	81.25	0.020
O ₂	18.47	0.013
Total	110710 m³/d	854 t/d

Approximately 90 wt% of the air stream are recycled to the compressor at a pressure loss of 1 bar. The estimated net work of the compressor is 5.65 MW at

an efficiency of 80 % and an outlet temperature of 378.14°C. Mechanical efficiency is set to 90 %.

5.1.2 Process simulation using filtration

As shown in Figure 34, a crystallizer is installed downstream the reactor to obtain solid FDCA, which is removed by filtration. For achieving the same input fractions as mentioned in the patent of Lilga et al., following flow stream and mass fractions of the process feed stream F are determined [17]:

Table 12: Flow rate and mass fractions of feed stream of the process with the filter

Component	Mass fraction Feed Stream F [wt%]
Water	0
Acetic acid	6.20
HMF	93.8
Total [t/d]	11.1

Water is not required, because it is recycled in the process and losses are compensated by the formed water in the reactor. The acetic acid demand is low due to the recycling streams. 0.69 t/d acetic acid, 10.38 t/d HMF and 4842 m³/h air are required for the estimated process.

Feed streams of the reactor are shown in Table 13. Fractions and volume liquid to air ratio are in accordance with the patent of Lilga et al. [17].

Table 13: Fractions and flow rates of reactor inputs at the process with the filter

Component	Mass fraction Feed Stream 1 [wt%]	Mole fraction Air Stream A2 [m%]
Water	59.19	0.228
Acetic acid	38.68	0.022
HMF	0.505	2.1e-9
FFCA	0.112	0
DFF	2.5e-3	0
FDCA ²⁻	0.047	0
H ⁺	6.2e-4	0
N ₂	0.862	80.78
O ₂	0.606	18.97
Total	2233 t/d	249433 m³/d

There are no solid particles in the inputs of the reactor. The estimated net heat duty is 513.54 kW, which is approximately 8 times smaller than the net heat duty of the reactor in the process using centrifugation for separating FDCA from the solvent. In both simulations, the total mass flows and fractions are approximately the same, but the temperatures of the stream 1 are different in the process with the hydrocyclone and in the process with the filter, namely 22.2°C and 71.7°C, respectively.

The estimated outlet vapor fraction of the reactor is 37.9 %, which is approximately the same as in the process using centrifugation for removing FDCA.

In the product stream of the reactor, air and part of the solvent are removed using a flash separator, at which the liquid phase is fed to the crystallizer at 150°C and 9.5 bar, containing 54.14 wt% water, 44.28 wt% acetic acid and 1.07 wt% solute FDCA (Table 14).

Considering the linear extrapolation of Table 2 and the weak dependence of the solubility of solids in liquids, FDCA is completely soluble in the input of the crystallizer [28].

Table 14: Mass fractions and flow rate of crystallizer input at the process with the filter

Component	Mass fraction Stream 4 [wt%]
Water	54.14
Acetic acid	44.28
HMF	0.067
FFCA	0.195
DFF	4.3e-3
FDCA ²⁻	1.070
H ⁺	0.014
N ₂	0.148
O ₂	0.084
Total [t/d]	1284

FDCA is crystallized at 25°C and 2.5 bar, obtaining 1 wt% solid FDCA in the product stream of the crystallizer. As shown in Table 15, the mass fractions of the liquid phase changed due to the lower fraction of solute FDCA.

Table 15: Mass fractions and flow rate of crystallizer output at the process with the filter

Component Liquid phase	Mass fraction Stream 5 [wt%]
Water	54.68
Acetic acid	44.73
HMF	0.067
FFCA	0.197
DFF	4.4e-3
FDCA ²⁻	0.083
H ⁺	1.1e-3
N ₂	0.149
O ₂	0.085
Solid FDCA [t/d]	12.85
Total [t/d]	1284

At the crystallizer, 12.85 t/d solid FDCA are formed at a determined volume of the crystallizer of 10 m³ and an estimated residence time of 11 min, which is the same as in the process with the hydrocyclone. The calculated cooling duty is approximately 6.5 MW, which is comparable to the cooling duty of the crystallizer at the process with the hydrocyclone.

Solid FDCA is removed from the product stream of the crystallizer using filtration at a calculated volume flow rate of the filtrate of 52.3 m³/h. The mass fraction of solids in the filter cake is 98 % at an estimated cake thickness of 1.97 mm. The calculated filter diameter and width are 1.5 cm and 3 cm, respectively.

Table 16 shows the average mass flow and fractions of the filter cake. The mass fractions of the liquid phase are the same as in stream 5. 12.85 t/d solid FDCA are produced at the process with the filter for removing solid FDCA. The overall yield of FDCA is 99.999 % due to the recycling of unreacted HMF and intermediates.

Table 16: Average mass flow and fractions of the filter cake

Liquid fraction [t/d]	0.262
Solid FDCA [t/d]	12.85
Total [t/d]	13.11

The filtrate is recycled to the reactor by mixing with feed stream F. For this purpose water is removed at a part using a flash separator to satisfy mass

balance. The estimated heat duty of the flash separator is 3.67 MW at 103.4°C and 2 bar. Table 17 shows the flow streams and the mass fractions of the vapor and the liquid phase of the flash separator B8.

Table 17: Mass fraction of liquid phase and mole fraction of vapor phase of flash separator B8

Component	Mole fraction Stream 11 [m%]	Mass fraction Stream 12 [wt%]
Water	45.99	54.75
Acetic acid	6.361	44.81
HMF	1.5e-4	0.068
FFCA	9.9e-8	0.197
DFF	4.5e-7	4.4e-3
FDCA ²⁻	0	0.083
H ⁺	0	1.1e-3
N ₂	35.02	0.045
O ₂	12.62	0.042
Total	2098 m³/d	1267 t/d

Recycling stream 12 consists of 54.75 wt% water and 44.81 wt% acetic acid and is mixed with feed stream F and recycling stream 8 and led to pump B5 at approximately 64°C. There are no solid particles in the feed stream of the pump, because the mass fraction of FDCA is 0.047 wt%, which is completely soluble according to Table 2. The vapor phase of the pump input is 1.44 % and should be attended at pump design. Required net work of the pump is 455.61 kW at a pump efficiency of 85.94 %. The estimated volumetric flow rate of the pump is 1568.5 m³/h, which is approximately 90 % higher compared to the pump flow rate in the process with the hydrocyclone. The reason is the higher temperature of the feed stream in the process with the filter, because the mass flows and fractions are approximately the same for stream 1 in both processes.

The vapor phase of the flash separator B8 comprises 47.64 m% air, 45.99 m% water and 6.361 m% acetic acid and should be treated before discharging due to relatively high acetic acid fraction.

The vapor phase of flash separator B4 contains 53.93 m% air, 40.39 m% water and 5.689 m% acetic acid (Table 18) and is recycled to the reactor, at which air is

separated from the solvent at flash separator B10. The estimated heat duty of flash separator B4 is 19.36 MW.

Table 18: Flow rate and mole fractions of vapor phase of flash separator B4 at the process with the filter

Component	Mole fraction Stream 3 [m%]
Water	40.39
Acetic acid	5.689
HMF	3.7e-4
FFCA	1.0e-6
DFF	1.5e-6
FDCA ²⁻	0
H ⁺	0
N ₂	43.56
O ₂	10.37
Total [m³/d]	315127

As shown in Table 19, the vapor phase of flash separator B10 consists of 99.72 m% air and is recycled to the compressor at 9 bar. 10 % of the air stream have to be removed due to the lower oxygen concentration of 18.73 m% compared to ambient air. The liquid phase of the flash separator contains 65.77 wt% water and 30.91 wt% acetic acid and is recycled to the reactor (Table 19). The estimated cooling duty of flash separator B10 is 23.35 MW.

Table 19: Mass fraction of liquid phase and mole fraction of vapor phase of flash separator B10 at the process with the filter

Component	Mole fraction Stream 7 [m%]	Mass fraction Stream 8 [wt%]
Water	0.254	65.77
Acetic acid	0.025	30.91
HMF	2.3e-9	4.2e-3
FFCA	0	1.3e-5
DFF	0	1.7e-5
FDCA ²⁻	0	0
H ⁺	0	0
N ₂	80.99	1.955
O ₂	18.73	1.360
Total	123828 m³/d	955 t/d

At the compressor, 90 % of the input is recycled air at a pressure of 9 bar. The estimated outlet temperature is 378.09°C, which is comparable to the outlet temperature of the compressor in the process with the hydrocyclone. The required net work of the compressor is 6.32 MW at an efficiency of 80 %. The mechanical efficiency is estimated to be 90 %.

5.2 Process simulation using distillation

Figure 37 shows the flowsheet of the HMF conversion to FDCA by separating FDCA from the solvent using a distillation column. For this purpose trioctylamine is introduced as a solvent to accomplish the distillation. The feed stream of the process is estimated to comply with the reactor inputs of the patent of Lilga et al. (Table 20) [17].

Table 20: Flow rate and mass fractions of feed stream of the process with the distillation column

Component	Mass fraction Feed Stream F [wt%]
Water	1.6
Acetic acid	0.4
HMF	98
Total [t/d]	10.9

0.17 t/d water, 0.04 t/d acetic acid, 10.67 t/d HMF and 4404 m³/h air are required for the simulated process. Table 21 shows the reactor inputs those fractions are based on the patent of Lilga et al. [17]. The estimated heat duty of the reactor is 2.98 MW at a vapor fraction of 35.11 %.

Table 21: Fractions and flow rates of reactor inputs at the process with the distillation column

Component	Mass fraction	Mole fraction
	Feed Stream 1 [wt%]	Air Stream A2 [m%]
Water	59.07	0.218
Acetic acid	39.64	0.019
HMF	0.514	1.4e-9
FDCA	0.034	0
FFCA	0.112	0
DFF	2.5e-3	0
N ₂	0.472	80.95
O ₂	0.149	18.81
Trioctylamine	3.8e-3	0
Total	2258 t/d	25170 m³/d

Air and part of the solvent are removed at the flash separator B4 downstream the reactor at 150°C and 9.5 bar at a required heat duty of 17.83 MW. As shown in Table 22, the vapor phase of the flash drum consists of 39.83 m% water, 5.22 m% acetic acid and 54.94 m% air at an estimated flow rate of 284948 m³/d.

Table 22: Flow rate and mole fractions of vapor phase of flash separator B4 at the process with the distillation column

Component	Mole fraction Stream 3 [m%]
Water	39.83
Acetic acid	5.222
HMF	2.9e-4
FDCA	7.9e-9
FFCA	7.1e-7
DFF	1.1e-6
N ₂	44.70
O ₂	10.24
Trioctylamine	1.9e-8
Total [m³/d]	284948

To separate air from water and acetic acid, a cooling duty of 20.49 MW is required in the flash separator B9 at a temperature of 21°C. As shown in Table 23, vapor phase of the flash separator contains of 99.74 m% air and is recycled to the compressor at 9 bar. Due to the lower oxygen concentration in the air

recycling stream of 18.56 m% compared to ambient air, 10 % of the recycling flow is exhausting and ambient air is sucked in.

The required net work of the compressor is 5.83 MW at an efficiency of 80 %, whereas the mechanical efficiency is set to 90 %. The estimated outlet temperature is 381.55°C.

Table 23: Mass fraction of liquid phase and mole fraction of vapor phase of flash separator B9 at the process with the distillation column

Component	Mole fraction Stream 20 [m%]	Mass fraction Stream 21 [wt%]
Water	0.243	68.70
Acetic acid	0.021	30.06
HMF	1.6e-9	3.5e-3
FDCA	0	1.2e-7
FFCA	0	9.6e-6
DFF	0	1.3e-5
N ₂	81.18	0.935
O ₂	18.56	0.308
Trioctylamine	0	6.5e-7
Total	114244 m³/d	801 t/d

The liquid phase of the flash separator B9 consists of 68.70 wt% water and 30.06 wt% acetic acid, is mixed with recycling streams 10 and 18 and recycled to the reactor by mixing with feed stream F.

The liquid phase of flash separator B4 is fed to the extractor to introduce the solvent trioctylamine. As shown in Table 24, input 4 of the extractor contains 53.73 wt% water, 44.79 wt% acetic acid and 0.956 wt% FDCA, which is completely soluble according to Table 2.

Table 24: Mass fractions and flow rate of aqueous extractor input

Component	Mass fraction Stream 4 [wt%]
Water	53.73
Acetic acid	44.79
HMF	0.061
FDCA	0.956
FFCA	0.173
DFF	3.9e-3
N ₂	0.217
O ₂	0.062
Trioctylamine	5.9e-3
Total	1461 t/d

Table 25 shows the K-values of the components in every stage of the extractor. A K-value close to 1 signifies similar solubility of the substance in both solvents, which involves low separation efficiency. Flow rates of both feed streams of the extractor are approximately 0.65 kmol/s. As shown in Table 25, K-value of FFCA is close to 1, which means that this component is the most difficult substance being extracted by trioctylamine, followed by HMF, FDCA and DFF.

Table 25: K-values of the components in the 4 stages of the extractor

N	H₂O	AcOH	HMF	FDCA	FFCA	DFF	N₂	O₂	TOA
1	62.9	0.00182	0.0674	0.0129	7.06	0.0102	4e-5	5.6e-4	8e-23
2	62.7	0.00182	0.0672	0.0129	7.04	0.0102	4e-5	5.6e-4	8e-23
3	60.3	0.00190	0.0675	0.0134	7.00	0.0107	4e-5	5.8e-4	1e-22
4	37.4	0.00293	0.0658	0.0182	5.74	0.0157	8e-5	9.2e-4	7e-22

Mass fractions and flow rates of the aqueous and the organic outlet streams of the extractor are shown in Table 26. The aqueous stream contains 99.56 wt% water and is mixed with streams 10, 21 and F and recycled to the reactor, at which due to formed water in the reactor, 1.52 t/d of the recycling stream are removed to satisfy mass balance. The mass fraction of FDCA in the aqueous stream is 0.101 wt% at 34°C, which is completely soluble at this temperature.

Table 26: Mass fractions and flow rates of the aqueous and organic outlet streams of the extractor

Component	Mass fraction	Mass fraction
	Aqu. Stream 16 [wt%]	Org. Stream 5 [wt%]
Water	99.56	0.162
Acetic acid	7.4e-6	3.157
HMF	4.0e-6	4.3e-3
FDCA	0.101	0.461
FFCA	0.335	3.2e-3
DFF	4.6e-5	5.0e-4
N ₂	0	0.015
O ₂	0	4.3e-3
Triethylamine	0	96.19
Total [t/d]	755	20730

The organic outlet stream of the extractor consists of 0.162 wt% water, 3.157 wt% acetic acid, 0.461 wt% FDCA and 96.19 wt% triethylamine and is fed to a flash separator to decrease the input of the first column B8. The estimated heat duty of the flash separator B7 is 154.02 MW at 300°C and 3.5 bar.

Mass fractions and flow rates of the liquid and the vapor phase of the flash separator are shown in Table 27.

Table 27: Mass fractions and flow rates of liquid and vapor phase of flash separator B7 at the process with the distillation column

Component	Mass fraction	Mass fraction
	Stream 6 [wt%]	Stream 7 [wt%]
Water	4.042	0.035
Acetic acid	65.35	1.120
HMF	0.057	2.6e-3
FDCA	5.5e-3	0.475
FFCA	9.5e-4	3.3e-3
DFF	1.1e-3	4.8e-4
N ₂	0.480	1.1e-4
O ₂	0.136	3.1e-5
Triethylamine	29.93	98.36
Total [t/d]	658	20072

The vapor phase consists of 4.042 wt% water, 65.35 wt% acetic acid and 29.93 wt% triethylamine and is mixed with the distillate of the first column to separate acetic acid and triethylamine in the second column B18. The liquid

phase comprises 0.475 wt% FDCA, 1.120 wt% acetic acid and 98.36 wt% trioctylamine and is fed to the first distillation column at the second stage.

The estimated condenser cooling duty of the first distillation column is 148.37 MW at a condenser temperature of 289.96°C. The distillate rate and the reflux rate are estimated to be 20058 t/d and 2006 t/d, respectively. The calculated reboiler heat duty is 140.91 MW and the bottoms rate and the boilup rate are 13.6 t/d and 37015 t/d, respectively. The resultant boilup ratio at the first distillation column is 2719. At an estimated reboiler temperature of 453.89°C, FDCA in bottoms is liquid and could be used for further processing.

Mass fraction and flow rate of the distillate and the bottoms are shown in

Table 28. The distillate contains 1.120 wt% acetic acid, 0.410 wt% FDCA and 98.43 wt% trioctylamine and is fed to the second distillation column B18. The bottoms consists of 3 wt% trioctylamine and 97 wt% FDCA. 13.20 t/d FDCA are produced at the process using distillation at an overall yield of FDCA of 99.95 %.

Table 28: Mass fraction and flow rate of distillate and bottoms of distillation column B8

Component	Mass fraction Distillate [wt%]	Mass fraction Bottoms [wt%]
Water	0.035	0
Acetic acid	1.120	0
HMF	2.6e-3	0
FDCA	0.410	97.0
FFCA	3.3e-3	1.4e-7
DFF	4.8e-4	0
N ₂	1.1e-4	0
O ₂	3.1e-5	0
Trioctylamine	98.43	3.0
Total [t/d]	20058	13.6

The split fraction of FDCA in the distillate and the bottoms are 86 % and 14 %, respectively. Figure 41 shows the mass fractions of the liquid phase in every stage and the temperature profile of the first distillation column, which enables FDCA separation from the solvent trioctylamine. The temperature is decreasing from 453.75°C in the bottom tray to 423.76°C in the top tray, resulting in liquid

FDCA in all stages. The estimated temperatures in the condenser and in the reboiler are 289.96°C and 453.89°C, respectively.

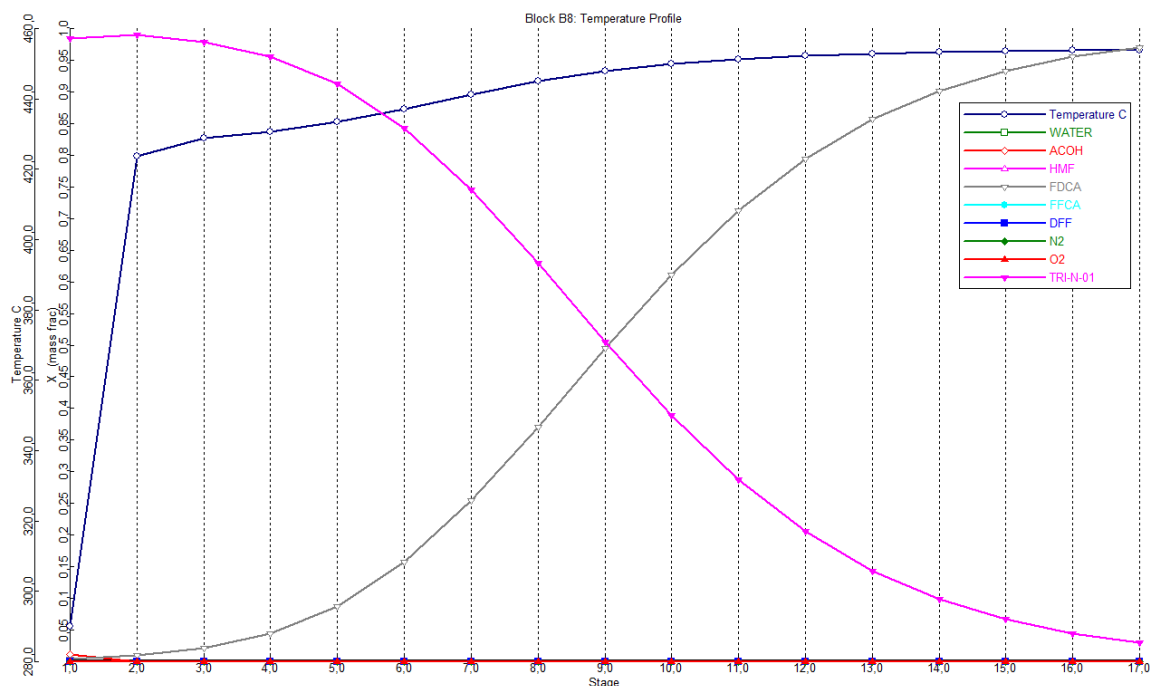


Figure 41: Mass fractions of liquid phase and temperature profile of distillation column B8

As shown in Table 29, the input of the second distillation column B18 contains 3.159 wt% acetic acid, 0.397 wt% FDCA and 96.25 wt% trioctylamine.

Table 29: Mass fraction and flow rate of the input of distillation column B18

Component	Mass fraction Stream 9 [wt%]
Water	0.162
Acetic acid	3.159
HMF	4.3e-3
FDCA	0.397
FFCA	3.2e-3
DFF	5.0e-4
N ₂	0.015
O ₂	4.3e-3
Trioctylamine	96.25
Total [t/d]	20716

The calculated condenser temperature is -81.93°C to liquefy the distillate. The required condenser cooling duty is 9.73 MW at a distillate rate of 693 t/d and a

reflux rate of 416 t/d. The estimated reboiler heat duty is 103.84 MW at a temperature of 416.34°C. The bottoms rate and the boilup rate are estimated to be 20023 t/d and 65054 t/d, respectively. The split fractions of the components are shown in Table 30, in which air, water, acetic acid and HMF go out the distillate and FFCA, FDCA and trioctylamine go out the bottoms. DFF is split 55 % and 45 % in top and bottoms, respectively.

Table 30: Split fraction in the distillate and bottoms of distillation column B18

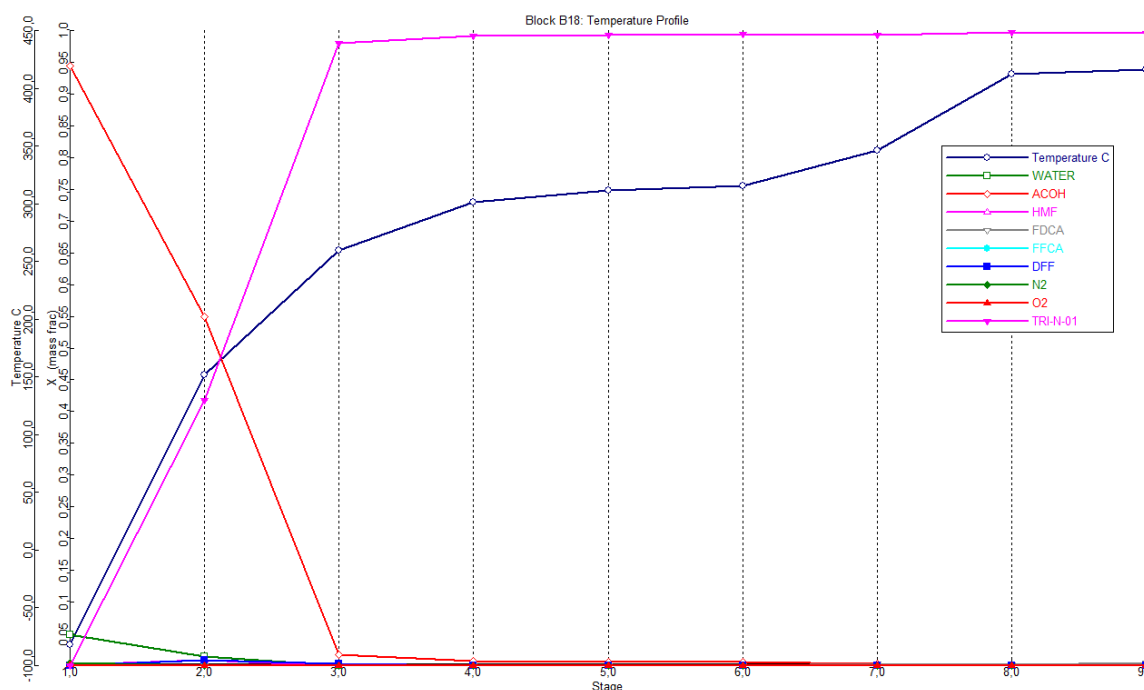
Component	Distillate [%]	Bottoms [%]
Water	100	6.4e-4
Acetic acid	100	6.5e-3
HMF	99.94	0.059
FDCA	0	100
FFCA	2.2e-4	100
DFF	54.83	45.17
N ₂	100	5.7e-9
O ₂	100	4.9e-9
Trioctylamine	4.3e-4	100

Table 31 shows the estimated mass fractions and flow rates of the distillate and the bottoms of the distillation column B18. The distillate consists of 4.849 wt% water, 94.41 wt% acetic acid and 0.012 wt% trioctylamine, which fulfills the defined flow stream of the organic solvent of 0.001 kg/s. Due to the recycling of the distillate to the reactor, trioctylamine fraction has to be low in the distillate to avoid dissolving of FDCA in the organic solvent in the reactor. The bottoms contains 0.411 wt% FDCA and 99.59 wt% trioctylamine and is recycled to the extractor.

Table 31: Mass fraction and flow rate of distillate and bottoms of distillation column B18

Component	Mass fraction Distillate [wt%]	Mass fraction Bottoms [wt%]
Water	4.849	1.1e-6
Acetic acid	94.41	2.1e-4
HMF	0.129	2.6e-6
FDCA	0	0.411
FFCA	2.1e-7	3.3e-3
DFF	8.2e-3	2.3e-4
N ₂	0.458	0
O ₂	0.130	0
Trioctylamine	0.012	99.59
Total [t/d]	693	22023

The mass fractions of the liquid phase in every stage and the temperature profile of the distillation column B18 are shown in Figure 42. Large parts of trioctylamine and FDCA are separated from the rest in the first three stages. The purification of the streams is accomplished in stages 4 to 9 to obtain the defined concentrations. The temperature in the trays varies from 151.71°C to 412.62°C.

**Figure 42:** Mass fractions of liquid phase and temperature profile of distillation column B18

The distillate of column B18 is mixed with the streams 18, 21 and F and fed to the pump B5. The input of the pump contains 0.034 wt% FDCA at 14°C, which

should be completely soluble according to linear interpolation of a solubility of 0.153 wt% at 25°C (Table 2) and determined immiscibility at 0°C. The estimated vapor fraction of the pump input is 0.43 % and should be regarded at pump design. The required net work of the pump is 144.55 kW at an estimated efficiency of 81.89 %. The calculated volumetric flow rate of the pump is 474 m³/h.

The bottoms of distillation column B18 is cooled down to 50°C at 2.5 bar to obtain the same temperature as in the extractor. Due to a FDCA concentration of 0.411 wt%, it is completely soluble in accordance with Table 2. The cooling duty of the heat exchanger is 247.34 MW.

The output flow of the heat exchanger is mixed with the trioctylamine feed stream to satisfy mass balance due to losses of the organic solvent in the product stream P. 0.406 t/d trioctylamine are required for the process. The mixed flow stream is fed to pump B2 at a volumetric flow rate of 1049 m³/h. The required net work of the pump is 68.02 kW at an efficiency of 85.64 %.

Pump outlet stream 15 is fed to the extractor to form the organic solvent. As shown in Table 32, the organic input of the extractor contains 0.411 wt% FDCA and 99.59 wt% trioctylamine at a flow rate of 20023 t/d.

Table 32: Mass fraction and flow rate of the organic input of the extractor

Component	Mass fraction Stream 15 [wt%]
Water	1.1e-6
Acetic acid	2.1e-4
HMF	2.6e-6
FDCA	0.41
FFCA	3.3e-3
DFF	2.3e-4
N ₂	0
O ₂	0
Trioctylamine	99.59
Total [t/d]	20023

5.3 Process optimization

5.3.1 Process simulation using crystallization and filtration

For economic reasons, which are discussed in 5.4.2, the flash separator B8 in the process using filtration for removing solid FDCA is replaced by a splitter (Figure 43).

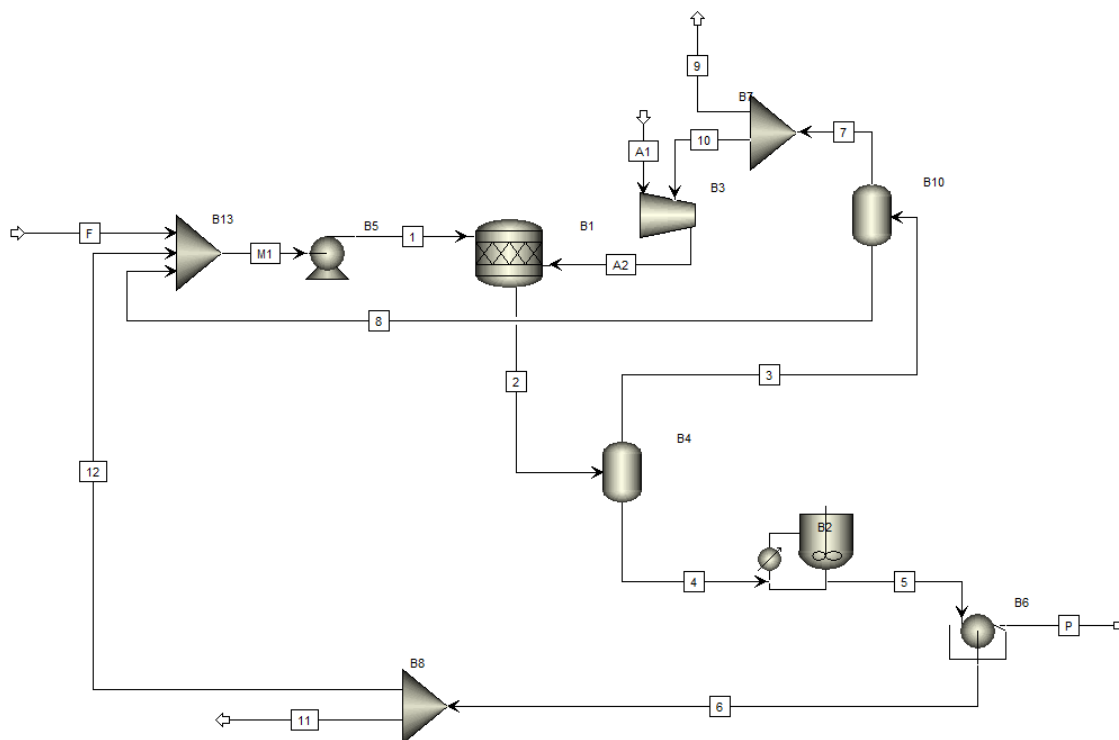


Figure 43: Flowsheet of HMF conversion to FDCA using a crystallizer and a filter for removing solid FDCA with a splitter for discharging solvent at a fraction

The operating conditions are the same as in the process using a flash separator for discharging the solvent at a part. The mass fractions and the volume ratio of feed stream to air stream at the reactor input are according to the US patent of Lilga et al. [17]. Mass fractions and flow stream of the feed stream F are shown in Table 33.

Table 33: Flow rate and mass fractions of feed stream of the process with the filter and splitter

Component	Mass fraction
	Feed Stream F [wt%]
Water	0
Acetic acid	10.5
HMF	89.5
Total [t/d]	11.7

1.23 t/d acetic acid, 10.49 t/d HMF and 4198 m³/h air are required for the process. As shown in Table 34, fractions and flow streams of the reactor inputs are comparable to those of the reactor feed streams in the process using filtration for obtaining solid FDCA and a flash separator for discharging solvent at a part. FDCA is completely soluble in the feed stream due to its low concentration of 0.051 wt%.

Table 34: Fractions and flow rates of the reactor inputs at the process with the filter and splitter

Component	Mass fraction	Mole fraction
	Feed Stream 1 [wt%]	Air Stream A2 [m%]
Water	58.05	0.227
Acetic acid	39.92	0.023
HMF	0.504	1.9e-9
FFCA	0.110	0
DFF	2.4e-3	0
FDCA ²⁻	0.051	0
H ⁺	6.7e-4	0
N ₂	0.817	81.01
O ₂	0.548	18.74
Total	2260 t/d	218158 m³/d

The estimated heat duty of the reactor is 4.67 MW that is approximately the same as in the process using centrifugation for FDCA removing due to comparable flow streams and temperatures. Air and part of the solvent are removed from the product stream of the reactor in a similar way as in the other process with the filter.

The feed stream of the crystallizer contains 53.67 wt% water, 44.87 wt% acetic acid and 0.979 wt% solute FDCA at a flow rate of 1427 t/d (Table 35).

Table 35: Mass fractions and flow rate of the crystallizer input at the process with the filter and splitter

Component	Mass fraction Stream 4 [wt%]
Water	53.67
Acetic acid	44.87
HMF	0.061
FFCA	0.175
DFF	3.9e-3
FDCA ²⁻	0.979
H ⁺	0.013
N ₂	0.148
O ₂	0.083
Total [t/d]	1427

Due to the higher flow rate, the estimated cooling duty is greater than in the other process with the filter, namely 7.10 MW at a solid product rate of 12.98 t/d. The calculated resistance time is 10 min at a defined volume of the crystallizer of 10 m³.

FDCA is removed using filtration at an estimated volume flow rate of the filtrate of 58.1 m³/h. The average mass fractions and the flow rate of the filter cake are shown in Table 36. 12.98 t/d FDCA are produced at the process with the filter for removing solid FDCA and the splitter at the recycling stream. The overall yield of FDCA with reference to HMF conversion is 99.93 %.

Table 36: Average mass flow and fractions of the filter cake at the process with the filter and splitter

Liquid fraction [t/d]	0.292
Solid FDCA [t/d]	12.98
Total [t/d]	13.24

Table 37 shows the mass flows of the outlet stream 11 of both processes using filtration for obtaining purified FDCA. In the process with the splitter, twice as much acetic acid is removed compared to the process with the flash separator. Hence, the mass fraction of acetic acid is higher in feed stream F. The water flow rates in both outlets are comparable, namely 1.232 t/d and 1.327 t/d, respectively. In the process with the flash separator, approximately 360 times more air is removed compared to the other process.

Table 37: Mass flows of outlet streams 11 of both processes using a filter

Component	Mass flow Flash Outlet [t/d]	Mass flow Splitter Outlet [t/d]
Water	1.117	1.204
Acetic acid	0.515	1.007
HMF	2.5e-5	0.001
FFCA	1.9e-8	0.004
DFF	7.6e-8	8.7e-5
FDCA ²⁻	0.0	0.002
H ⁺	0.0	2.4e-5
N ₂	1.323	0.003
O ₂	0.545	0.002
Total [t/d]	3.50	2.22

5.3.1.1 Oxidant: Use of Oxygen

To decrease oxidant flow rate, air is substituted for oxygen in the process using filtration for obtaining purified FDCA and a splitter for discharging part of the solvent, at which oxygen flow rates are equal in both processes (Figure 44). Compared to the process using air as oxidant, no splitter is required for emitting a part of the oxidant due to the usage of pure oxygen.

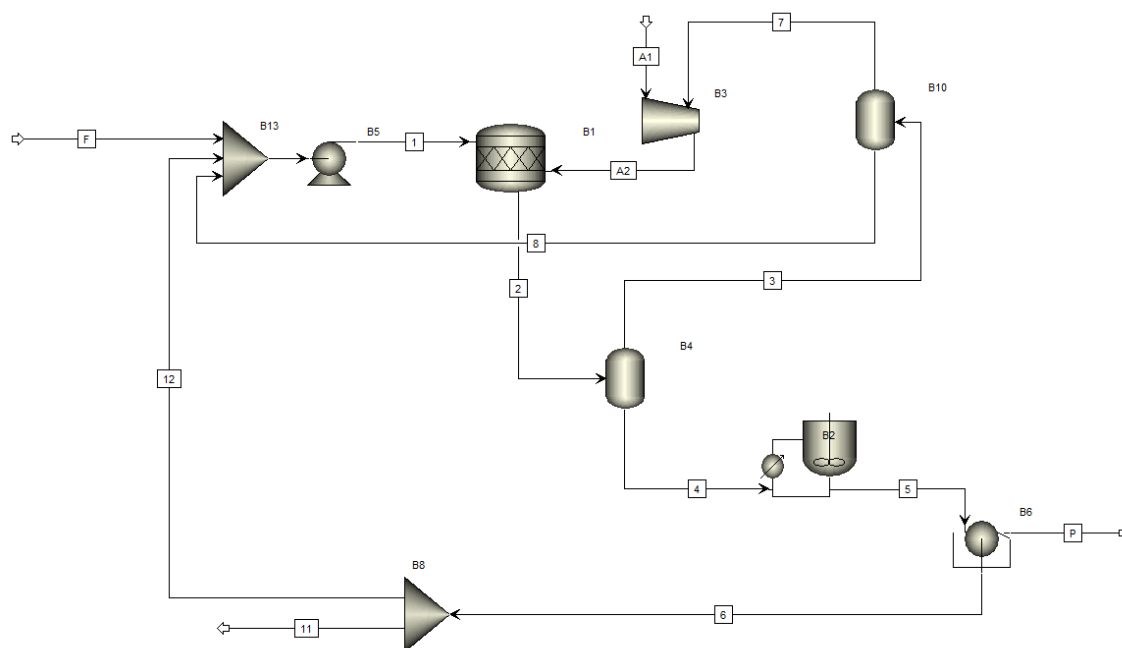


Figure 44: Flowsheet of HMF conversion to FDCA using a crystallizer and a filter for removing solid FDCA with a splitter for discharging solvent at a fraction and pure O₂ as oxidant

As shown in Table 38, the mass fractions and the flow rate of the feed stream F is comparable to the feed stream of the other processes using crystallization for obtaining solid FDCA.

Table 38: Flow rate and mass fractions of feed stream of the process with filter, splitter and pure O₂ as oxidant

Component	Mass fraction Feed Stream F [wt%]
Water	1
Acetic acid	10
HMF	89
Total [t/d]	12

0.12 t/d water, 1.2 t/d acetic acid, 10.48 t/d HMF and 127 m³/h oxygen are required for the process. The mass fractions of the feed streams of the reactor are according to the patent of Lilga et al. (Table 39) [17]. Volume ratio of the oxygen stream to the liquid input is set to 20/1. FDCA concentration in feed stream 1 is 0.078 wt%, which is completely soluble according to linear interpolation of a solubility of 0.153 wt% at 25°C (Table 2) and determined immiscibility at 0°C.

Table 39: Fractions and flow rates of the reactor inputs at the process with filter, splitter and pure O₂ as oxidant

Component	Mass fraction Feed Stream 1 [wt%]	Mole fraction Air Stream A2 [m%]
Water	58.56	0.248
Acetic acid	39.63	0.021
HMF	0.503	1.5e-7
FFCA	0.110	0
DFF	2.4e-3	0
FDCA ²⁻	0.078	0
H ⁺	1.0e-3	0
O ₂	1.108	99.73
Total	2263 t/d	43468 m³/d

The estimated vapor fraction in the reactor is 8.76 %. The required net heat duty is 5.98 MW, which is approximately 30 % greater than in the process using air as oxidant.

The product stream of the reactor is fed to flash separator B4 for recycling oxygen and part of the solvent at a specified temperature of 155°C. Due to the lower oxidant fraction, the temperature in the flash separator has to be higher to obtain comparable solvent evaporation. The estimated heat duty of the flash separator is 8.25 MW, which is half of the energy that is required in the flash separator B4 in the process using air as oxidant. The vapor phase contains 47.38 m% water, 5.69 m% acetic acid and 46.94 m% oxygen and is fed to flash B10 for separating oxygen from the solvent (Table 40). The volumetric flow of stream 3 is approximately 4 times smaller compared to the process using air as oxidant.

Table 40: Flow rate and mole fractions of vapor phase of flash separator B4 at the process with the filter, splitter and pure O₂ as oxidant

Component	Mole fraction Stream 3 [m%]
Water	47.38
Acetic acid	5.687
HMF	2.9e-4
FFCA	8.5e-7
DFF	1.2e-6
FDCA ²⁻	0
H ⁺	0
O ₂	46.94
Total [m³/d]	67301

A 3.6 times smaller net heat duty at the flash separator B10 of 5.65 MW is estimated compared to the process using air. Mass fraction and flow rate of the liquid phase and mole fraction and volumetric flow rate of the vapor phase of flash separator B10 are shown in Table 41 at a vapor fraction of 44.1 %. Volumetric vapor stream 7 is 5 times smaller than in the process using air due to the volumetric oxygen fraction of 21 vol% in air.

Table 41: Mass fraction of liquid phase and mole fraction of vapor phase of flash separator B10 at the process with the filter, splitter and pure O₂ as oxidant

Component	Mole fraction Stream 7 [m%]	Mass fraction Stream 8 [wt%]
Water	0.252	66.15
Acetic acid	0.021	26.49
HMF	1.5e-9	2.8e-3
FFCA	0	9.2e-6
DFF	0	1.1e-5
FDCA ²⁻	0	0
H ⁺	0	0
O ₂	99.73	7.353
Total	21844 m³/d	236 t/d

Stream 7 is recycled to the compressor at 9 bar to minimize oxygen demand. The required net work of the compressor is 1.12 MW, which is 5 times smaller than in the other process using air, at an efficiency of 80 %. The calculated outlet temperature is 361.69°C at 10 bar.

The liquid phase of flash separator B4 is fed to the crystallizer to solidify FDCA. The input of the crystallizer contains 57.64 wt% water, 41.09 wt% acetic acid and 0.718 wt% solute FDCA (Table 42). Due to the lower solvent evaporation at flash separator B4, the flow stream of the crystallizer feed is approximately 40 % higher in comparison to the input of the crystallizer in the process using air. As a result, FDCA concentration is lower, which leads to a higher crystallizer cooling duty at an equal FDCA flow rate compared to the process using air.

Table 42: Mass fractions and flow rate of crystallizer input at the process with filter, splitter and pure O₂ as oxidant

Component	Mass fraction Stream 4 [wt%]
Water	57.64
Acetic acid	41.09
HMF	0.044
FFCA	0.123
DFF	2.7e-3
FDCA ²⁻	0.718
H ⁺	9.4e-3
O ₂	0.380
Total	2031 t/d

0.174 t/d water, 0.044 t/d acetic acid, 10.67 t/d HMF, 4480 m³/d air and 0.415 t/d trioctylamine are required for the process to produce 13.20 t/d FDCA at an overall yield of 99.95 %. The fractions and mass flows of the inputs and the output of the reactor and the air recycling streams are comparable to those of the simulation with liquid distillates.

Due to the higher temperature of the distillate recycling stream of the second distillation column, temperature of the feed stream 1 is 38°C compared to 16°C in the other process using distillation. As a result, required net power of the reactor is 2.5 times lower compared to the process using total condenser at both distillation columns, namely 1.17 MW at a vapor fraction of 36.18 %.

The results of the extractor, flash separator B7 and distillation column B8 are comparable to the process with total condensers at both distillation columns. Variation is approximately 10 %, due to a 10 % lower flow rate in the process with vapor distillate in column B18.

At the second distillation column, the number of stages is set to 7, at which stage 5 is estimated as feed tray. Reflux ratio of 0.4 is specified and the distillate to feed rate is varied to obtain a flow rate of trioctylamine of 0.001 kg/s in the distillate.

The mass fractions of the feed stream of distillation column B18 are comparable in both processes using distillation for obtaining purified FDCA. The variation of the flow rates in both processes is approximately 10 % (Table 44).

Table 44: Mass fractions and flow rate of the input of distillation column B18 with gaseous distillate

Component	Mass fraction Stream 9 [wt%]
Water	0.166
Acetic acid	3.201
HMF	4.7e-3
FDCA	0.401
FFCA	3.3e-3
DFF	5.0e-4
N ₂	0.016
O ₂	4.6e-3
Trioctylamine	96.20
Total [t/d]	18890

Compared to the other process using distillation, less number of stages are required due to slightly varying mass fractions and same settings of mass flow specification of trioctylamine in the distillate at different flow rates in both processes. Another reason for the different number of stages compared to the other process is that the total condenser is counting as one stage in the process with the liquid distillates.

The required condenser cooling duty is 4.25 MW at an estimated condenser temperature of 151.98°C. The calculated distillate rate and reflux rate are 641 t/d and 432 t/d, respectively. Estimated reboiler heat duty is 95.56 MW, which is 10 % lower in comparison to the process using total condenser at both distillation columns. The reboiler temperature is 416.38°C that is equal to the other distillation column process. The calculated bottoms rate and boilup rate are 18249 t/d and 63696 t/d, respectively.

The mass fractions of the distillate and the bottoms are comparable to those of the other process using distillation. As shown in Table 45, distillate contains 4.897 wt% water, 94.33 wt% acetic acid and 0.013 wt% trioctylamine. Bottoms consists of 0.415 wt% FDCA and 99.58 wt% trioctylamine. Flow rates are approximately 10 % lower due to decreased mass flows.

Table 45: Mass fractions and flow rate of distillate and bottoms of column B18 with gaseous distillate

Component	Mass fraction Distillate [wt%]	Mass fraction Bottoms [wt%]
Water	4.897	5.7e-7
Acetic acid	94.33	1.1e-4
HMF	0.139	1.4e-6
FDCA	0	0.415
FFCA	3.1e-7	3.4e-3
DFF	8.8e-3	2.1e-4
N ₂	0.475	0
O ₂	0.135	0
Trioctylamine	0.013	99.58
Total [t/d]	641	18249

Figure 46 shows the mass fractions of vapor phase in every stage and the temperature profile of distillation column B18 with gaseous distillate. Due to the high difference of boiling points of acetic acid and trioctylamine of 247°C,

separation is operating effectively at a small number of stages. The temperature varies from 267.26°C in the top tray to 414.29°C in the bottom tray.

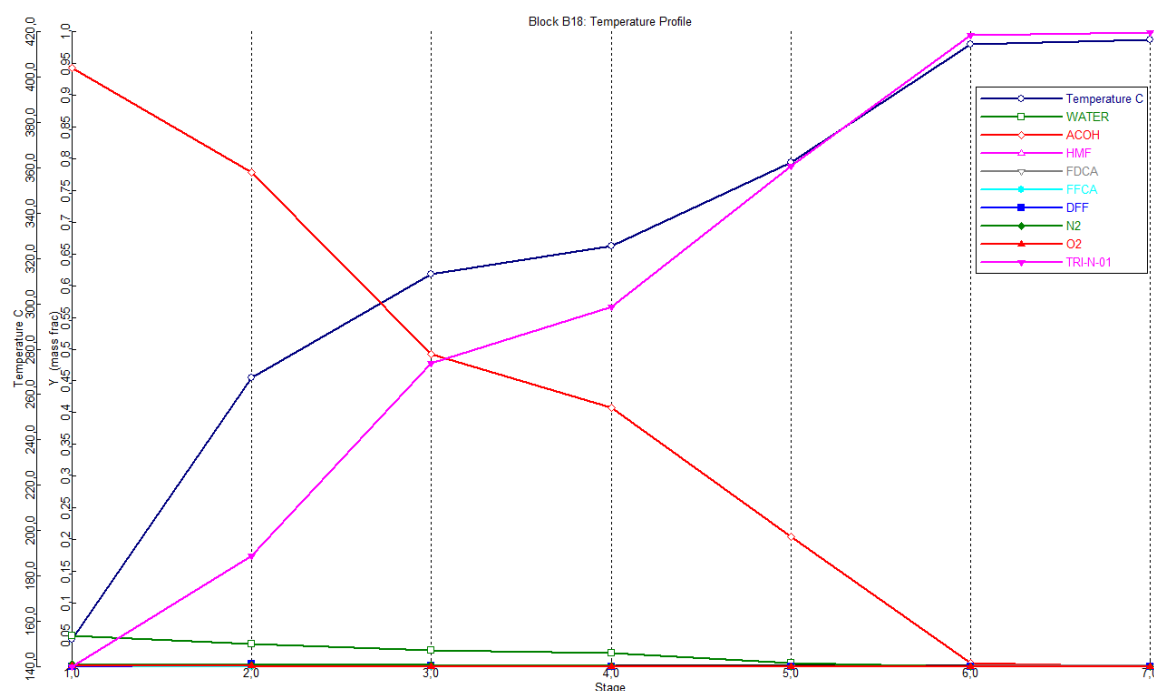


Figure 46: Mass fractions of vapor phase and temperature profile of column B18 with gaseous distillate

5.3.2.1 Decreased trioctylamine flow rate

According to the literature, organic acids are highly soluble in trioctylamine [32-36]. Therefore feed stream of trioctylamine in the extractor is decreased 10 times to reduce the flow rates in the distillation columns. The distillate of the second column B18 is gaseous to minimize costs. Figure 45 shows the flowsheet of the simulated process with lower trioctylamine flow stream.

Flow rates, mass fractions and operating conditions are comparable to those in the process using partial condenser at the second distillation column. 0.173 t/d water, 0.043 t/d acetic acid, 10.58 t/d HMF and 4492 m³/h air are required for the process. Hence, the estimated heating duties of the flash separators for recycling air and the part of the aqueous solvent and the required works of pump B5 and compressor B3 are approximately the same in both processes using different trioctylamine flow rates.

As shown in Table 46, the mass fractions and the flow rate of the aqueous input of the extractor are comparable to those of the other process with the partial condenser in the distillation column B18.

Table 46: Mass fractions and flow rate of the aqueous extractor input at the process with reduced trioctylamine flow rate

Component	Mass fraction Stream 4 [wt%]
Water	53.78
Acetic acid	44.67
HMF	0.061
FDCA	1.026
FFCA	0.172
DFF	3.9e-3
N ₂	0.217
O ₂	0.062
Trioctylamine	5.9e-3
Total	1452 t/d

Table 47 shows the K-values of the components in every stage of the extractor. Due to 10 times lower trioctylamine flow rate, K-values are closer to 1, which means worse separation results.

Table 47: K-values of the components in the 4 stages of the extractor at the process with reduced trioctylamine flow rate

N	H ₂ O	AcOH	HMF	FDCA	FFCA	DFF	N ₂	O ₂	TOA
1	37.3	0.00320	0.0718	0.0220	6.6702	0.0182	8e-5	9.2e-4	9e-22
2	21.2	0.00596	0.0794	0.0401	6.3456	0.0343	2e-4	1.6e-3	1e-20
3	11.3	0.01241	0.0941	0.0808	5.9787	0.0707	5e-4	3.2e-3	2e-19
4	5.01	0.04035	0.1503	0.2157	5.0038	0.1915	3e-3	0.0111	5e-18

The aqueous product stream of the extractor contains 99.39 wt% water and 0.254 wt% FDCA, which is twice as much as in the process with 10 times higher trioctylamine flow rate. The organic product stream of the extractor contains 2.72 wt% water, 24.57 wt% acetic acid, 0.847 wt% FDCA and 71.67 wt% trioctylamine at 138°C (Table 48). Due to the lower trioctylamine flow stream, FDCA fraction is twice as high compared to the other processes using distillation.

In accordance with linear extrapolation of Table 2, FDCA is completely soluble in stream 5.

Table 48: Mass fractions and flow rates of the aqueous and organic outlet streams of the extractor at the process with reduced trioctylamine flow rate

Component	Mass fraction	Mass fraction
	Aqu. Stream 16 [wt%]	Org. Stream 5 [wt%]
Water	99.39	2.720
Acetic acid	4.7e-4	24.57
HMF	2.8e-3	0.033
FDCA	0.254	0.847
FFCA	0.351	8.8e-3
DFF	2.4e-4	2.4e-3
N ₂	0	0.120
O ₂	3.7e-9	0.034
Trioctylamine	0	71.67
Total [t/d]	714	2641

Stream 5 is fed to a flash separator to minimize flow rate of the first distillation column B8. Due to the lower trioctylamine fraction, the temperature in the flash separator is lower than in the other processes with the distillation columns, namely 270°C instead of 300°C. The estimated heat duty of the flash separator is 15.3 MW.

As shown in Table 49, the vapor phase of flash separator B7 contains 8.599 wt% water, 75.78 wt% acetic acid and 15.02 wt% trioctylamine and is mixed with the distillate of the first distillation column to separate trioctylamine from water and acetic acid. The liquid phase of the flash separator B7 consists of 0.096 wt% water, 1.702 wt% acetic acid, 1.223 wt% FDCA and 96.96 wt% trioctylamine and is fed to the first distillation column.

Table 49: Mass fractions and flow rates of liquid and vapor phase of flash separator B7 at the process with reduced trioctylamine flow rate

Component	Mass fraction Stream 6 [wt%]	Mass fraction Stream 7 [wt%]
Water	8.599	0.096
Acetic acid	75.78	1.702
HMF	0.092	6.4e-3
FDCA	3.7e-3	1.223
FFCA	1.6e-3	0.012
DFF	3.0e-3	2.2e-3
N ₂	0.387	7.9e-5
O ₂	0.110	2.3e-5
Trioctylamine	15.02	96.96
Total [t/d]	815	1826

To minimize the operating cost, the number of stages in the distillation column B8 is set to 17 at a reflux ratio of 0.1. The second stage is chosen as feed stage due to low ratio of bottoms to distillate.

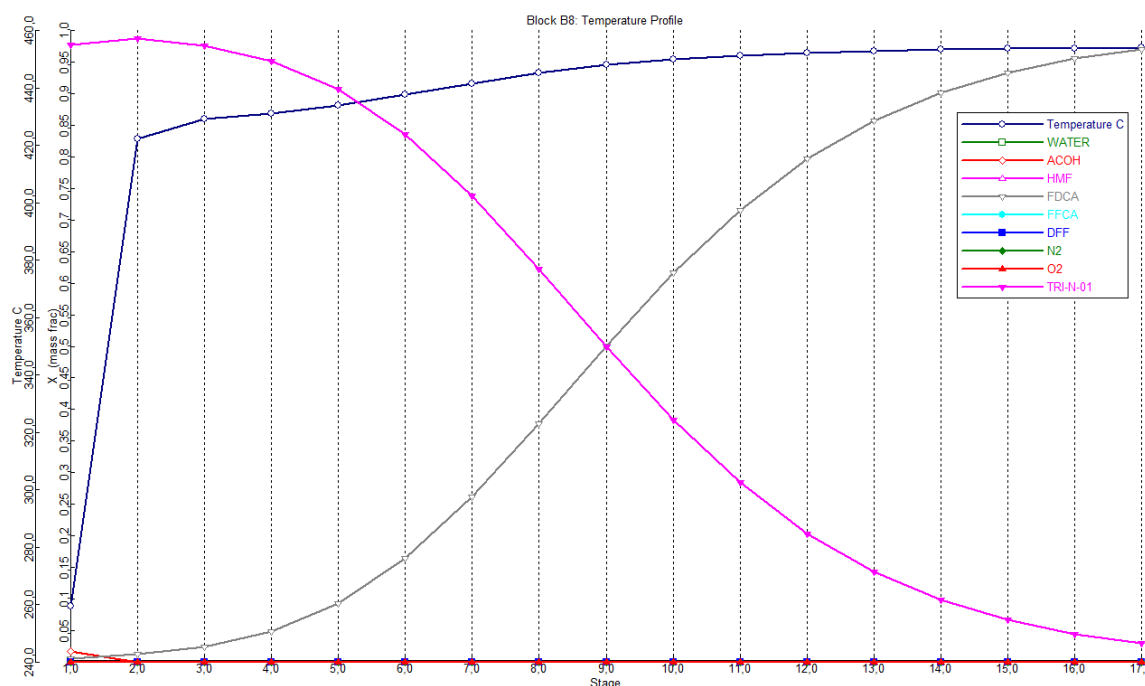
At a temperature of 259.67°C, the estimated condenser cooling duty is 15.37 MW, which is 9.5 times smaller compared to the condenser duty of distillation column B8 in the processes with 10 times higher trioctylamine flow rate. The calculated distillate rate is 1812 t/d at a reflux rate of 181 t/d. The temperature in the reboiler is estimated to be 453.88°C. The bottoms rate and the boilup rate are 13.5 t/d and 3910 t/d, respectively. Calculated reboiler heat duty is 14.88 MW, which is 8.6 times smaller in comparison to those of the distillation columns B8 in the other processes.

The distillate contains 0.097 wt% water, 1.714 wt% acetic acid, 0.51 wt% FDCA and 97.66 wt% trioctylamine at an estimated flow rate of 1812 t/d. The bottoms consists of 97 wt% FDCA and 3 wt% trioctylamine (Table 50). 13.49 t/d FDCA are produced, which is comparable to the other processes using distillation for obtaining purified liquid FDCA. The overall yield of FDCA with reference to HMF conversion is 99.92 %. Reducing trioctylamine flow rate at 10 times enables smaller equipment and lower flow streams.

Table 50: Mass fractions and flow rates of distillate and bottoms of column B8 at the process with reduced trioctylamine flow rate

Component	Mass fraction Distillate [wt%]	Mass fraction Bottoms [wt%]
Water	0.097	0
Acetic acid	1.714	0
HMF	6.5e-3	0
FDCA	0.510	97.0
FFCA	0.012	5.3e-7
DFF	2.2e-3	0
N ₂	8.0e-5	0
O ₂	2.3e-5	0
Trioctylamine	97.66	3.0
Total [t/d]	1812	13.5

Due to similar mass fractions and same column settings compared to the other processes, the temperature profile and the mass fractions in every stage of the distillation column B8 are comparable to the processes using high trioctylamine flow rates (Figure 47). The temperature ranges from 422.13°C in the top tray to 453.76°C in the bottom tray.

**Figure 47:** Mass fractions of liquid phase and temperature profile of column B8 at the process with reduced trioctylamine flow rate

At the second distillation column B18, the number of stages is set to 6 at a reflux ratio of 0.2, using a partial condenser for economic reasons. Feed stream of the distillation column contains 2.734 wt% water, 24.69 wt% acetic acid, 0.353 wt% FDCA and 72.02 wt% trioctylamine at a flow rate of 2627 t/d, which is 7 times smaller compared to the other processes using distillation columns (Table 51).

Table 51: Mass fractions and flow rate of the input of column B18 with gaseous distillate

Component	Mass fraction Stream 9 [wt%]
Water	2.734
Acetic acid	24.69
HMF	0.033
FDCA	0.353
FFCA	8.9e-3
DFF	2.5e-3
N ₂	0.120
O ₂	0.034
Trioctylamine	72.02
Total [t/d]	2627

The estimated condenser temperature is 149.27°C at a condenser cooling duty of 3.04 MW. The distillate rate and the condenser rate are 726 t/d and 256 t/d, respectively. At the bottoms, calculated temperature is 416.45°C at a reboiler heat duty of 13.02 MW, which is approximately 7 times lower compared to the process with the partial condenser and high trioctylamine flow. The estimated bottoms rate and boilup rate are 1902 t/d and 9078 t/d, respectively.

As shown in Table 52, the distillate of column B18 contains 9.9 wt% water, 89.4 wt% acetic acid and 0.012 wt% trioctylamine, is condensed at heat exchanger B14 and recycled to the reactor. The required cooling duty for condensation and subcooling to 50°C is 6.02 MW.

The bottoms consists of 0.488 wt% FDCA and 99.5 wt% trioctylamine, is cooled down to 50°C at a required cooling duty of 23.49 MW and mixed with the trioctylamine input to be recycled to the extractor. For this purpose pump B2 is required with an estimated net work of 11.78 kW to increase pressure of the recycling stream 15 to 4 bar. Estimated mass fraction of FDCA in stream 15 is

0.488 wt% at a temperature of 50°C. Therefore, FDCA is completely soluble according to linear interpolation of FDCA solubility in Table 2.

Table 52: Mass fractions and flow rates of distillate and bottoms of column B18 at the process with reduced trioctylamine flow rate

Component	Mass fraction Distillate [wt%]	Mass fraction Bottoms [wt%]
Water	9.900	3.6e-7
Acetic acid	89.40	3.7e-5
HMF	0.119	6.1e-7
FDCA	0	0.488
FFCA	8.3e-7	0.012
DFF	7.5e-3	5.2e-4
N ₂	0.435	0
O ₂	0.124	0
Trioctylamine	0.012	99.50
Total [t/d]	726	1902

Figure 48 shows the mass fractions of the vapor phase in every tray and the temperature profile of distillation column B18. The temperature varies from 250.35°C in the top tray to 415.5°C in bottom tray.

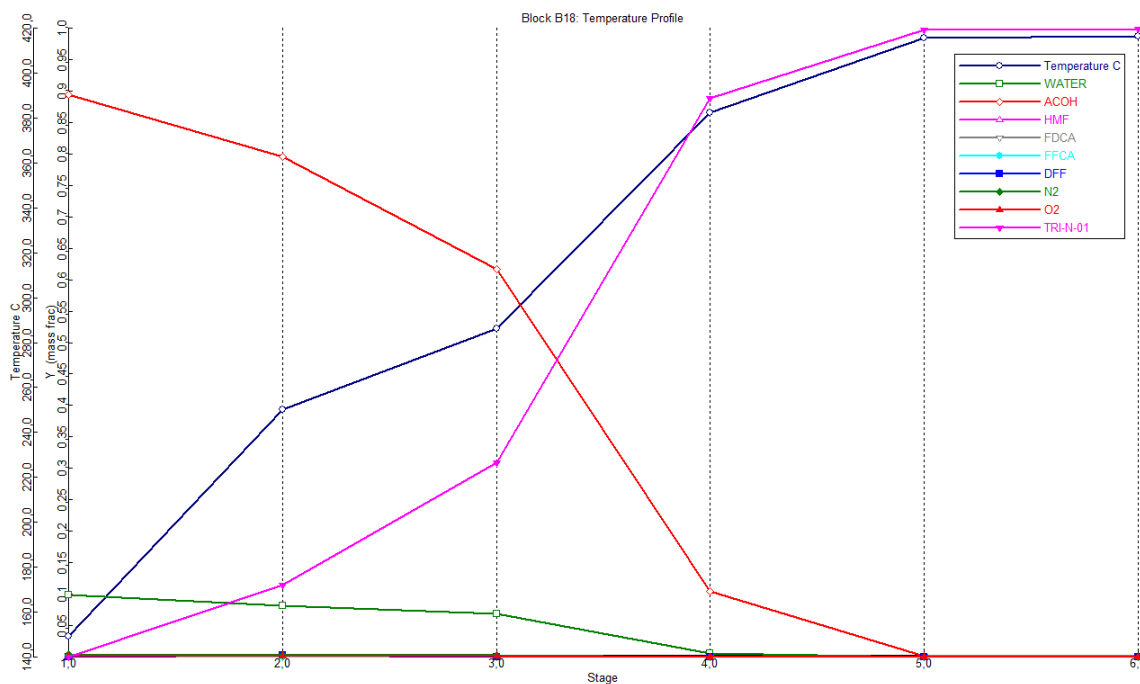


Figure 48: Mass fractions of vapor phase and temperature profile of column B18 with gaseous distillate

distillation. At the temperature of 139°C, FDCA is completely soluble in the input of the first column.

Table 53: Mass fractions and flow rate of distillation column B8 input at the process with reduced trioctylamine flow rate and no flash separator

Component	Mass fraction Stream 5 [wt%]
Water	2.815
Acetic acid	25.11
HMF	0.034
FDCA	0.593
FFCA	9.2e-3
DFF	2.4e-3
N ₂	0.122
O ₂	0.035
Trioctylamine	71.2
Total [t/d]	2577

At the first column, the number of stages is set to 16 at a reflux ratio of 0.1. The feed stage is defined as the second stage. Due to the higher acetic acid fraction in distillation column B8 compared to the other processes, the temperature of the condensed distillate would be too low for using water as cooling medium. Therefore, a partial condenser is used at the column to get gaseous distillate.

The estimated temperature at the condenser is 354.31°C at a cooling duty of 2.56 MW. The calculated distillate rate and the condensate rate are 2563 t/d and 691 t/d, respectively. The reboiler heat duty is 28.09 MW at an estimated temperature of 453.88°C. The bottoms rate and the boilup rate are 13.5 t/d and 7379 t/d, respectively.

Table 54 shows mass fractions and flow rates of the distillate and the bottoms of distillation column B8.

Table 54: Mass fractions and flow rates of distillate and bottoms of column B8 at the process with reduced trioctylamine flow rate and no flash separator

Component	Mass fraction Distillate [wt%]	Mass fraction Bottoms [wt%]
Water	2.829	0
Acetic acid	25.24	0
HMF	0.034	0
FDCA	0.086	97.0
FFCA	9.3e-3	9.1e-7
DFF	2.5e-3	0
N ₂	0.122	0
O ₂	0.035	0
Trioctylamine	71.64	3.0
Total [t/d]	2563	13.5

The bottoms contains 97 wt% FDCA and 3 wt% trioctylamine at a flow rate of 13.5 t/d, which is comparable to the other processes using a distillation for obtaining purified FDCA. 13.08 t/d FDCA are produced at the process without the flash separator upstream column B8.

The distillate consists of 2.829 wt% water, 25.24 wt% acetic acid, 0.086 wt% FDCA and 71.64 wt% trioctylamine at an estimated flow rate of 2563 t/d and is fed to heat exchanger B7 to be cooled down to 250°C at 3 bar. The estimated cooling duty of the heat exchanger is 12.20 MW to obtain an outlet flow with a vapor fraction of 71.53 %, which is comparable to the feed stream of the process using a flash separator to minimize the flow rate of the first distillation column.

Figure 50 shows the mass fractions of the liquid phase in every stage and the temperature profile of distillation column B8. The temperature ranges from 367.13°C in the top tray to 453.75°C in the bottom tray.

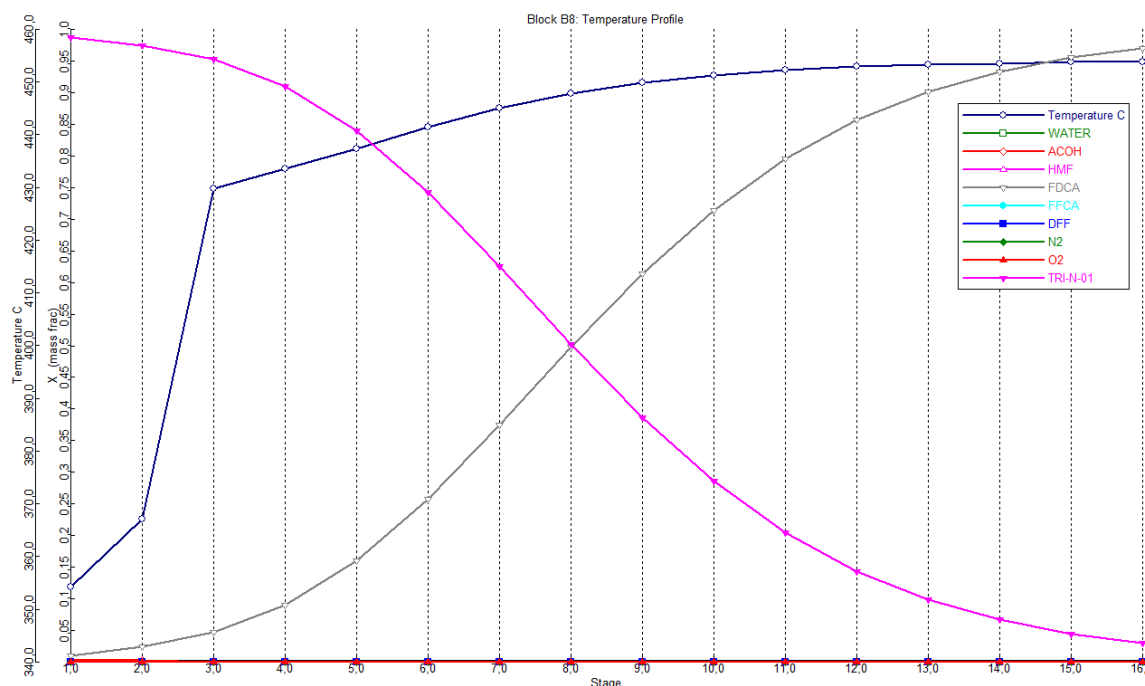


Figure 50: Mass fractions of liquid phase and temperature profile of column B8 at the process with reduced trioctylamine flow rate and no flash separator

Due to the higher acetic acid and the lower trioctylamine fraction in the feed stream, the temperature in stage 2 is lower compared to the other processes (Figure 47 and Figure 50).

5.4 Economic analysis of the process using crystallization

5.4.1 Process using centrifugation

The total capital costs of the process using centrifugation for separating part of the solvent from FDCA are shown in Table 55. The row noted as "Other" includes costs for design, engineering and procurement, material freight and taxes, and construction field indirect costs, such as equipment rental, small tools, field services, plant startup and fringe benefits. G and A stands for General and Administrative. The estimated total capital costs are \$43.73 million. The main cost of equipment purchasing, which is \$2.93 million, comprises of the acquisition cost of the air compressor, namely \$2.23 million. The costs of the reactor and the crystallizer are \$139 T and \$173 T, respectively. The largest part of the capital cost is the initial cost of the Pt/ZrO₂ catalyst, which is \$35 million. All indirect

costs, such as general and administrative overheads, contract fee, contingencies and other costs make up \$3.88 million, which equates to 8.9 % of the total capital costs.

Table 55: Capital costs of the process with the hydrocyclone

Element	Cost [\$]
Pt/ZrO ₂ catalyst	35,000,000
Purchased Equipment	2,898,300
Equipment Setting	55,069
Piping	270,174
Civil	101,228
Steel	27,586
Instrumentation	614,265
Electrical	794,959
Insulation	68,132
Paint	19,965
Other	2,086,600
G and A Overheads	177,008
Contract Fee	284,917
Contingencies	1,331,677
Total Capital Costs	43,729,879

As shown in Table 56, the total operating costs are \$42.2 million per year, whose implies \$33.6 million raw material cost due to the large acetic acid throughput compared to FDCA fraction. The acetic acid cost and the HMF cost make up approximately 88.6 % and 11.4 %, respectively, of the total raw material cost. Therefore, recycling or selling of the acetic acid in the product stream is indispensable. The operating labor cost and the maintenance cost are charged at \$920 T and \$106 T, respectively. The estimated utility cost is \$3.6 million, at which operation of the compressor represents the largest part. Granted that acetic acid in the product stream is sold at a price of 550 \$/t, a minimum sale price of FDCA of 4435 \$/t is estimated.

Table 56: Operating costs of the process with the hydrocyclone

Element	Cost [\$/a]
Raw Materials	33,649,623
Catalyst Current Cost	100,000
Operating Labor Cost	920,000
Maintenance Cost	106,000
Utilities	3,604,940
Operating Charges	230,000
Plant Overhead	513,000
Subtotal Operating Costs	39,023,564
G and A Costs	3,121,885
Total Operating Costs	42,245,449

5.4.2 Process using filtration

At the process with the filter for removing solid FDCA, two versions were simulated using a flash separator and a splitter, respectively, for discharging part of the solvent at the recycling stream. Table 57 shows the total capital costs of both processes.

Table 57: Capital costs of the processes with the filter

Element	Process Flash Cost [\$]	Process Splitter Cost [\$]
Pt/ZrO ₂ catalyst	35,000,000	35,000,000
Purchased Equipment	3,026,800	2,930,500
Equipment Setting	52,349	50,569
Piping	312,881	270,548
Civil	104,756	91,003
Steel	37,653	27,706
Instrumentation	675,234	630,493
Electrical	798,385	782,360
Insulation	82,176	62,554
Paint	23,084	21,810
Other	2,213,500	2,069,900
G and A Overheads	186,667	177,415
Contract Fee	300,483	283,314
Contingencies	1,406,514	1,331,671
Total Capital Costs	44,220,480	43,729,844

The costs for the purchased equipment of the processes with the filter are comparable to that of the process with the hydrocyclone, namely \$3.03 million and \$2.93 million, respectively. In both processes using filtration, the cost of the compressor makes up 83 % of the total purchased equipment cost. The direct costs, such as catalyst, piping, civil, steel, instrumentation and electrical costs are approximately equal in all processes using crystallization. The estimated indirect costs are \$4.12 million and \$3.86 million, respectively. In the process with the flash separator, the total capital costs are \$44.22 million, whose are comparable to those of to the process with the splitter, whose are \$43.73 million.

As shown in Table 58, the total annual operating costs of the processes using filtration are \$10.5 million and \$10.1 million, respectively. Due to the high energy consumption of the flash separator, the difference of the utility costs is 14 %, whose are \$4.02 million and \$3.54 million, respectively. The raw material costs in both processes with the filter are approximately 8.5 times smaller in comparison with the process using centrifugation due to the lower acetic acid input. The HMF cost make up 95 % of the total raw material costs due to the recycling of large part of the solvent. The catalyst current costs are the same for all processes with the crystallizer, namely \$100 T.

Table 58: Operating costs of the processes with the filter

Element	Process Flash Cost [\$/a]	Process Splitter Cost [\$/a]
Raw Materials	3,828,313	3,967,191
Catalyst Current Cost	100,000	100,000
Operating Labor Cost	920,000	920,000
Maintenance Cost	112,000	109,000
Utilities	4,022,597	3,535,562
Operating Charges	230,000	230,000
Plant Overhead	516,000	514,500
Subtotal Operating Costs	9,628,911	9,276,253
G and A Costs	770,313	742,100
Total Operating Costs	10,399,224	10,018,354

The estimated minimum sale price of FDCA is 3301 \$/t at the process with the flash separator. Due to the lower utility and purchased equipment costs, FDCA sale price is 4.4 % lower in the process with the splitter, namely 3157 \$/t.

5.4.2.1 Oxidant: Use of Oxygen

Due to the high acquisition and operation costs of the compressor, pure oxygen is introduced to lower the flow rate of the oxidant. Table 59 shows the total capital costs of the process with the filter for obtaining purified FDCA, the splitter for discharging part of the solvent and pure oxygen as oxidant. The initial cost of the catalyst is the same as in all other processes. Due to the acquisition cost of the compressor of \$1.51 million, the purchased equipment cost is 37 % lower compared to the process using air as oxidant, namely \$2.14 million. The other initial expenses are in comparison with the other processes. The estimated total capital costs are \$42.39 million, whose are 3 % lower than those of the process using air.

Table 59: Capital costs of the process with the filter and pure O₂

Element	Cost [\$]
Pt/ZrO ₂ catalyst	35,000,000
Purchased Equipment	2,136,800
Equipment Setting	40,322
Piping	237,113
Civil	75,824
Steel	26,921
Instrumentation	619,437
Electrical	721,638
Insulation	64,745
Paint	18,853
Other	1,919,300
G and A Overheads	145,733
Contract Fee	255,396
Contingencies	1,127,175
Total Capital Costs	42,389,255

The total operating costs of the process using pure oxygen are \$7.46 million per year (Table 60). The raw material cost is 8 % higher compared to the other processes with the filter due to the cost of the oxygen feed of 250 \$/t. The utility

cost is reduced at 4.5 times to \$781 T compared to the process using air, due to the lower operating cost of the compressor. The maintenance cost and general and administrative cost are decreased by 25 % and 35 %, respectively, in comparison with the other process using a filter and a splitter. The estimated minimum sale price of FDCA at the process using oxygen is 2458 \$/t.

Table 60: Operating costs of the process with the filter and pure O₂

Element	Cost [\$/a]
Raw Materials	4,287,430
Catalyst Current Cost	100,000
Operating Labor Cost	920,000
Maintenance Cost	88,100
Utilities	780,741
Operating Charges	230,000
Plant Overhead	504,050
Subtotal Operating Costs	6,810,321
G and A Costs	544,826
Total Operating Costs	7,455,146

5.5 Economic analysis of the process using distillation

Table 61 shows the total capital costs of the processes with the distillation columns and a molar ratio of trioctylamine to water and acetic acid of 1/1 in the extractor. In the first process total condenser are used at both distillation columns (Figure 37), in the second one distillate of the column B18 is gaseous (Figure 45).

The purchased equipment costs of both processes are comparable, namely \$8.52 million and \$8.21 million, respectively. Most expensive elements are the distillation column B8 and the compressor, with acquisition costs of approximately \$3.5 million and \$2.3 million, respectively. The estimated cost of the distillation column B18 with a total condenser is \$521 T, whereas the same column with a partial condenser is more expensive, namely \$630 T, due to the higher temperature of the distillate. The acquisition cost of the condenser for cooling down bottoms of distillation column B18 is approximately \$500 T in both processes. Piping and instrumentation costs are approximately \$7 million and

\$1.5 million, respectively. The estimated total indirect costs in both processes are approximately \$17 million. The total capital costs in the processes using the distillation columns are \$72.8 million and \$73.1 million, respectively, whose are comparable. In both processes, the acquisition cost of the catalyst makes up approximately half of the total capital costs.

Table 61: Capital costs of the processes with distillation columns

Element	Total Condenser Cost [\$]	Gaseous Distillate Cost [\$]
Pt/ZrO ₂ catalyst	35,000,000	35,000,000
Purchased Equipment	8,515,801	8,205,500
Equipment Setting	246,600	228,741
Piping	7,020,898	7,527,220
Civil	870,582	881,367
Steel	220,740	216,919
Instrumentation	1,461,607	1,483,101
Electrical	1,003,813	997,449
Insulation	1,079,560	1,045,319
Paint	100,841	102,055
Other	9,556,801	9,643,500
G and A Overheads	804,937	811,337
Contract Fee	1,172,891	1,176,395
Contingencies	5,769,912	5,817,403
Total Capital Costs	72,824,982	73,136,304

The total operating costs of both processes with the distillation columns are shown in Table 62. Due to the trioctylamine feed stream, the raw material costs are 15 % higher in comparison with the process using crystallization and filtration, namely \$4.50 million. In the process with the total condensers at both distillation columns, the utility cost is \$209 million, which is 17 times higher compared to the process with the partial condenser at the distillation column B18. The reason is the low temperature of -82°C of the distillate in the second column, which requires high energy consumption for cooling down. Introducing a partial condenser decreases the utility cost in large part. The total operating costs of both processes with the distillation columns are \$234 million and \$20.6 million, respectively.

Table 62: Operating costs of the processes with distillation columns

Element	Total Condenser Cost [\$/a]	Gaseous Distillate Cost [\$/a]
Raw Materials	4,491,805	4,506,205
Catalyst Current Cost	100,000	100,000
Operating Labor Cost	920,000	920,000
Maintenance Cost	583,000	558,000
Utilities	209,439,449	12,024,185
Operating Charges	230,000	230,000
Plant Overhead	751,500	739,000
Subtotal Operating Costs	216,415,754	18,977,389
G and A Costs	17,313,260	1,518,191
Total Operating Costs	233,829,014	20,595,580

The estimated minimum sale price of FDCA at the process with the total condenser at both distillation columns is 56,795 \$/t, which is approximately 18 times higher in comparison with the FDCA price at the process using crystallization and filtration. The minimum sale price of FDCA at the process with the partial condenser at the second distillation column is 6674 \$/t, which is 8.5 times smaller compared to the other process using distillation.

5.5.1 Decreased trioctylamine flow rate

The total capital costs of both processes introducing trioctylamine with a ratio of trioctylamine to water and acetic acid of 1/10 in the extractor are shown in Table 63. The first process uses the flash separator B7 upstream the distillation column B8 to reduce the flow rate of the column (Figure 45). At the second one, the whole output of the extractor is fed to the distillation column B8 (Figure 49).

As shown in Table 63, the estimated purchased equipment costs are in both processes approximately \$3.9 million, whose are roughly 45 % of the equipment costs of the processes with 10 times higher trioctylamine flow rate. The most expensive element is the compressor, with an acquisition cost of \$2.24 million, which is comparable to that of the other processes. The costs for the distillation column B8 and B18 are in both processes approximately \$500 T and \$260 T, respectively. The estimated piping and instrumentation costs are \$2 million and \$1.3 million, respectively and the indirect costs make up \$8.65 million in both

processes. The total capital costs of the processes with decreased trioctylamine flow rate are \$52.77 million and \$52.34 million, whose are approximately 28 % smaller compared to the total capital costs of the processes with 10 times higher trioctylamine flow rate. The catalyst cost makes up 67 % of the total capital costs at both processes.

Table 63: Capital costs of the processes with distillation columns and reduced trioctylamine flow rate

Element	With Flash Cost [\$]	Without Flash Cost [\$]
Pt/ZrO ₂ catalyst	35,000,000	35,000,000
Purchased Equipment	3,951,500	3,855,500
Equipment Setting	73,057	70,119
Piping	2,033,242	1,996,132
Civil	306,061	293,447
Steel	122,098	110,509
Instrumentation	1,288,156	1,248,560
Electrical	808,356	803,833
Insulation	431,698	395,036
Paint	69,552	66,994
Other	5,040,301	4,942,100
G and A Overheads	345,421	336,538
Contract Fee	588,259	576,396
Contingencies	2,710,386	2,645,130
Total Capital Costs	52,768,085	52,340,294

Table 64 shows the total operating costs of both processes with decreased trioctylamine flow rate. The raw material cost and the catalyst current cost are comparable to those of the other processes using distillation. The estimated utility cost at the process with the flash separator upstream the first distillation column is \$4.86 million, which is 2.5 times smaller in comparison with the utility cost of the same process with a 10 times higher trioctylamine flow rate. Due to omitted flash separator B7, the utility cost is 3.5 % lower at the process with no flash separator upstream the distillation column B8. The estimated total operating costs of the processes with decreased trioctylamine flow rate are \$12.23 million and \$12.06 million, respectively.

Table 64: Operating costs of the processes with distillation columns and reduced trioctylamine flow rate

Element	With Flash Cost [\$/a]	Without Flash Cost [\$/a]
Raw Materials	4,467,924	4,467,924
Catalyst Current Cost	100,000	100,000
Operating Labor Cost	920,000	920,000
Maintenance Cost	199,000	201,000
Utilities	4,858,061	4,692,690
Operating Charges	230,000	230,000
Plant Overhead	559,500	560,500
Subtotal Operating Costs	11,234,485	11,072,114
G and A Costs	898,759	885,769
Total Operating Costs	12,233,244	12,057,883

The resulting minimum sale price of FDCA at the process with the flash separator upstream the first distillation column is 3946 \$/t, which is 41 % lower compared to the process with a higher trioctylamine flow stream. The estimated FDCA price at the process with no flash separator upstream the distillation column B8 is 3885 \$/t, which is comparable to the sale price of the other process.

5.6 Sensitivity analysis

Comparison of all processes producing FDCA with air as oxidant shows that the process using crystallization and filtration for removing solid FDCA, and the splitter for discharging part of the solvent has the lowest production costs, at a minimum sale price of FDCA of 3157 \$/t (Figure 43). Introducing pure oxygen as an oxidant reduces FDCA price to 2458 \$/t (Figure 44).

Sensitivity analysis was carried out for the process using pure oxygen as oxidant to investigate the impact of temperature and pressure at the crystallizer, and conversion and selectivity at the reactor. Decreasing the temperature at the crystallizer leads to lower solubility of FDCA, which increases the solid fraction of FDCA. A temperature under ambient conditions increases the cost of cooling medium, therefore a minimum temperature of 15°C was chosen. As shown in Table 65, reducing temperature from 25°C to 15°C decreases the price of FDCA

by 0.25 %. Due to the low pressure dependence of the solubility of solids, changing the pressure of the crystallizer from 2.5 bar to 8.5 bar has no impact on the minimum sale price of FDCA (Table 65) [28].

As shown in Table 65, varying conversion and selectivity of FDCA at the reactor have a slight impact on the minimum sale price of FDCA due to the recycling of HMF and the intermediates that leads to an overall FDCA yield of 99.94 %. 100 % conversion of HMF at a yield of FDCA of 97.95 % reduces the minimum sale price of FDCA by 4.42 %. Increasing the selectivity of FDCA by enhancing the FDCA yield of FFCA and DFF conversion to 50 % respectively decreases the sale price of the product by 0.10 %. Reduction of HMF conversion at estimated yields of FDCA, FFCA and DFF of 60 %, 1.33 % and 0.033 %, respectively increases the sale price of FDCA slightly by 0.10 %. Decreasing selectivity of FDCA at determined yields of HMF conversion of 60 % FDCA, 30 % FFCA and 0.75 % DFF increases the minimum sale price of the product by 0.45 %.

Table 65: Influence of temperature and pressure at the crystallizer, and conversion and selectivity at the reactor at the process with the filter and pure oxygen as oxidant

	Low Temp.	High Pres.	High Conv.	High Sel.	Low Conv.	Low Sel.
Temp. Crystallizer [°C]	15	25	25	25	25	25
Pres. Crystallizer [bar]	2.5	8.5	2.5	2.5	2.5	2.5
Yield FDCA [%]	90	90	97.95	90	60	60
Yield FFCA [%]	2	2	2	2	1.33	30
Yield DFF [%]	0.05	0.05	0.05	0.05	0.033	0.75
Conv. FFCA to FDCA [%]	10	10	10	50	10	10
Conv. DFF to FDCA [%]	10	10	10	50	10	10
Change of FDCA price [%]	-0.25	-0.04	-4.42	-0.10	+0.10	+0.45

The estimated annual product flow rate of the process with the crystallizer and the filter for obtaining solid FDCA and pure oxygen as oxidant is 4830 t/a. Doubling plant capacity reduces the minimum sale price of FDCA by 14.7 % to 2095 \$/t. A three times larger plant decreases the product sale price by 19.3 % to 1983 \$/t FDCA.

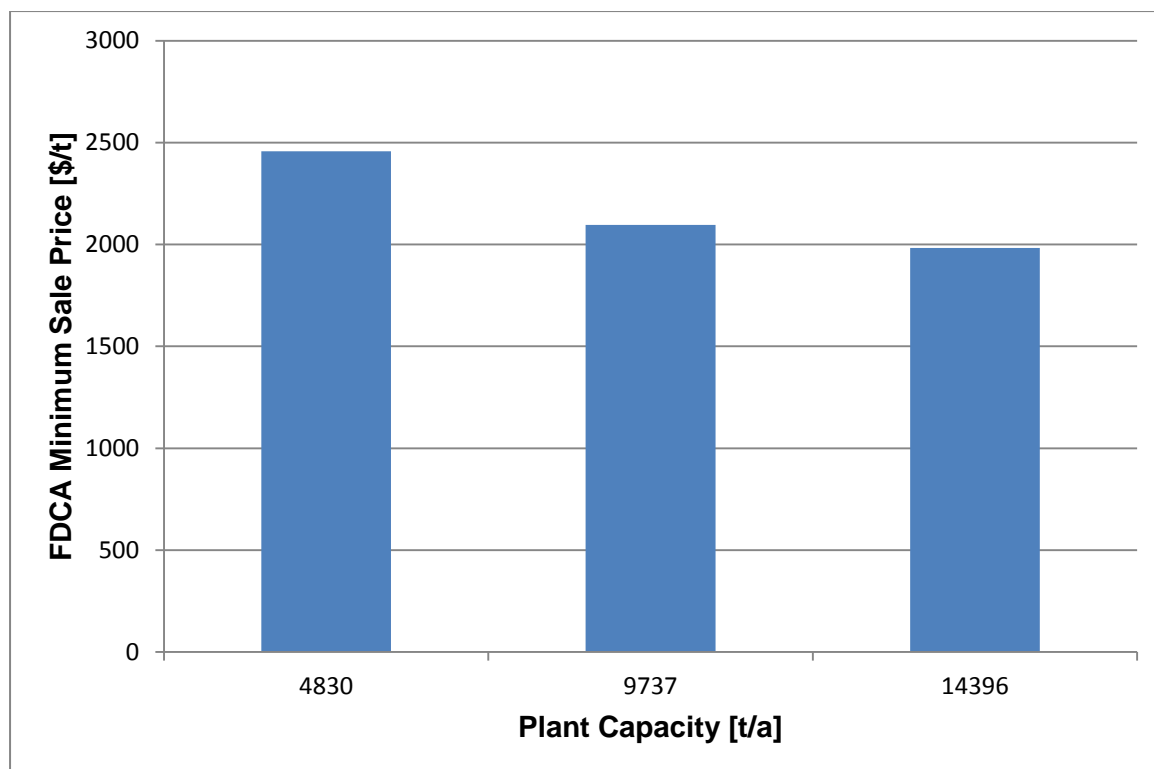


Figure 51: Minimum sale price of FDCA as a function of the plant capacity

Catalyst cost makes up 19 % of the total annual costs of the process due to high acquisition cost of the catalyst. Decreasing the catalyst cost by half of the original estimated catalyst cost reduces the minimum sale price of FDCA by 7.79 % to 2266 \$/t. Doubling the catalyst cost increases the FDCA price by 15.58 % to 2841 \$/t.

As shown in Figure 52, 39 % of the annual costs is the cost of HMF. Hence the price of HMF has a big impact on the minimum sale price of FDCA. Due to recycling of large parts of acetic acid and oxygen, their prices have a small influence on the total production cost of FDCA, namely 2 % and 4 %, respectively.

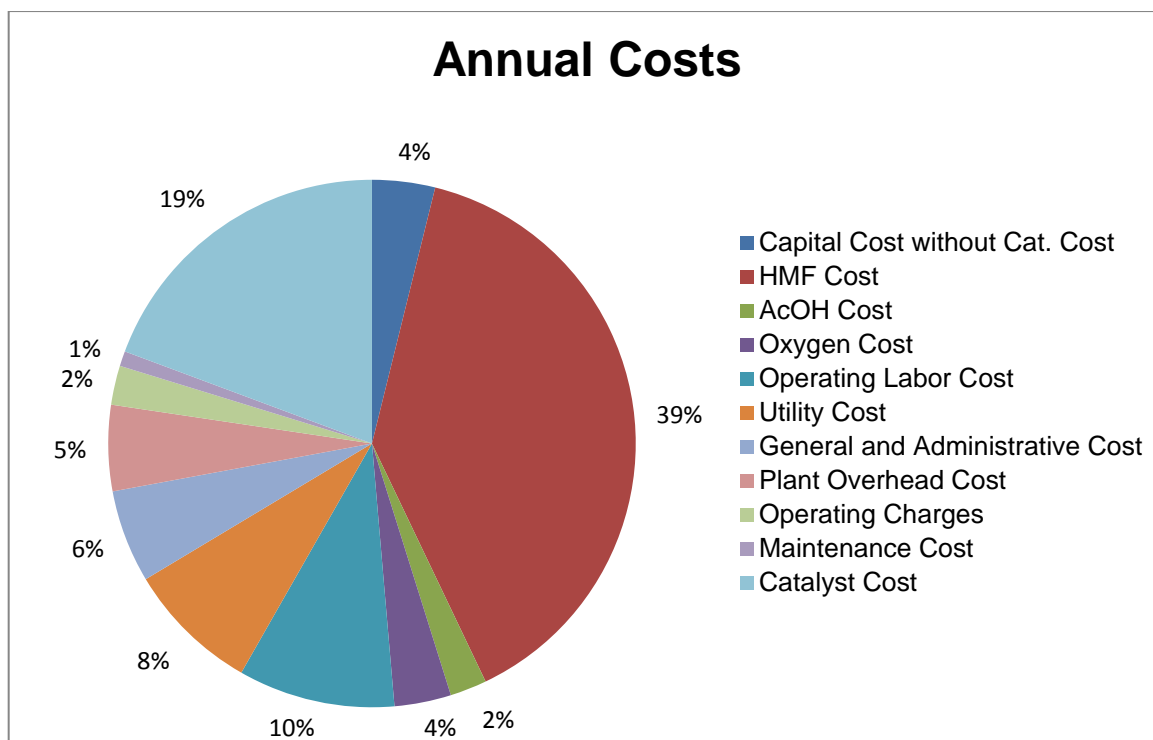


Figure 52: Annual costs of the process with the crystallizer and the filter using pure oxygen as oxidant

Figure 53 shows the sale price of FDCA as a function of the raw material market prices. Oxygen market price of 500 \$/t instead of 250 \$/t increases FDCA minimum sale price by 88 \$. Reducing the price of acetic acid from 550 \$/t to 400 \$/t decreases FDCA sale price by 15 \$/t, while reducing the market price of HMF to 500 \$/t leads to a minimum sale price of FDCA of 1936 \$/t, which is approximately 45 % higher than the market price of purified terephthalic acid [42].

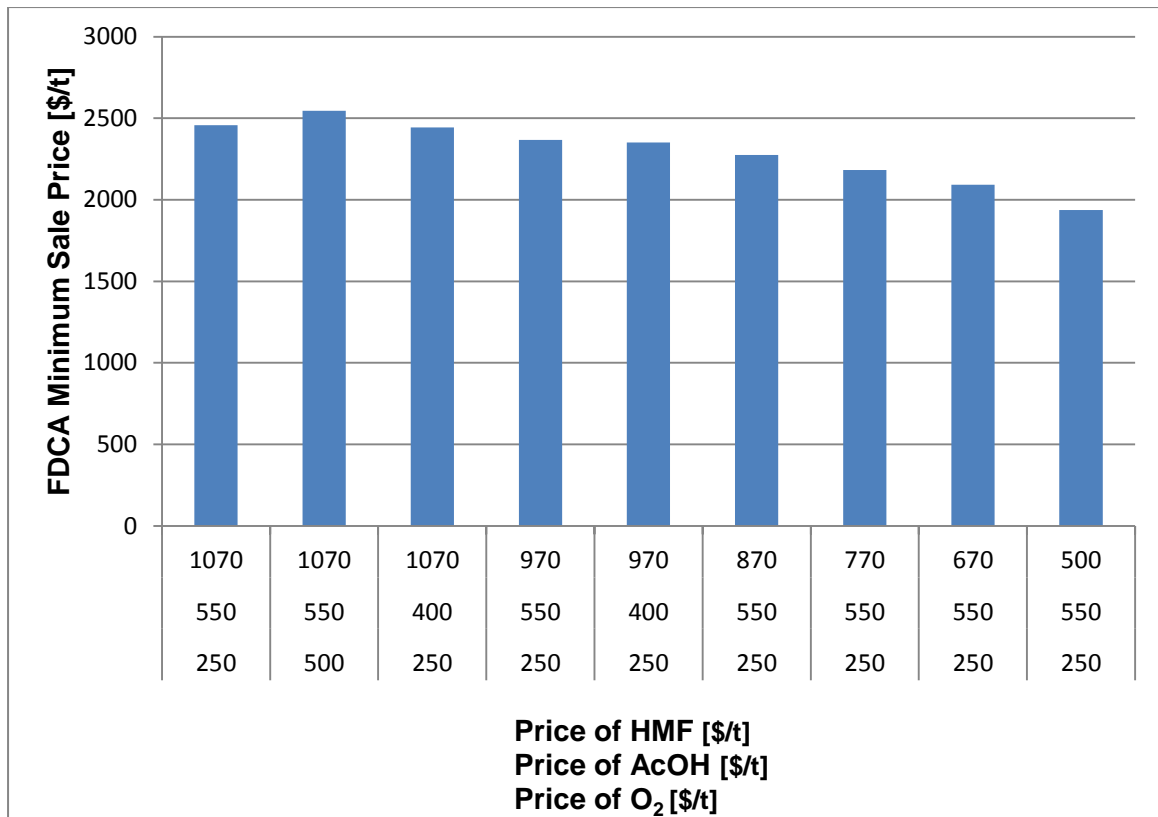


Figure 53: Minimum sale price of FDCA as a function of raw material market prices

6 Summary and Outlook

In this thesis the processes used to convert HMF to FDCA in a continuous steady state operation are developed and simulated using Aspen [1]. A tubular reactor was chosen to model catalytic oxidation of HMF to FDCA at 10 bar and 100°C. Since no commercial processes exist to produce FDCA in large quantities, further research is needed on the continuous steady state catalytic reaction of HMF to FDCA in scaled up processes. Attention should be paid on the reactor design and the oxidant feed to minimize the size and cost of the reactor. Introducing a new solvent with higher solubility of FDCA also has an impact on the reactor size. For process simulation, reaction kinetics and thermochemistry of the HMF conversion to FDCA is crucial. Further research is necessary to obtain data of the physical properties of FDCA for the process simulation.

The high melting point of FDCA (342°C) requires high process temperatures and thus high energy demand in the processes producing liquid FDCA. Solvents with high boiling points have to be introduced those are expensive in comparison to aqueous solutions. For separating FDCA from the solvent, distillation has to be used that require high temperatures for removing FDCA.

At the simulated processes, trioctylamine is introduced at the extractor to enable FDCA purification at the distillation column. Due to missing data of the solubility of FDCA in trioctylamine, two different flow rates of trioctylamine were investigated. The specified ratios of trioctylamine to water and acetic acid are 1/1 and 1/10, respectively.

Further research is needed to investigate the solubility of HMF, FDCA, DFF and FFCA in trioctylamine. At the simulations, the solubility was calculated by using estimated properties of the components. Optimization has to be done to minimize the trioctylamine flow rate at constant plant capacities.

Due to a distillate temperature of -82°C at the distillation column for separating trioctylamine from acetic acid, high utility cost for cooling down the distillate is required. To minimize the process costs, a partial condenser was introduced at the distillation column to produce gaseous distillate and reduce cost for cooling.

Process optimization at the distillation columns is required to reduce costs for the separation processes. Increasing number of stages and reflux ratio could lead to high purified FDCA in the bottoms of the first distillation column.

Due to the high capital cost of the required equipment and the catalyst, high utility and raw material costs, the resulting minimum sale prices of FDCA at the processes with the high and the low trioctylamine flow rate are 6674 \$/t and 3885 \$/t, respectively.

At the processes with the crystallizer, FDCA is successfully solidified at ambient conditions. Experiments on the crystallization of FDCA in aqueous acetic acid solution should be done to investigate the solubility of FDCA and to get data on the growth kinetics and the nucleation rate to simulate size dependent growth rate. As a result, models of the particle size distribution could be estimated for the average crystal size of FDCA, which is required for layout design of the filter and the hydrocyclone.

Using centrifugation for removing part of the solvent, downstream processes have to be investigated to recycle the acetic acid in the product flow stream due to its market price of 550 \$/t [40]. Assuming that the acetic acid is sold, the estimated minimum sale price of FDCA is 4435 \$/t. The calculated solid fraction in the product stream is 3 wt%. Purified FDCA could be obtained by installing a filter or a dryer downstream the hydrocyclone.

Due to the larger recycling part of the solvent compared to the process with the hydrocyclone, the resulting minimum sale price of FDCA is 29 % lower at the process with the filter, namely 3157 \$/t. For detailed layout design of the filter and storage of the filter cake, research is needed on the particle size distribution of FDCA at the crystallizer. To purify the FDCA filter cake, a dryer could be installed downstream the filter.

At the processes producing solid FDCA, attention should be paid on the solid fraction in the product stream at the process layout. Sediments and abrasions cause many problems under operating conditions. Due to the low solubility of FDCA in water, large part of the solvent and huge equipment in comparison to the FDCA fraction are required for maintaining liquid flows. Therefore, the operating costs and the capital costs are high for a comparatively low plant capacity.

One approach for diminishing the costs at the processes is decreasing the oxidant flow rate. Due to the large ratio of the liquid to the oxidant in the reactor, huge amount of air is required for the process. Hence the compressor represents a large part of the total capital and operating costs. One opportunity for decreasing the oxidant flow stream is to use pure oxygen instead of air, which reduces the minimum sale price of FDCA by 22.6 % from 3175 \$/t to 2458 \$/t.

Due to the low LHSV of 3 h^{-1} , a huge amount of catalyst is required in comparison to the FDCA flow rate. Using a 5 % Pt catalyst involves high acquisition cost due to the high price of platinum. Research has to be done on processes using different catalysts at varying LHSVs to minimize the catalyst cost.

The cost of raw materials, especially of HMF, has a big impact on the sale price of FDCA. Up to 54 % of the total operating cost is due to HMF cost. Increasing the production output, improved technologies of the processes, and lower cost of fructose and glucose feedstock as raw materials for HMF production can lead to lower HMF price, which is comparable to the market prices of chemicals derived from petroleum.

On the other hand, improving selectivity of FDCA and conversion of HMF does not implicate a lower minimum sale price of FDCA. The reason is the recycling of HMF and the intermediates to the reactor. Since no other byproducts are formed, the overall yield of FDCA is close to 100 %. Additional work is needed to investigate the formed byproducts of the catalytic HMF conversion to FDCA at scaled up processes.

To obtain a competitive market price compared to petroleum based chemicals, process optimization and decreased HMF cost are required. One opportunity to minimize process costs is to reduce stream flows of the solvent and the oxidant relative to FDCA flow.

Further research has to be done on subsequent processing to transform FDCA to PEF or purified terephthalic acid. Gandini et al. [11] describe FDCA reaction with ethylene glycol to form FDCA dimethyl ester, which is converted to PEF and ethylene glycol via transesterification. Due to similar properties to PET, PEF could be used to replace PET to manufacture biobased products. Research is

needed to investigate properties of PEF in its application areas. Studies on the toxicity of PEF are necessary for its possible usage as starting material for bottles.

According to the patent of Gong [10], FDCA is reacting with ethylene to form water and terephthalic acid. Process optimizations have to be done due to the small yield of FDCA conversion to terephthalic acid of 0.14 %. Biobased terephthalic acid and ethylene glycol could be used to produce 100 % biobased PET. Due to existing market and logistic infrastructure of PET, the adjustment to biobased PET would not implicate higher expenses.

7 Bibliography

1. Aspen Plus V7.3 (25.0.4987). 2011, Aspen Technology, Inc.
2. Aspen Process Economic Analyzer V.7.3.1 (19.0.0.2556). 2011, Aspen Technology, Inc.
3. Román-Leshkov, Y., et al., *Production of dimethylfuran for liquid fuels from biomass-derived carbohydrates*. Nature, 2007. **447**: p. 982 - 986.
4. Kazi, F.K., et al., *Techno-economic analysis of dimethylfuran (DMF) and hydroxymethylfurfural (HMF) production from pure fructose in catalytic processes*. Chemical Engineering Journal, 2011. **169**: p. 329 - 338.
5. Davis, S.E., et al., *Oxidation of 5-hydroxymethylfurfural over supported Pt, Pd and Au catalysts*. Catalysis Today, 2011. **160**: p. 55 - 60.
6. Tong, X., Y. Ma, and L. Yongdan, *Biomass into Chemicals: Conversion of sugars to furan derivatives by catalytic processes*. Applied Catalysis A: General, 2010. **385**: p. 1 - 13.
7. Assary, R.S., et al., *Predicted thermochemistry for chemical conversions of 5-hydroxymethylfurfural*. Chemical Physics Letters, 2010. **497**: p. 123 - 128.
8. Ribeiro, M.L. and U. Schuchardt, *Cooperative effect of cobalt acetylacetonate and silica in the catalytic cyclization and oxidation of fructose to 2,5-furandicarboxylic acid*. Catalysis Communications, 2003. **4**: p. 83 - 86.
9. Moreau, C., M.N. Belgacemb, and A. Gandini, *Recent catalytic advances in the chemistry of substituted furans from carbohydrates and the ensuing polymers*. Topics in Catalysis, 2004. **27**: p. 11 - 30.
10. Gong, W.H., *Terephthalic acid composition and process for the production thereof*, 2008, US: 7385081.
11. Gandini, A., et al., *The Furan Counterpart of Poly(ethylene terephthalate): An Alternative Material Based on Renewable Resources*. Journal of Polymer Science, Part A: Polymer Chemistry, 2008. **47**: p. 295 - 298.
12. Schmidt, L.D. and P.J. Dauenhauer, *Hybrid routes to biofuels*. Nature, 2007. **447**: p. 914 - 915.
13. Chidambaram, M. and A.T. Bell, *A two-step approach for the catalytic conversion of glucose to 2,5-dimethylfuran in ionic liquids*. Green Chemistry, 2010. **12**: p. 1253 - 1262.
14. Bozell, J.J. and G.R. Petersen, *Technology development for the production of biobased products from biorefinery carbohydrates - the US Department of Energy's "Top 10" revisited*. Green Chemistry, 2010. **12**: p. 539 - 554.
15. Werpy, T. and G. Petersen, *Top Value Added Chemicals from Biomass*. 2004.
16. *Guidechem - HMF*. [cited 2012 March 26]; Available from: <http://www.guidechem.com/cas-67/67-47-0.html>.
17. Lilga, M.A., et al., *Hydroxymethyl furfural oxidation methods*, 2012, US: 8193381.
18. *Guidechem - FDCA*. [cited 2012 March 26]; Available from: <http://www.guidechem.com/cas-323/3238-40-2.html>.
19. Casanova, O., S. Iborra, and A. Corma, *Biomass into Chemicals: Aerobic Oxidation of 5-Hydroxymethyl-2-furfural into 2,5-Furandicarboxylic Acid with Gold Nanoparticle Catalysts*. ChemSusChem, 2009. **2**: p. 1138 - 1144.
20. Koopman, F., et al., *Efficient whole-cell biotransformation of 5-(hydroxymethyl)furfural into FDCA, 2,5-furandicarboxylic acid*. Bioresource Technology, 2010. **101**: p. 6291 - 6296.
21. *World of Plastic*. [cited 2012 March 28]; Available from: <http://www.worldofplastic.net/PolyethyleneTerephthalate.htm>.
22. Ullmann, F., *Ullmann's encyclopedia of industrial chemistry* 1986.
23. Partenheimer, W. and V.V. Grushin, *Synthesis of 2,5-Diformylfuran and Furan-2,5-Dicarboxylic Acid by Catalytic Air-Oxidation of 5-Hydroxymethylfurfural. Unexpectedly*

- Selective Aerobic Oxidation of Benzyl Alcohol to Benzaldehyde with Metal/Bromide Catalysts*. *Advanced Synthesis & Catalysis*, 2001. **343**: p. 102 - 111.
24. Gorbanev, Y.Y., et al., *Gold-Catalyzed Aerobic Oxidation of 5-Hydroxymethylfurfural in Water at Ambient Temperature*. *ChemSusChem*, 2009. **2**: p. 672 - 675.
 25. Kröger, M., U. Prüße, and K.-D. Vorlop, *A new approach for the production of 2,5-furandicarboxylic acid by in situ oxidation of 5-hydroxymethylfurfural starting from fructose*. *Topics in Catalysis*, 2000. **13**: p. 237 - 242.
 26. Munoz de Diego, C., M.A. Dam, and G.J.M. Gruter, *Method for the preparation of 2,5-furandicarboxylic acid and esters thereof*, 2001, WO: 2011/043660.
 27. Munoz de Diego, C., et al., *Method for the preparation of 2,5-furandicarboxylic acid and for the preparation of the dialkyl ester of 2,5-furandicarboxylic acid*, 2011, WO: 2011/043661.
 28. Perry, R.H. and D.W. Green, *Perry's Chemical Engineers' Handbook*. 7th ed. 1999, New York: McGraw-Hill.
 29. *NIST Database*. [cited 2012 May 03]; Available from: <http://webbook.nist.gov/cgi/cbook.cgi?ID=C3238402&Units=SI&Mask=4#Thermo-Phase>.
 30. *Aspen Plus Help*. 2012, Aspen Technology, Inc.
 31. *SciFinder*. [cited 2012 April 27]; Available from: <https://scifinder.cas.org/scifinder/view/scifinder/scifinderExplore.jsf>.
 32. Brient, J.A., *Removal of acidic organic contaminants from refinery waste water*, 1998, US: 5705074.
 33. Tolan, J.S., B. Foody, and V. Anand, *Recovery of volatile carboxylic acids by a stripper-extractor system*, 2011, WO: 2011/022811.
 34. Tolan, J.S., B. Foody, and V. Anand, *Recovery of volatile carboxylic acids by extractive evaporation*, 2011, WO: 2011/022812.
 35. Galaction, A.I., L. Kloetzer, and D. Cascaval, *Influence of Solvent Polarity on the Mechanism and Efficiency of Formic Acid Reactive Extraction with Tri-n-Octylamine from Aqueous Solutions*. *Chemical Engineering & Technology*, 2011. **34**: p. 1341 - 1346.
 36. Jain, S.K. and S. Chand, *Removal/recovery of carboxylic acids from waste water*. *Chemical Engineering World*, 1995. **30**: p. 55 - 61.
 37. *Chemical Land*. [cited 2012 May 10]; Available from: <http://www.chemicaland21.com/industrialchem/organic/TRIOCTYLAMINE.htm>.
 38. *The Chemical World*. [cited 2012 May 10]; Available from: <http://www.thechemicalworld.com/products/detail.asp?id=52264>.
 39. Douglas, J.M., *Chemical Engineering Series - Conceptual Design of Chemical Processes*. 1988.
 40. *Alibaba AcOH*. [cited 2012 April 18]; Available from: <http://price.alibaba.com/price/priceLeafCategory.htm?spuld=100073989&categoryId=100001625>.
 41. *Alibaba Pt Al2O3*. [cited 2012 July 18]; Available from: http://www.alibaba.com/product-gs/558966580/Platinum_Alumina_Catalyst.html.
 42. *ICIS Pricing*. [cited 2012 July 02]; Available from: http://www.icispricing.com/il_shared/Samples/SubPage177.asp.
 43. Seader, J.D. and E.J. Henley, *Separation Process Principles*. 1998, New York: John Wiley & Sons, Inc.
 44. Luyben, W.L., *Distillation Design and Control using Aspen Simulation*. 2006, Hoboken: John Wiley & Sons, Inc.
 45. Leubner, I.H., *Precision Crystallization - Theory and Practise of Controlling Crystal Size*. 2010, Boca Raton: CRC Press.

46. Strickland-Constable, R.F., *Kinetics and Mechanism of Crystallization*. 1968, London: Academic Press.
47. Garside, J. and S.J. Jancic, *Prediction and measurement of crystal size distributions for size-dependent growth*. *Chemical Engineering Science*, 1978. **33**: p. 1623 - 1630.
48. Mydlarz, J. and A.G. Jones, *On modelling the size-dependent growth rate of potassium sulphate in an MSMPR crystallizer*. *Chemical Engineering Communications*, 1990. **90**: p. 47 - 56.
49. Abegg, C.F., J.D. Stevens, and M.A. Larson, *Crystal Size Distributions in Continuous Crystallizers when Growth Rate is Size Dependent*. *AIChE Journal*, 1968. **14**: p. 118 - 122.
50. Randolph, A.D. and M.A. Larson, *Theory of Particulate Processes: Analysis and Techniques of Continuous Crystallization*. 2nd ed. 1988, San Diego: Academic Press.

8 Appendix: Theory of Simulated Unit Operations

8.1 Distillation

Distillation separates a feed containing two or more components into two products, the distillate and the bottoms, whose fractions are different to that of the feed. The separation requires a liquid and a gaseous phase that are in equilibrium, where concentrations of the components differ in each phase due to different volatilities. For improving separation, multiple trays are necessary, stacked one above the other and varying in temperature to form a column (Figure 54). At one tray feed stream is introduced, at which due to different densities, liquid is running down and vapor is flowing up in every stage. Stages above the feed tray are called rectifying section and stages below are the stripping section. Liquid that reaches bottom of the distillation column is partially vaporized at the reboiler returning to the column and partially providing the product bottoms. Vapor that reaches the top of the column is partially or totally condensed in the overhead condenser and led to the reflux drum. One part is sent as reflux stream back to the distillation column and the other part is forming the product stream distillate, which could be liquid or gaseous. The ratio between reflux stream and distillate is called reflux ratio. Fractions introduced in the distillation column are separated by their volatility, which means that components with higher boiling points are preferably going down to the bottoms and components with a lower boiling point are concentrating in the distillate. [28, 43]

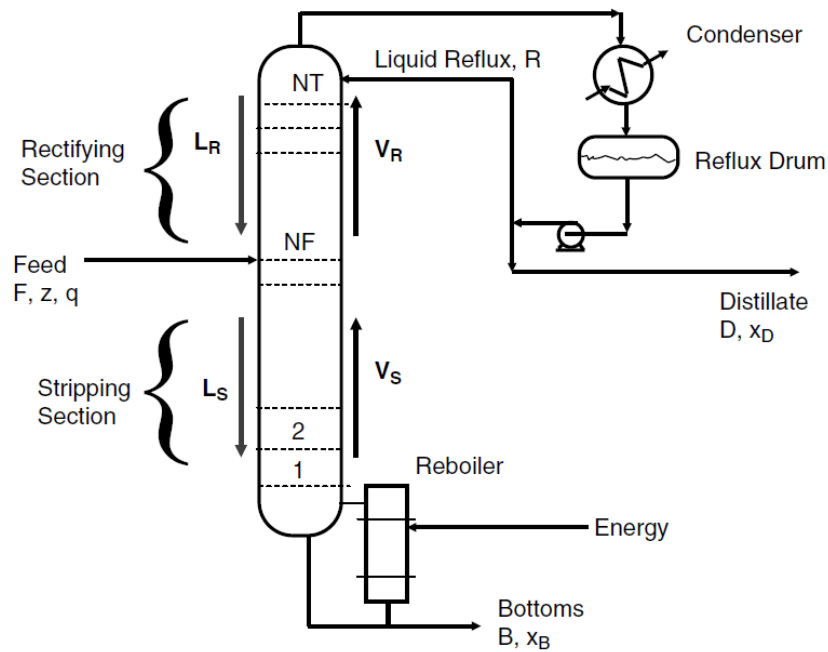


Figure 54: Schematic illustration of a distillation column with reboiler and total condenser [44]

For calculating the distillation column, mass balance and component balance for the rectifying section and the stripping section of the distillation column have to be set up.

Figure 55 shows the flow rates and mass fractions of all inputs and outputs of the rectifying section.

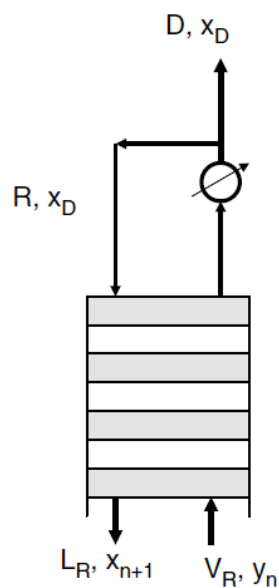


Figure 55: Mass flows and fractions of the rectifying section for component balance [44]

Component balance of the rectifying section leads to:

$$V_R \cdot y_n = L_R \cdot x_{n+1} + D \cdot x_D \quad 8-1$$

$$y_n = \frac{L_R}{V_R} \cdot x_{n+1} + \frac{D \cdot x_D}{V_R} \quad 8-2$$

where V_R is the vapor flow rate, y_n is the mass fraction of the component in the vapor phase of the n^{th} stage, L_R is the liquid flow rate, x_{n+1} is the mass fraction of the component in the liquid phase of the $(n+1)^{\text{th}}$ stage, D is the distillate flow rate and x_D the mass fraction of the component in the distillate.

Figure 56 shows the flow rates and mass fractions of all inputs and outputs of the stripping section.

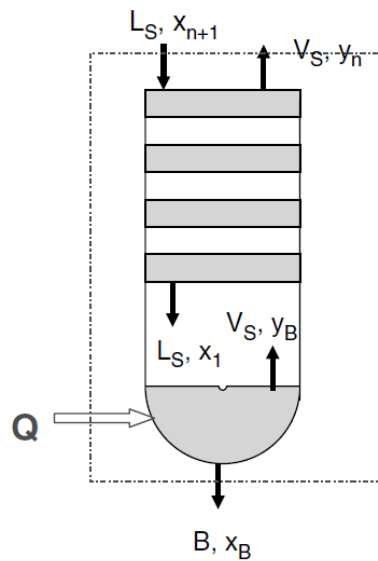


Figure 56: Mass flows and fractions of the stripping section for component balance [44]

Component balance of the stripping section leads to:

$$L_S \cdot x_{n+1} = B \cdot x_B + V_S \cdot y_n \quad 8-3$$

$$y_n = \frac{L_S}{V_S} \cdot x_{n+1} + \frac{B \cdot x_B}{V_S} \quad 8-4$$

where L_S is the liquid flow rate, x_{n+1} is the mass fraction of the component in the $(n+1)^{\text{th}}$ stage, B is the bottoms, x_B is the mass fraction of the component in the bottoms, V_S is the vapor flow rate and y_n is the mass fraction of the component in the n^{th} stage.

Using 8-2 and 8-4, rectifying operation line (ROL) and stripping operation line (SOL) are drawn in the McCabe-Thiele diagram as shown in Figure 57, in which ROL and SOL intersect 45° line at x_D and x_B , respectively. Line q is connecting the intersection of ROL and SOL with the 45° line at feed composition z . [44]

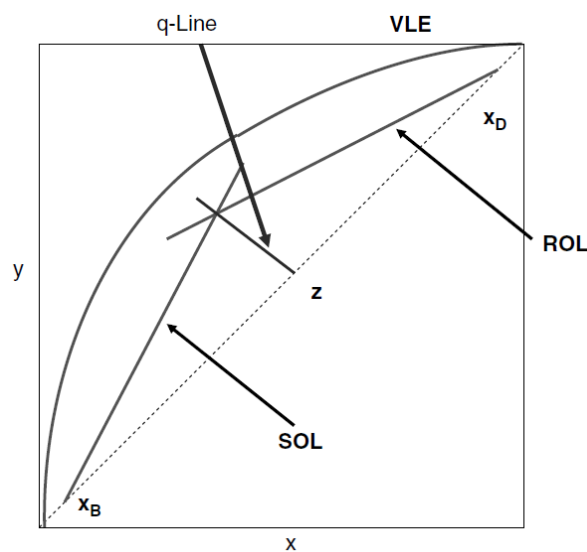


Figure 57: SOL, ROL and q-line in the McCabe-Thiele diagram [44]

In Figure 58, the vertical line from x_B intersects with the equilibrium line at point 1, which represents vapor concentration in the reboiler. Horizontal line from point 1 to SOL intersects at the liquid concentration in stage 1. Vertical line from that point to the equilibrium line intersects at point 2 at the vapor concentration in stage 1 and so on. Every step represents one stage at the distillation column. Therefore, this method is used for estimating the number of trays. [28]

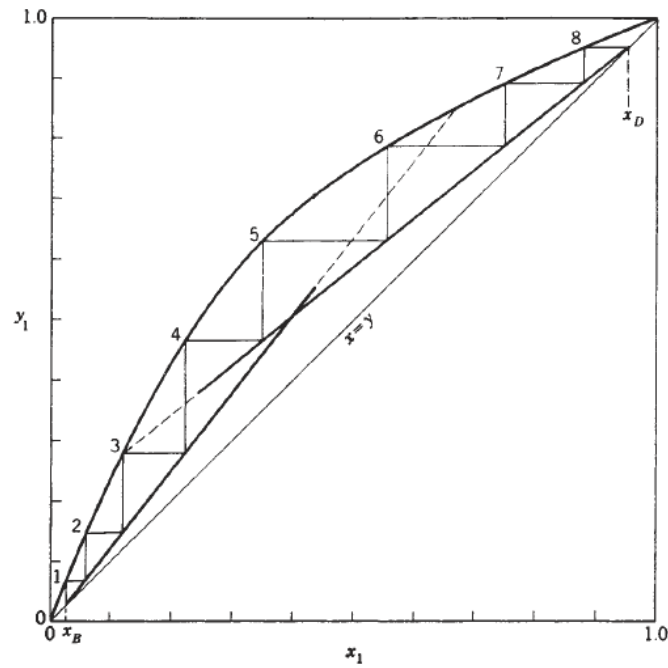


Figure 58: Graphical evaluation of the number of stages in McCabe-Thiele diagram using SOL and ROL [28]

Limiting cases are shown in Figure 59 and Figure 60. First represents a distillation column with total reflux, which means that the distillate is zero and minimum stages are required. Figure 60 shows a distillation column with no reflux, which leads to infinite number of stages. [28]

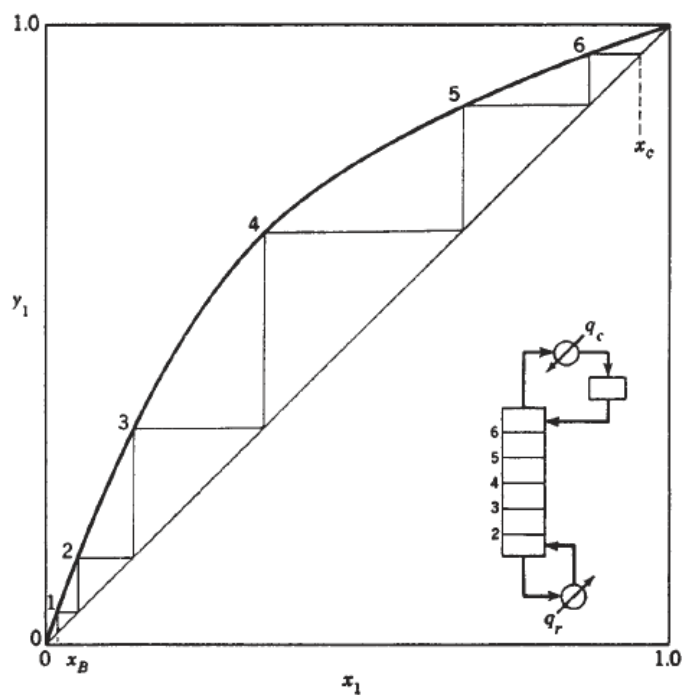


Figure 59: Minimum number of stages at a distillation column with total reflux (distillate is zero) [28]

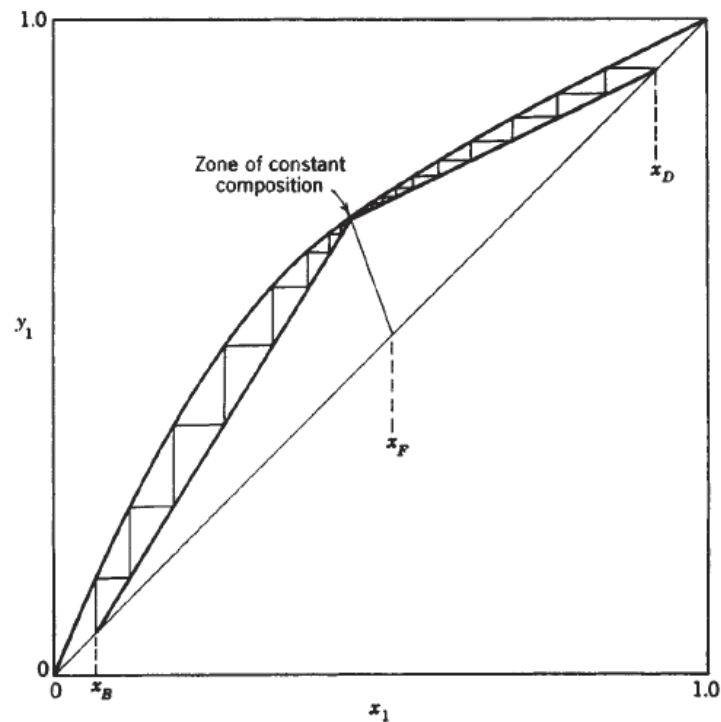


Figure 60: Infinite number of stages at a distillation column with no reflux [28]

8.2 Liquid-liquid extraction

Liquid-liquid extraction is used for separating components due to their different solubility in two immiscible liquids. An example is the transfer of a solute substance into a second liquid that is not miscible with the other solvent. To achieve better results, liquid-liquid extraction in multiple stages is preferred, at which each stage is in phase equilibrium, which implies that the activity of any component is the same in each liquid phase. Figure 61 shows crosscurrent and countercurrent liquid-liquid extraction. Feed stream F contains the component to be extracted from the liquid F, stream S is the solvent used for the extraction, the raffinate R is the liquid from which the component is extracted and E contains the solvent plus the extracted component. [28]

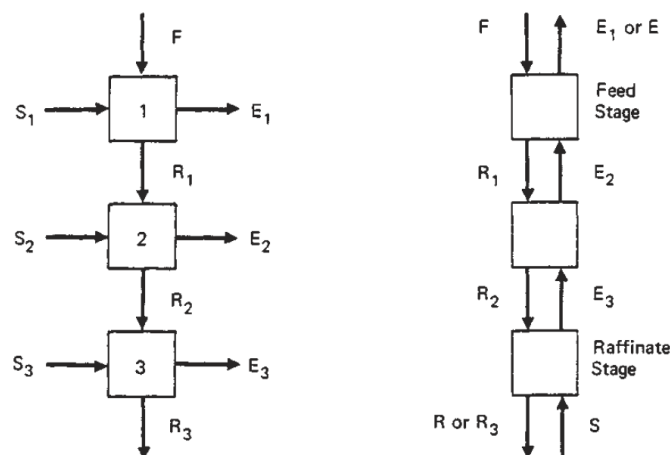


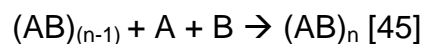
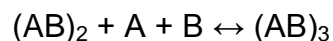
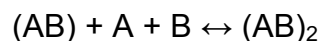
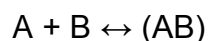
Figure 61: Schematic illustration of crosscurrent and countercurrent liquid-liquid extraction [28]

8.3 Crystallization

In crystallization, assumptions are made on the nascent crystal size or the nucleation time, which is defined as the time from the beginning of the addition of the reactant to the time the slurry attains a given density. This density only reveals on the number and the size of the crystals, nucleation stopped earlier. Clouding is the result of the growth of small crystals and occurs after nucleation. [45]

8.3.1 Classical Nucleation Model

The classical nucleation model was originally developed for explaining condensation. It was adapted to crystallization for describing several steps to gain a stable critical cluster $(AB)_n$, at which size the nucleus has the same probability for growing or dissolving. [45]



Critical nucleus size is depending on its thermodynamic stability.

8.3.2 Continuous Crystallization

For simulating continuous crystallization, the continuous stirred tank reactor (CSTR), or mixed-suspension, mixed-product-removal (MSMPR) system, and the stop flow system are common. [45]

The yield is depending on the reaction addition rate and the residence time, which is calculated by the ratio of the reaction volume in the reactor to the sum of inputs or outputs, respectively. Crystal population is conditioned by the reaction conditions, solubility, temperature, reactant addition rate, presence of restrainers, or ripeners, and the residence time. The steady-state suspension density may also influence the crystal population. [45]

8.3.3 Nucleation

Crystal nucleation is a combination of different processes, implying homogenous nucleation and nucleation due to contact between crystals and other crystals, walls of the container and the impeller of the reactor. The number of formed crystals B^0 is calculated by the sum of the nucleation rates of crystal-impeller contacts (B_e), crystal-crystal contacts (B_c) and the number of new crystals due to the driving force of supersaturation (B_{ss}). [28]

$$B^0 = B_{ss} + B_e + B_c \quad 8-5$$

Supersaturation S is defined as the difference between the solute concentration C and the solute saturation concentration C_s . [45]

$$S = C - C_s \quad 8-6$$

Predominant effects on forming new crystals in processes with low supersaturation are contacts between crystals. Another approach for calculating nucleation rate is by using supersaturation or growth rate. The number of new crystals B^0 is a power function to the supersaturation, where k and i are constants. [28]

$$B^0 = k \cdot S^i \quad 8-7$$

8.3.4 Crystal Growth Rate

Crystal growth appears on the face of a crystal, and is determined by the diffusion behavior of the solvent and the manner of integrating the new molecules on the surface. For a crystal with the characteristic length L the growth rate over time interval is defined as [28]:

$$G = \lim_{\Delta L \rightarrow 0} \frac{\Delta L}{\Delta t} = \frac{dL}{dt} \quad 8-8$$

McCabe developed the delta L law indicating that the growth rate of similar crystals of the same material in the same solution is the same. [28]

Growth rate is depending on mass transfer from the bulk of the solution to the surface of the crystal and the growth of the surface itself. Mass transfer is calculated by the difference of the concentration in the bulk of the solution (C) and the concentration on the surface of the crystal (C_c), where J is the molecular flux and k_1 the mass transfer coefficient. [46]

$$J = k_1 \cdot (C - C_c) \quad 8-9$$

Reaction on the surface of the crystal is determined by the difference of the concentration on the surface of the crystal (C_c) and the saturated concentration (C_s), where k_2 is a constant. [46]

$$J = k_2 \cdot f(C_c - C_s) \quad 8-10$$

In stirred reactors, concentrations in the bulk of the solution and on the surface of the crystal are equal and the growth rate is defined by [46]:

$$J = k_2 \cdot f(S) \quad 8-11$$

Analyses of experimental data lead to the empirical form [46]:

$$J = k_3 \cdot S^m \quad 8-12$$

where k_3 and m are constants determined by experimental results. J is directly proportional to the growth rate that leads to the equation [46]:

$$G = k_4 \cdot S^m \quad 8-13$$

where G is the rate of growth of the crystals, S is the supersaturation of the solution and k_4 is a constant. 8-7 and 8-13 lead to the correlation between growth rate G and nucleation B^0 , where k_5 and n are constants. [28]

$$B^0 = k_5 \cdot G^n \quad 8-14$$

Another approach for nucleation includes beside supersaturation or growth rate the density of the crystal slurry (M_T), where k_6 , n and p are constants. [28]

$$B^0 = k_6 \cdot G^n \cdot M_T^p \quad 8-15$$

In stirred reactors, nucleation is a power function to the rotation rate of the impeller (R) and is defined as [28]:

$$B^0 = k_7 \cdot G^n \cdot M_T^p \cdot R^q \quad 8-16$$

where k_7 , n , p and q are constants.

8.3.4.1 Size-dependent Growth Rate

In most crystallization processes, resistance in consequence of surface reaction is significant, which leads to growth rates determined by reaction using McCabe's delta L law. At appearance of size-dependent growth rate, McCabe's delta L law cannot be used. For mixed-suspension, mixed-product-removal (MSMPR) crystallizers three size-dependent growth rate equations were developed, proposed by Bransom in 1960 [47, 48]:

$$G(L) = a \cdot L^b \quad 8-17$$

by Canning and Randolph in 1967 [47, 48]:

$$G(L) = G^0 \cdot (1 + a \cdot L^b) \quad 8-18$$

and by Abegg, Stevens and Larson in 1968 [49]:

$$G(L) = G^0 \cdot (1 + a \cdot L)^b \quad \text{for } b < 1 \text{ and } L \geq 0 \quad 8-19$$

Where G^0 is the growth rate at zero size, depending on temperature, supersaturation and agitation etc., L is the characteristic length of the crystal, and a and b are constants. Model for calculating size-depending growth rate should imply following points [47, 48]:

- Calculation of continuous growth rate function including boundary condition for $L = 0$.
- Estimation of finite growth rates for nuclei ($G(0) \neq 0$)
- Compliance with population balance, at which calculated moments of population density distributions should converge.
- Generation of appropriate growth models for crystallization with a growth rate proportional to crystal sizes.
- For small crystal sizes, model for calculating growth rate should not diverge greatly from delta L law.

Equation by Abegg, Stevens and Larson is the only equation that fulfills these points. [47]

8.3.5 Population Balance

The population density n_i is the number of particles in a specific size range (ΔN_i) divided by this size range (ΔL_i). [28]

$$n_i = \frac{\Delta N_i}{\Delta L_i} \quad 8-20$$

For infinitesimal small size ranges the population density n is defined as [28]:

$$n = \frac{dN}{dL} \quad 8-21$$

Figure 62 shows the determination of the population density (n). [28]

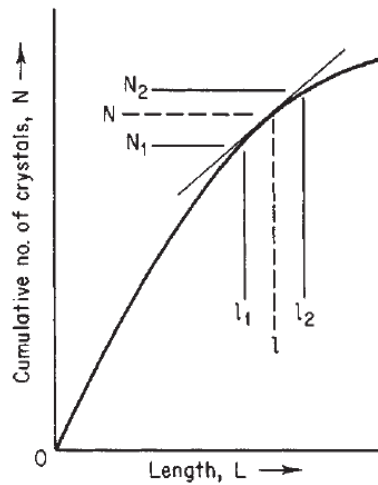


Figure 62: Population density (n): Number of particles in a specific size range (ΔN_i) divided by this size range (ΔL_i) [28]

For calculating the population density, the macroscopic population balance is required. [50]

$$\frac{\partial n}{\partial t} + \frac{\partial(Gn)}{\partial L} + D - B + n \frac{d(\log V)}{dt} = - \sum_k \frac{n_k \cdot Q_k}{V} \quad 8-22$$

where n is the population density, t is the time, G the growth rate, L the characteristic length of the crystal, D and B are the empirical death and birth density functions depending on position, $d(\log V)/dt$ is the logarithmical solids-free liquid volume change at its free surface per time, and V is an external phase space volume having inputs and outputs of the flow rate Q_k and the population density n_k . [50]

For steady state systems, d/dt terms and the birth and death functions are equal to zero. For introducing the crystal residence time $\tau = V/Q$ and assuming McCabe's delta L law, the equation is simplified to [50]:

$$G \cdot \frac{dn}{dL} + \frac{n}{\tau} = 0 \quad 8-23$$

Using the population density of nuclei (n^0), integral of 8-23 is formed. [28]

$$\int_{n^0}^n \frac{dn}{n} = - \int_0^L \frac{dL}{G \cdot \tau} \quad 8-24$$

Solving 8-24 for n gives [50]:

$$n = n^0 \cdot \exp \left[\frac{-L}{G \cdot \tau} \right] \quad 8-25$$

8.3.6 Magma Density

The magma density or slurry density is the total mass of crystals per unit volume of slurry. [50]

$$M_T = \rho_c \cdot k_v \cdot \int_0^\infty L^3 \cdot n(L) dL \quad 8-26$$

M_T is the magma density, ρ_c the density of the crystal, k_v is the volume shape factor of the crystal, n the crystal population density and L the characteristic length of the crystal. In 8-25, n^0 can be specified as the ratio of the nucleation (B^0) to the crystal growth rate at zero size (G^0). 8-16 can be substituted into 8-25, which leads to:

$$n(L) = \frac{k_7 \cdot G^n \cdot M_T^p \cdot R^q}{G^0} \cdot \exp \left[\frac{-L}{G \cdot \tau} \right] \quad 8-27$$

The resulting equation for the magma density is:

$$M_T = \rho_c \cdot k_v \cdot \int_0^\infty L^3 \cdot k_7 \cdot \frac{G^n}{G^0} \cdot M_T^p \cdot R^q \cdot \exp\left[\frac{-L}{G \cdot \tau}\right] dL \quad 8-28$$

where the growth rate G is defined according to 8-19 [49].

8.4 Thermodynamics

8.4.1 Equation-of-state models

8.4.1.1 Ideal Gas solution model

Equation-of-state models calculate the relationship between pressure, specific volume and temperature, P , v and T . For ideal gas and ideal gas solution, following equations are given to estimate specific molar vapor volume v_V , specific molar vapor enthalpy h_V and specific molar vapor entropy s_V [43]:

$$v_V = \frac{V}{\sum_{i=1}^c N_i} = \frac{M}{\rho_V} = \frac{R \cdot T}{P} \quad 8-29$$

$$h_V = \sum_{i=1}^c y_i \cdot \int_{T_0}^T (C_P^0)_{iV} dT = \sum_{i=1}^c y_i \cdot h_{iV}^0 \quad 8-30$$

$$s_V = \sum_{i=1}^c y_i \cdot \int_{T_0}^T \frac{(C_P^0)_{iV}}{T} dT - R \cdot \ln\left(\frac{P}{P_0}\right) - R \cdot \sum_{i=1}^c y_i \cdot \ln y_i \quad 8-31$$

where V is the volume, N_i the number of moles of component i , M is the molar mass, ρ_V the density of vapor phase, R is the gas constant, T the temperature, P is the pressure, y_i the mole fraction of vapor phase, $(C_P^0)_{iV}$ is the ideal gas heat capacity of component i at constant pressure, h_{iV}^0 the ideal gas molar enthalpy of component i , and T_0 and P_0 temperature and pressure at reference condition. [43]

8.4.1.2 Soave-Redlich-Kwong equation-of-state model

Non-ideal gas equation-of-state models imply molecular and intermolecular forces, whose impact volume. Soave-Redlich-Kwong (SRK) is one of these non-ideal gas equation-of-state models describing a semi-empirical approach for estimating equation of state as follows [43]:

$$P = \frac{R \cdot T}{v - b} - \frac{a}{v^2 + b \cdot v} \quad 8-32$$

where

$$a = 0.42748 \cdot R^2 \cdot T_c^2 \cdot [1 + f_\omega \cdot (1 - T_r^{0.5})]^2 / P_c \quad 8-33$$

$$b = 0.07780 \cdot R \cdot T_c / P_c \quad 8-34$$

$$f_\omega = 0.48 + 1.574 \cdot \omega - 0.176 \cdot \omega^2 \quad 8-35$$

$$\omega = \left[-\log \left(\frac{P^s}{P_c} \right)_{T_r=0.7} \right] - 1 \quad 8-36$$

P is the pressure, R the gas constant, T is the temperature, v the specific molar volume, T_c and P_c are the critical temperature and pressure, T_r is the reduced temperature T/T_c , P^s the vapor pressure and ω is the acentric factor. [43]

8.4.2 NRTL

For estimating non-ideal systems containing components with different polarities, ideal liquid calculation cannot be used. Non-random, two-liquid (NRTL) equation is used for modeling multicomponent vapor-liquid, liquid-liquid and vapor-liquid-liquid systems for various compounds. Binary interaction parameters have to be available from experimental data. NRTL is estimating the activity coefficient by following equation [43]:

$$\ln \gamma_i = \frac{\sum_{j=1}^C \tau_{ji} \cdot G_{ji} \cdot x_j}{\sum_{k=1}^C G_{ki} \cdot x_k} + \sum_{j=1}^C \left[\frac{x_j \cdot G_{ij}}{\sum_{k=1}^C G_{kj} \cdot x_k} \cdot \left(\tau_{ij} - \frac{\sum_{k=1}^C x_k \cdot \tau_{kj} \cdot G_{kj}}{\sum_{k=1}^C G_{kj} \cdot x_k} \right) \right] \quad 8-37$$

where

$$G_{ji} = \exp(-\alpha_{ji} \cdot \tau_{ji}) \quad 8-38$$

$$\tau_{ij} = \frac{g_{ij} - g_{jj}}{R \cdot T} \quad 8-39$$

$$\tau_{ji} = \frac{g_{ji} - g_{ii}}{R \cdot T} \quad 8-40$$

γ_i is the activity coefficient of component i , g_{ij} , g_{ji} and so on are interaction energies of molecule pairs, R is the gas constant, T the temperature, α_{ji} is a parameter for non-randomly distribution of component j and i , and x is the mole fraction of liquid phase.